Marian Bică

Generalized Multicarrier Radar: models and performance

School of Electrical Engineering

Thesis submitted for examination for the degree of Master of Science in Technology.
Espoo November 22, 2012

Thesis supervisor and instructor:

Professor Visa Koivunen

Aalto University
School of Electrical
Engineering

AALTO UNIVERSITY
SCHOOL OF ELECTRICAL ENGINEERING

ABSTRACT OF THE
MASTER'S THESIS

Author: Marian Bică

Title: Generalized Multicarrier Radar: models and performance

Date: November 22, 2012 Language: English Number of pages:8+79

Department of Signal Processing and Acoustics

Professorship: Signal Processing Code: S-88

Supervisor and instructor: Professor Visa Koivunen

Radar has been an area of extensive research over the last decades. Due to wide availability and applicability of multicarrier systems in wireless communications the idea of multicarrier radar has emerged. Multicarrier waveforms bring several major advantages over single carrier waveforms in radar systems. One major advantage, if not the most significant, is frequency diversity. This allows to overcome problems like jamming, interference or attenuation by allocating power to subcarriers where the channel quality is high. Another great advantage is that only one pulse is required to obtain range and Doppler information. Waveform diversity is also an advantage. Designing the waveforms both in time and frequency brings in additional degrees of freedom. Last but not least, the possibility to optimize the transmitted waveform is important for radar systems. Traditionally, only the receiver has been adaptive and optimized in radars. Interesting waveform designs have been proposed in the literature already. However, no effort has been done in order to create a general model that can describe all these proposed waveforms and allow the design of new ones in an easy and intuitive way. This work takes the initiative and derives such a general model that can accommodate various design options. The derivation of this model is done using equations in a matrix form. This matrix formulation allows for an easy and intuitive implementation of multicarrier radar waveforms just by filling in the elements to corresponding matrices accordingly. Moreover, generation of different radar waveforms in Matlab in an intuitive way is facilitated. A spread spectrum waveform is proposed and generated using the derived model. The radar performance of this waveform is investigated through simulations. The choice of different design parameters is discussed and suggestions are made in order to achieve the best possible radar performance. The derivation of this general model is key enabler for future implementations of multicarrier radar waveforms.

Keywords: Radar, Multicarrier, OFDM, MCPC, Spread Spectrum

Preface

The work for this thesis has been carried out in the Department of Acoustics and Signal Processing, Aalto University.

I am deeply grateful to my supervisor, Prof. Visa Koivunen, for his constant guidance and support and for giving me the opportunity to be part of his research group. Thank you for the privilege of working on such interesting subject. I feel honoured for the chance of meeting and working with such distinguished person and researcher.

I would like to thank all my colleagues in the department for creating such a friendly place to work. Especially, I would like to thank Dr. Jussi Salmi and Mário Costa for valuable and numerous discussions related to this work. Their feedback and guidance have helped me achieve a better understanding on the subject. I would also like to thank Tuomas Aittomäki for his valuable comments and feedback.

Special thanks are due to Dr. Traian Abrudan for his support and great confidence he has shown in my skills and my desire to learn. I can only hope to never disappoint.

I would like to thank my girlfriend Delia for her constant encouragement and support. Thank you for believing in me and bearing with me in my hard times.

Last but not least, I would like to thank my parents, Gheorghe and Mariana, for all the love and immense support, for being so close to me despite the distance. I am deeply grateful and I dedicate this thesis to them. În cele din urmă, dar nu mai puţin important, doresc să le mulţumesc părinţilor mei, Gheorghe şi Mariana, pentru toate dragostea şi nemăsurata susţinere oferită, pentru că mi-au fost atât de aproape sufleteşte, în ciuda distanţei fizice. Le sunt profund recunoscător şi le dedic această teză.

Otaniemi, November 22, 2012

Marian Bică

Contents

List of Acronyms

COCS	Consecutive Ordered Cyclic Shift
CP	Cyclic Prefix
CW	Continuous Wave
DAB	Digital Audio Broadcast
DFT	Discrete Fourier Transform
DS-CDMA	Direct Sequence CDMA
DVB	Digital Video Broadcast
ECM	Electronic Countermeasure
FDC	Frequency Domain Coding
FDRW	Frequency Diversity Radar Waveform
FFT	Fast Fourier Transform
ICS	Identical Complementary Set
IDFT	Inverse Discrete Fourier Transform
IFFT	Inverse Fast Fourier Transform
IS	Identical Sequence
ISI	Inter-Symbol Interference
LFM	Linear Frequency Modulation
LTE	Long Term Evolution
LTI	Linear Time-Invariant
MC	Multicarrier Communication
MC-CDMA	Multicarrier CDMA
MC-DS-CDMA	Multicarrier Direct Sequence CDMA
MCPC	Multicarrier Phase-Coded
MLS	Maximum Length Sequence
MOCS	Mutually Orthogonal Complementary Set
MPS	Minimum Peak Sequence
MT-CDMA	Multitone CDMA
NLFM	Non-Linear Frequency Modulation
OFDM	Orthogonal Frequency Division Multiplexing
PACF	Periodic Autocorrelation Function
PAPR	Peak-to-Average Power Ratio
PDR	Pulsed Doppler Radar
PMEPR	Peak-to-Mean Envelope Power Ratio
PR	Pulsed Radar
PRC	Pseudo Random Code
PRF	Pulse Repetition Frequency
PRI	Pulsed Repetition Interval
PRN	Pseudo Random Sequence
PSLL	Peak Sidelobe Level
QRS	Quadratic Residue Sequence

RCS	Radar Cross Section
SNR	Signal-to-Noise Ratio
SOJ	Stand-Off Jammer
SSJ	Self-Screening Jammer
TDC	Time Domain Coding
TDRW	Time Diversity Radar Waveform
WAF	Wideband Ambiguity Function
WiMAX	Worldwide Interoperability for Microwave Access
WLAN	Wireless Local Area Network

List of Symbols

A_e	antenna aperture
B	bandwidth
B_J	jammer's bandwidth
c	speed of light
$c_{n,m}$	m^{th} chip on the n^{th} subcarrier
D	diameter
d_n	information symbol on the n^{th} subcarrier
F	noise figure
f_D	Doppler frequency
f	frequency
f_0	central frequency
f_b	beat frequency
f_{bd}	beat frequency on the negative slope
f_{bu}	beat frequency on the positive slope
$\dot{f}$	rate of the frequency change
f_m	modulating frequency
f_r	pulse repetition frequency
G	gain of the antenna
G'	gain in the direction of the jammer
G_j	jammer's antenna gain
k	$= 1.38 \times 10^{-23}$ joule/degree Kelvin Boltzman's constant
L	loss
L_j	jammer's operating loss
L_p	propagation losses
L_r	receiver losses
L_t	transmitter losses
L_{win}	losses associated with the type of utilized window
M	number of chips in the modulating code
N	number of subcarriers

n_b	number of positions required to cover the solid angle
n_p	number of pulses that will hit the target
P_{av}	average power applied on the target
P_{cw}	average transmitter power over the dwell time
P_D	peak power density
P_{Dr}	power delivered to the radar
P_j	jammer's peak power
P_{min}	minimum power level for which the target is detected
P_r	power reflected from the target
P_{refl}	power density at the receiving antenna for bistatic radar
P_{SOJ}	power of the Stand-Off Jammer
P_{SSJ}	power received by the radar from a Self-Screening Jammer
P_t	peak transmitted power
$\dot{R}$	range rate
R	range of the target
R_j	jammer's range
R_{max}	maximum distance at which a detectable target can be from the radar
v	target speed
T	pulse duration
T_c	chip duration
T_{CP}	duration of the cyclic prefix
T_d	duration of a serial symbol
T_{dwell}	dwelling time
T_e	effective noise temperature in degree Kelvin
T_i	time on target
T_r	pulse repetition interval
t_r	round-trip time
T_s	OFDM symbol duration
T_{sc}	scan time, the time the radar needs to scan a volume in space
$u_{n,m}$	m^{th} weight on the n^{th} subcarrier
w_n	weight of the n^{th} subcarrier
Δf	intercarrier spacing
$\Delta\phi$	phase difference
Δt	time difference
λ	wavelength
μ	complex amplitude introduced by the target
Ω	solid angle
Φ	matrix of polyphase codes
ϕ	vector of a polyphase code

π	ratio of circumference of circle to its diameter
σ	radar cross section
σ_B	bistatic radar cross section
τ	delay
Θ	shift of a modulating code
θ_{3dB}	beam width at 3dB
φ	phase
ξ	scaling factor

1 Introduction

1.1 Motivation

Radar was first developed as a military technology in the 1940's. Nevertheless, its operating principle was based on the developments achieved by scientists in the field of electromagnetic waves many years earlier. Since then, extensive research has been done on radar technology and its use in civilian applications has grown also.

The idea of multicarrier data transmission was introduced in 1960's [23, 35] and since 1980's it has been of great interest for the research community [5]. This was facilitated by the progress in digital circuit technology as well as single and multi-user communication systems. Nowadays, Multicarrier Communication (MC) systems such as Orthogonal Frequency Division Multiplexing (OFDM) are included in the digital television systems (Digital Video Broadcast (DVB) [25]), digital radio systems (Digital Audio Broadcast (DAB) [30]), local area mobile wireless networks (WLAN [6, 33]), wireless communications (WiMAX [8]) and cellular communications (LTE [12]) [34].

Given the wide spread of multicarrier waveforms in communication systems, multicarrier transmissions found their place in radar as well. Multicarrier type of signals bring many advantages to radar. Frequency diversity, reduced time on target, waveform diversity and optimization of both transmitter and receiver are just a few key benefits. Another incentive to use multicarrier signals in radar is the wide availability and reduced cost of the hardware. Plenty of research has been done in this area. Multicarrier radar signal models that employ OFDM ([14, 13, 20, 26]) and its special case Multicarrier Phase-Coded (MCPC) waveform ([16, 15, 22]) have been proposed in the literature. However, no attention has been paid to a general model that could describe all these multicarrier waveform designs as well as most commonly used other waveforms. Such model should allow for easy implementation of various multicarrier waveforms.

1.2 Scope of the Thesis

This work focuses on the development of a general signal model that would describe the already proposed multicarrier radar signals as well as many other. The formulation of this model is done in matrix form that would allow easy implementation of many different waveforms by modifying the matrices accordingly. Several waveform examples are presented after the derivation of the model is complete. The radar performance of some of these examples is then compared with an already proposed waveform in the literature.

1.3 Contributions of the Thesis

The main contribution of this work is the proposed general multicarrier radar model. Since it is formulated using matrix representation, it allows for easy implementation

of the different new waveforms. This is achieved by modifying the corresponding matrices accordingly.

The generalized multicarrier radar model is able to implement both single and multicarrier radar waveforms. Some of the techniques that can be implemented for the multicarrier radar waveforms using this model are:

- pulse compression over subbands and time
- frequency hopping
- resource allocation

Another main contribution is the introduction of a spread spectrum waveform using the general model that is called Time Diversity Radar Waveform (TDRW). This waveform is able to provide better radar performance than the MCPC waveform proposed in the literature. Nevertheless, it is shown that the MCPC waveform is a particular case of a Time Diversity Radar Waveform (TDRW). Recommendations are made on how better performance for TDRW can be obtained.

1.4 Structure of the Thesis

The content of this thesis is organized as follows. Chapter 2 presents an overview of radar principles. First, an overview of radar terminology is provided and then the radar equation is presented for different types of radars. Couple of the most used radar waveforms are also presented in this chapter. Chapter 3 reviews recent developments in the field of multicarrier radar. The two multicarrier radar concepts based on OFDM and MCPC are presented in more detail. In chapter 4, general multicarrier radar model is derived. A few waveform design examples are also presented and implemented using the derived general model. Chapter 5 focuses on the performance of a multicarrier waveform generated with the proposed general model. The performance is assessed by comparison with the MCPC waveform, already proposed in the literature. The conclusions of this work are presented in Chapter 6.

2 Overview of Radar Principles

2.1 Radar terminology

Radar stands for RAdio Detection And Ranging, first used by the U.S. Navy in the 1940's and then becoming a common word. Radars utilize radiated electromagnetic energy towards certain directions in order to detect targets that reflect back part of the energy. By analyzing the reflected energy (known as echoes or radar returns) information like range, velocity or angular position of the target can be extracted.

Radars can be classified in different categories based on the operating frequency, antenna type, utilized waveform or purpose. In terms of operating frequency radars are found in the range 1–40 GHz, while from the point of view of utilized waveform radars can be CW or Pulsed Radars (PRs). There are many other ways of characterizing a radar and as a result many ways to differentiate them. Surveillance radar, Moving target indication, Tracking radar, Image radar, Synthetic aperture radar are just a few that can be mentioned [27].

CW radars emit electromagnetic energy in a continuous manner. Separate antennas for transmission and reception are needed as a result. This type of radar can measure very precisely radial velocity and angular position. For measuring the range of the target it is necessary to utilize some form of modulation. Frequency modulation is commonly utilized so that the radar is able to detect the range of the target. This type of radar is known as Frequency Modulated CW radar.

Pulsed radars utilize a train of, usually, modulated pulses and are characterized by the Pulse Repetition Frequency (PRF). Based on the PRF, which can be low, medium or high, there is a trade-off in measuring the range or velocity of the target. When a high PRF is utilized, the radar performs better in measuring target velocity, while a low PRF is more suitable for measuring the range of the target [19].

Radar is capable of providing more information in addition to detecting targets and measuring the range. Detecting a target means only to be aware of its presence. Usually the interest lies in obtaining as much information about the parameters of the target from the observed data. The ability to determine and store the parameters of a target is called tracking. A tracking radar can follow one or many targets depending on its capability and purpose. The radar's ability to distinguish between multiple targets depends on the resolution in range and angle. These represent the dimensions of the resolution cell. It is considered that if two targets are in the same resolution cell, the radar can not distinguish between them. By analyzing the radar echo one can extract information such as:

Range determined by measuring the time for the radar signal to propagate to the target and back. It is typically the most important task of the radar. The most common waveform for measuring the range is a short pulse. The shorter the pulse, the more precise the range is.

Radial Velocity determined by successively measuring the range of the target and observing how often the range of the target is changing. Radial Velocity can also be determined from the Doppler frequency shift of the echo signal, but

this is not accurate for many pulsed radars. Commonly this is obtained with a CW type of radar. However, any of the methods requires time and the more time is used for observation the more accurate the results are, assuming the target state remains the same.

Angular Direction determined by analyzing the angle at which the echo arrives at the radar. This can be achieved by using a directive antenna or an antenna array and beamforming capability. The antenna radiation can be directed to a specific direction through beamsteering. This could be done either electronically, by changing the relative phase of the antenna elements, or mechanically, by tilting the antenna. Best results are obtained when using wide aperture antennas that can create a narrow beam width. As mentioned earlier, this is crucial when resolving between multiple targets.

Size determined by radars that provide enough resolution. The radar resolution must be considerably better than the size of the target (e.g. ten times) to enable this type of measurement. Alternatively, the target may be close-by.

Shape determined from the target's profile in range and cross range or by obtaining the two-dimensional profile of the target from measuring the phase and amplitude at different angles of observation.

There is also other information that can be extracted by analyzing the echo or by combining information, however, these are out of the scope of this work [27].

2.2 Radar equation

Also known as radar range equation, it represents a way of determining the range of a target based on the radar type and target characteristics. Such characteristics are the power radiated by the radar, the radar's antenna gain, target's radar cross section and the aperture of the receiving antenna of the radar [27]. These characteristics will be introduced in this section and the radar equation will be derived. There is a conventional radar equation, but this not used for any type of radar. As the purpose and main function of the radar can change, so does the radar equation have to be particularized for that specific task. In this section the radar equation will be derived for Doppler pulsed radars (with low and high PRF), CW radar, surveillance radar, radar in face of jamming and bistatic radar.

The starting point for the derivation of radar equation is the peak power density at distance R [19]. For an omni directional antenna this is defined as:

$$P_D = \frac{\text{Peak transmitted power}}{\text{Area of a sphere}} \quad \frac{\text{watts}}{\text{m}^2}. \tag{1}$$

If no losses and an isotropic radiation are considered, then the peak power density is:

$$P_D = \frac{P_t}{4\pi R^2}, \tag{2}$$

where P_t is the peak transmitted power and $4\pi R^2$ is the area of the sphere. In practice, radar systems utilize directional antennas. These give the radar the ability to concentrate the power density in one direction. Antenna aperture (A_e) and gain (G) are two characteristics of a directional antenna. The relation between antenna aperture and gain is given by:

$$A_e = \frac{G\lambda^2}{4\pi}, \tag{3}$$

where λ is the wavelength. Thus, for a directive antenna with gain G equation (2) becomes:

$$P_D = \frac{P_t G}{4\pi R^2}. \tag{4}$$

When the radiated energy hits a target it is radiated back in all directions. The spatial distribution of energy is called scattering, while the target is called a scatterer [27]. Only the energy radiated back to the radar is of interest. This is called the radar echo. The total power radiated back to the radar is defined by the Radar Cross Section (RCS). This is the characteristic of the target and it is important for the derivation of the radar equation. The RCS is given by the ratio of the power reflected back to the radar and the power density that hits the target:

$$\sigma = \frac{P_r}{P_D}, \tag{5}$$

where P_r is the power reflected from the target. The unit for a RCS is area and in this case can be m^2. An example of RCS is presented in Figure 1.

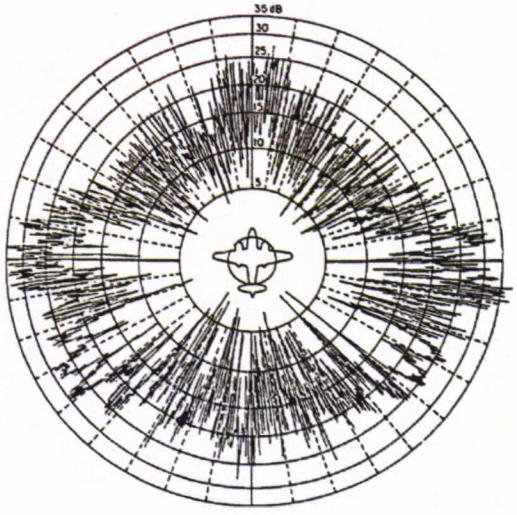

Figure 1: Example of Radar Cross Section (source of figure is [27])

It is common for radar to use the same antenna for transmission and reception. This means that the antenna gain will be the same for transmission and reception. Assuming this, the total power that is radiated by the target and observed by the radar is:

$$P_{Dr} = \frac{P_t G}{4\pi R^2} \frac{\sigma}{4\pi R^2} A_e \tag{6}$$

and by replacing A_e with its formula, the above equation becomes:

$$P_{Dr} = \frac{P_t G}{4\pi R^2} \frac{\sigma}{4\pi R^2} \frac{G\lambda^2}{4\pi}. \tag{7}$$

The right hand side of the equation is a product of three factors. The first one represents the power density of a radar that radiates the power P_t. The second one is the RCS divided by the area of a sphere. This accounts for the divergence of the echo signal returning to the radar. And the third one represents how much of the echo power is collected by the radar's receiving antenna. Regarding the units, range R is measured in meters, transmitted power P_t in watts, wavelength λ in meters and antenna aperture A_e in square meters. The gain G is considered to have no unit. The compact version of (7) is:

$$P_{Dr} = \frac{P_t G^2 \lambda^2 \sigma}{(4\pi)^3 R^4}. \tag{8}$$

If P_{min} is considered as the minimum power level for which the target is detected, then the maximum distance at which the target can be detected is given by:

$$R_{max} = \sqrt[4]{\frac{P_t G^2 \lambda^2 \sigma}{(4\pi)^3 P_{min}}}. \tag{9}$$

In practice the minimum detectable power P_{min} is limited by the receiver noise and can be written as:

$$P_{min} = kT_e BF(S/N)_0, \tag{10}$$

where k is Boltzmann's constant expressed in joules/degree Kelvin, T_e is the standard temperature of 290 Kelvin, B is the receiver bandwidth expressed in Hz and F is the noise figure. This is defined as the noise of a practical receiver over the noise of an ideal one and as a result it has no unit. $(S/N)_0$ is the factor by which the received signal has to be larger than the receiver noise in order to be detected. It is basically the radar detection threshold and it represents a Signal-to-Noise Ratio (SNR). This threshold is equivalent with:

$$(S/N)_0 = \frac{P_{min}}{kT_e BF}, \tag{11}$$

which, by using (8), can be further developed as:

$$(S/N)_0 = \frac{P_t G^2 \lambda^2 \sigma}{(4\pi)^3 R^4 kT_e BF}. \tag{12}$$

If L denotes the radar losses, that reduce the SNR, it is possible to write:

$$(S/N)_0 = \frac{P_t G^2 \lambda^2 \sigma}{(4\pi)^3 R^4 k T_e B F L}, \tag{13}$$

which is widely known as the radar equation [19].

2.2.1 Low PRF Radar

This section deals with one variation of (13) which is particularized for a low PRF radar. Such type of radar is able to detect targets at long ranges. The reason for this is the long time available to receive the echo before the next pulse is sent. Typically the range estimates produced by this radar are unambiguous, while Doppler estimates are ambiguous.

The pulse duration for such radar is assumed to be T, the Pulsed Repetition Interval (PRI) T_r and peak transmitted power P_t. For low PRF radars it can be assumed that $T << T_r$. This can be visualized in Figure 2.

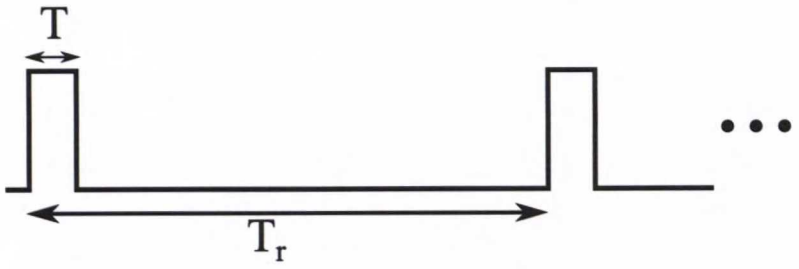

Figure 2: Pulses of a low PRF radar

The "time on target" T_i is the time that the beam is concentrated on the target. This time is related to the number of pulses that will hit the target n_p, and is given by:

$$n_p = T_i f_r, \tag{14}$$

where f_r is the PRF. Equation (13), which is valid for one pulse, is adapted for n_p pulses. Thus, for n_p coherently integrated pulses the radar equation is:

$$(SNR)_1 = \frac{P_t G^2 \lambda^2 \sigma n_p}{(4\pi)^3 R^4 k T_e B F L}. \tag{15}$$

Taking into account that $B = 1/T$ and replacing n_p with its formula equation, (15) can be written as:

$$(SNR)_{n_p} = \frac{P_t G^2 \lambda^2 \sigma T_i f_r T}{(4\pi)^3 R^4 k T_e F L}. \tag{16}$$

Equation (16) follows the equation (7) with the extra term $T_i f_r$, which accounts for the number of pulses utilized in target tracking.

2.2.2 High PRF Radar

This section deals with another variation of (13) which is particularized for a high PRF radar. This kind of radar utilizes a waveform similar with the one that a low PRF radar utilizes. The difference is that the rate at which the pulses are sent is very high. As a result the waveform resembles a train of pulses. In this case there is no time to receive the echo between consecutive pulse transmissions. This can be visualized in Figure 3.

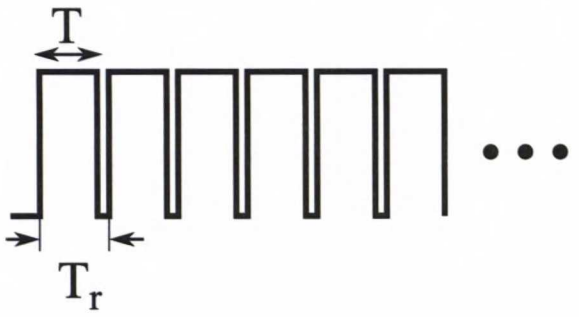

Figure 3: Pulses of a high PRF radar

If the pulse duration is T, as in the low PRF radar case, the bandwidth is not $1/T$ anymore. It is equal to the inverse of the integration time, in this case $1/T_i$. Another difference from the low PRF radar is the fact that the duty cycle can not be neglected. The duty cycle, or duty factor, is defined as the pulse duration over the duration between the pulses. This is very similar for both transmission and reception [19]. Thus, by denoting the duty cycle with d_t and d_r for transmission and reception respectively, equation (13) becomes :

$$SNR = \frac{P_t G^2 \lambda^2 \sigma d_t^2}{(4\pi)^3 R^4 k T_e B F L d_r} \tag{17}$$

and after the duty cycle is written as Tf_r and the appropriate reduction:

$$SNR = \frac{P_t G^2 \lambda^2 \sigma T T_i f_r}{(4\pi)^3 R^4 k T_e F L}. \tag{18}$$

The product $P_t T f_r$ is considered to be the average transmission power, denoted P_{av} and the final equation for high PRF radar is:

$$SNR = \frac{P_{av} T_i G^2 \lambda^2 \sigma}{(4\pi)^3 R^4 k T_e F L}. \tag{19}$$

The product between the average power and the PRI, $P_{av}T_i$, indicates that the detection performance can be improved by using a low transmission power and longer integration time [19].

2.2.3 CW Radar

The equation for this type of radar can be derived from (19) with the appropriate changes. The integration time T_i is replaced by the dwell time T_{dwell}. This is equal to the length of the data set that is processed at a time by the radar. The average transmitted power P_{av} is replaced by the average transmitted power over the dwell time P_{CW}. Also because different antennas are used for transmission and reception the gains for the respective antennas will be different. Introducing the new terms in (19), the equation for CW radar is obtained as:

$$SNR = \frac{P_{CW} T_{dwell} G_t G_r \lambda^2 \sigma}{(4\pi)^3 R^4 k T_e F L L_{win}}, \tag{20}$$

where the loss L_{win} is the loss associated with the type of window utilized for processing [19].

2.2.4 Surveillance Radar

This type of radar detects the presence of a target and determines its location in range and angle. It can also observe the target over a period of time, performing the task of tracking [27]. A certain volume in space is scanned in search of targets. The search of the target can be done in two ways, depending on the antenna and radar:

- the beam width covers the entire volume in elevation and scans in azimuth
- the beam width is smaller and has to scan in both azimuth and elevation

The scanning can be done either mechanically or electrically. Figure 4 presents how target searching can be done.

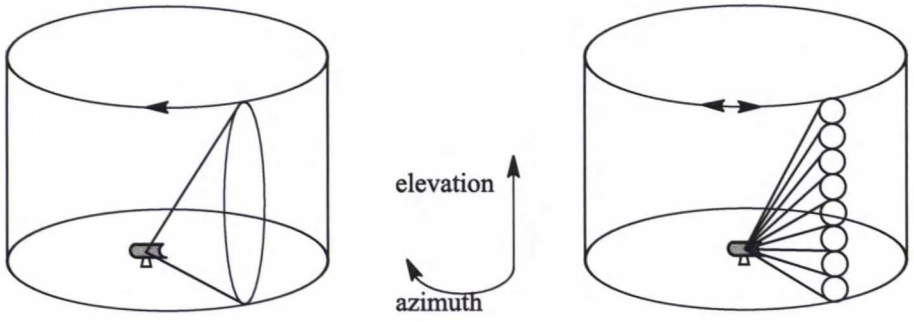

Figure 4: Surveillance radar search patterns [19]

Few assumptions need to be made before proceeding with the derivation of the equation for surveillance radar. When one is referring to beam width, it is assumed that the 3 dB beam width is taken into account. This means that the beam width is measured where the magnitude of the radiation pattern is reduced to half. Also it is considered that the radiation pattern is circular. What this means is that the angle of the radiation is the same in azimuth and elevation [19]. Solid angle Ω is

defined in order to specify the search volume. So, the number of positions that are needed to cover the solid angle Ω is:

$$n_b = \frac{\Omega}{\theta_{3dB}^2}, \tag{21}$$

where θ_{3dB} accounts for the beam width. For a circular aperture of diameter D it is considered that $\theta_{3dB} \approx \frac{\lambda}{D}$. Thus, the number of positions becomes:

$$n_b = \frac{D^2}{\lambda^2}\Omega. \tag{22}$$

In addition, the scan time T_{sc}, i.e. the time the radar needs in order to scan the volume, has to be defined. The time on target can be expressed in terms of T_{sc} as:

$$T_i = \frac{T_{sc}}{n_b} = \frac{T_{sc}\lambda^2}{D^2\Omega}. \tag{23}$$

The equation for surveillance radar can be obtained using (19). The formula for time on target is replaced in (19) and the equation becomes:

$$SNR = \frac{P_{av}G^2\lambda^2\sigma}{(4\pi)^3R^4kT_eFL}\frac{T_{sc}\lambda^2}{D^2\Omega}. \tag{24}$$

This can be factorized as:

$$SNR = \frac{P_{av}\sigma}{16R^4kT_eFL}\left(\frac{G\lambda^2}{4\pi}\right)^2\frac{4}{\pi D^2}\frac{T_{sc}}{\Omega}. \tag{25}$$

Recalling (3) and considering $A = \frac{\pi D^2}{4}$, the final equation for surveillance radar is obtained [19]:

$$SNR = \frac{P_{av}A\sigma}{16R^4kT_eFL}\frac{T_{sc}}{\Omega}. \tag{26}$$

2.2.5 Radar in the face of Jamming

Radars are subject to unintentional and intentional interference called jamming. Jamming is considered to be offensive Electronic Countermeasure (ECM). There are many ECMs, but here the focus is only on barrage jammers and deceptive jammers (repeaters). Barrage jammers try to increase the noise level in the whole radar operating bandwidth, while repeater jammers capture the radar transmissions and send back false echoes as an atempt to confuse the radar.

Self-Screening Jammers (SSJs)

SSJs are jammers that are carried with the target. For example, a fighter aircraft that needs to be invisible for enemy radar while it is in the air has to be equipped with a device that performs radar jamming. Equation (8) is utilized for the derivation of the equation for a radar in front of a SSJ. However, receiver loss L has to be taken into account, so the starting equation is [19]:

$$P_r = \frac{P_t G^2 \lambda^2 \sigma}{(4\pi)^3 R^4 L}. \tag{27}$$

The power received from a SSJ at the same range is

$$P_{SSJ} = \frac{P_J G_J}{4\pi R^2} \frac{A_e B}{B_J L_J}, \tag{28}$$

where P_J, G_J, B_J, L_J represent the jammer's peak power, antenna gain, operating bandwidth and losses respectively. Using (3) the following equation is obtained:

$$P_{SSJ} = \frac{P_J G_J}{4\pi R^2} \frac{\lambda^2 G}{4\pi} \frac{B}{B_J L_J}. \tag{29}$$

The bandwidth of the jammer over the bandwidth of the radar signal needs to be taken into account as less than unity. It is clear that the bandwidth of the jammer is larger than the one of the radar in general, as the jammer needs to operate against different radars. The equation for radar in front of a SSJ is obtained by dividing the power received by the radar in (27) with the power received from the jammer in (29) :

$$\frac{P_r}{P_{SSJ}} = \frac{P_t G \sigma B_J L_J}{4\pi P_J G_J R^2 B L}. \tag{30}$$

Stand-Off Jammers (SOJs)

SOJs emit ECM signals from long distances, thus the power received from such jammer has a similar formula as the one received from a SSJ:

$$P_{SOJ} = \frac{P_J G_J}{4\pi R_J^2} \frac{\lambda^2 G'}{4\pi} \frac{B}{B_J L_J}, \tag{31}$$

where R_J is the range to the jammer and G' is the radar antenna gain in the direction of the jammer [19]. The equation for a radar in front of a SOJ is obtained the same way as in front of a SSJ, by dividing the power received by the radar in (27) with the power received from the jammer in (31):

$$\frac{P_r}{P_{SOJ}} = \frac{P_t G^2 \sigma R_J^2 B_J L_J}{4\pi R^4 L P_J G_J G' B}. \tag{32}$$

2.2.6 Bistatic Radar

Bistatic radars are those type of radars that utilize different antennas for transmission and reception, situated in different locations. It is important to be aware of the fact that even though CW radars may have separate antennas for transmission and reception, these are not considered bistatic if the distance between them is not long enough. Usually, the distance between the transmitter and receiver has to be comparable with the expected target range [27]. Figure 5 presents the geometry of a bistatic radar. Transmitter and receiver need to be synchronized in order for this

type of radar to function. The angle between the two signal paths, the incident path and the reflected path, at the target, is called bistatic angle. This angle impacts the RCS since for a small angle the bistatic RCS is similar to the monostatic RCS, but for an angle that approaches 180° the bistatic RCS becomes very large compared to the monostatic one [19]. However, this is not always true for a target with a complex shape and the opposite can happen.

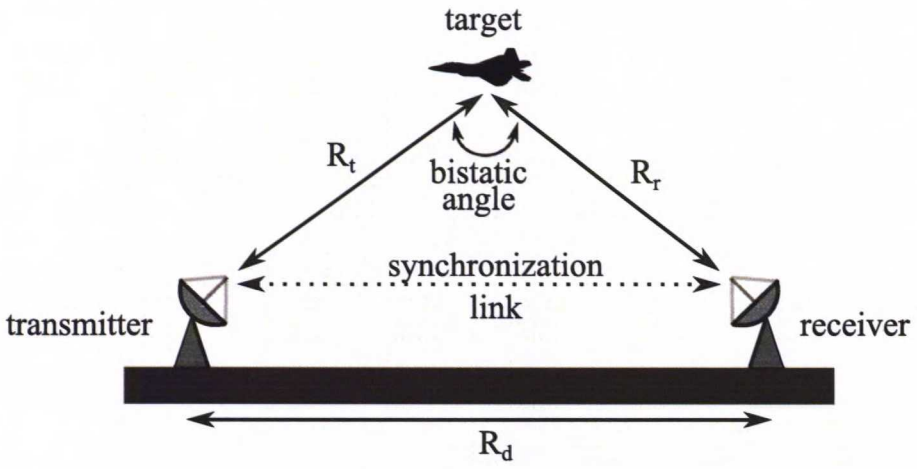

Figure 5: Bistatic radar [19]

The equation for a bistatic radar is derived in a similar way as for a monostatic radar. The formula for power density (4) at the target is the starting point. As the receiver and transmitter antennas are not the same, their gains are considered to be different, so that:

$$P_D = \frac{P_t G_t}{4\pi R_t^2}, \tag{33}$$

where the subscript "t" stands for transmission. The power density at the receiving antenna, reflected from the target, is:

$$P_{refl} = \frac{P_D \sigma_B}{4\pi R_r^2} = \frac{P_t G_t \sigma_B}{(4\pi)^2 R_t^2 R_r^2}, \tag{34}$$

where σ_B represents the bistatic RCS. The total received power taking into account the receiver antenna aperture is given by:

$$P_{Dr} = \frac{P_t G_t \sigma_B A_e}{(4\pi)^2 R_t^2 R_r^2}. \tag{35}$$

By replacing A_e with (3) and taking into account the losses for transmitter, receiver and propagation medium, L_t, L_r and L_p respectively, the bistatic radar equation can be defined as [19]:

$$P_{Dr} = \frac{P_t G_t G_r \lambda^2 \sigma_B}{(4\pi)^3 R_t^2 R_r^2 L_t L_r L_p}. \tag{36}$$

The interpretation of the above equation can tell which parameters influence the performance of the bistatic radar. The received power is directly proportional with the transmission power and gains of the transmission and reception antennas. It is also inversely proportional with the antennas and propagation losses and with the square distances from the target to receiver and transmitter.

2.3 Radar waveforms

This section deals with the radar waveforms which have a great influence on radar capabilities and possible applications. First, CW and pulsed radar are discussed and then pulse compression radar.

2.3.1 Continuous Wave Radar

As earlier described, the concept of radar implies the transmission of a pulse of energy and the analysis of the received echo. The information obtained is usually the target range. In order to obtain Doppler information, a different concept that uses continuous time waveforms exists. However, this concept does not allow for obtaining range information unless coding or some modulation technique is used. Other advantages of CW radar are its simplicity and potential minimum spread in the transmitted spectrum, which means lower interference. CW radar is less susceptible to being detected due to its minimum power requirement and great frequency diversity. Unmodulated CW radars are able to provide velocity information without ambiguities for targets of any range. Of course CW radar has its disadvantages that can not be neglected. The most important one is the leakage from the transmitter to the receiver. This leakage has to be separated from the true echoes that are received from the target. The leakage not only that confuses the receiver but also introduces noise [27].

The waveforms utilized by CW radars can be pure sine waves of the form $\cos(2\pi f_0 t)$. Spectra of the radar echo from stationary targets and clutter will be concentrated at f_0. The center frequency of the echoes from moving targets will be shifted by the Doppler frequency, f_D. Target radial velocity can be extracted from the difference of these central frequencies.

In order to avoid interruption of the continuous radar energy emission, two antennas are used in CW radars, one for transmission and one for reception. CW radars cannot measure target range since this is computed from the radar echoes by measuring a two-way time delay. In order for CW to be able to measure target range, the transmitted waveform needs to be modulated somehow. For example, Linear Frequency Modulation (LFM) can be used. In practical CW radars, the available bandwidth limits the continuously change of waveform in one direction. Hence, periodicity in the modulation has to be utilized. The modulation form can be triangular, sinusoidal, saw-tooth, or some other form. Figure 6 presents some examples of these modulation forms and their corresponding pulses.

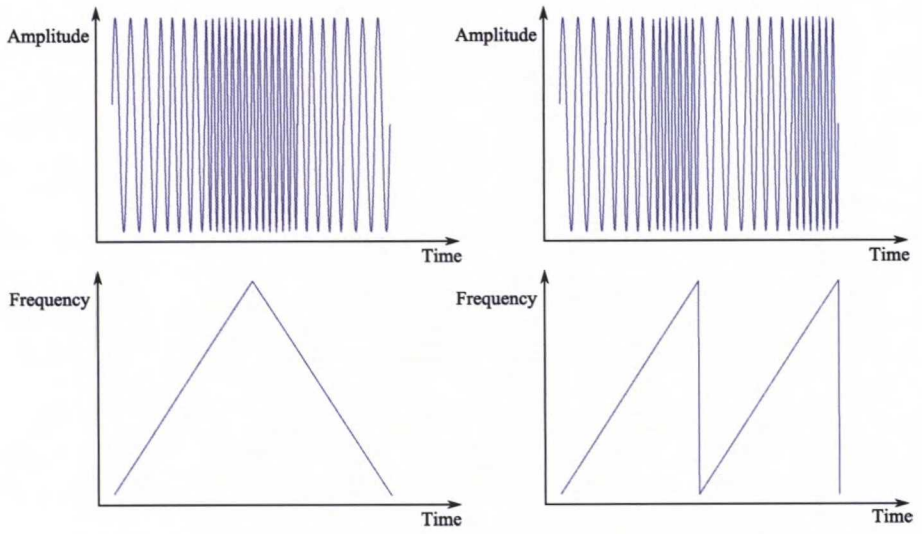

Figure 6: Triangle and saw-tooth modulation form

Due to heterodyning there will be a difference in frequency between the transmitted and received signals. This difference is defined as the beat frequency f_b [19]. Figure 7 presents the transmitted and received triangular LFM signals. The beat frequency is also pointed out.

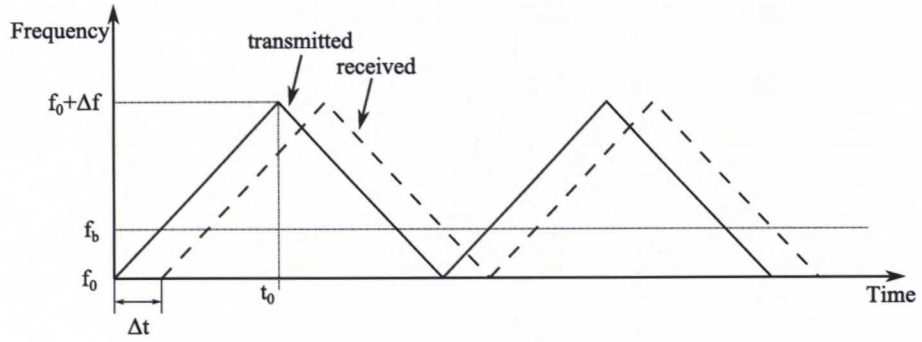

Figure 7: Triangular LFM pulses - received and transmitted [19]

The modulating frequency f_m is selected such that:

$$f_m = \frac{1}{2t_0}. \tag{37}$$

The rate of the frequency change is

$$\dot{f} = \frac{\Delta f}{t_0} = \frac{\Delta f}{(1/2f_m)} = 2f_m \Delta f, \tag{38}$$

where Δf is the peak frequency deviation. The beat frequency f_b is given by

$$f_b = \Delta t \dot{f} = \frac{2R}{c} \dot{f}, \tag{39}$$

which can be written as:

$$f_b = \frac{4Rf_m\Delta f}{c}. \tag{40}$$

If the radar is dealing with a moving target the beat frequency is defined as: $f_b = f_{received} - f_{transmitted}$. The received signal will contain a Doppler shift term in addition to the frequency shift due to time delay Δt. The Doppler shift term subtracts from the beat frequency during the positive slope and adds to it on the negative slope. Thus, the beat frequency on the positive slope f_{bu} and on the negative slope f_{bd} are:

$$f_{bu} = \frac{2R}{c}\dot{f} - \frac{2\dot{R}}{\lambda} \tag{41}$$

and

$$f_{bd} = \frac{2R}{c}\dot{f} + \frac{2\dot{R}}{\lambda}, \tag{42}$$

where $\dot{R}$ is the range rate or the target radial velocity as seen by the radar. From these two equations the range can be obtained as:

$$R = \frac{c}{4f}(f_{bu} + f_{bd}) \tag{43}$$

and the range rate as:

$$\dot{R} = \frac{\lambda}{4}(f_{bd} - f_{bu}). \tag{44}$$

Equations (43) and (44) show that CW radar with frequency modulation can extract both range and range rate information. In practice, the maximum delay time Δt is selected as $\Delta t_{max} = 0.1t_0$. Thus the maximum range is given by:

$$R_{max} = \frac{0.1ct_0}{2} = \frac{0.1c}{4f_m} \tag{45}$$

and the maximum unambiguous range will correspond to a shift equal to $2t_0$.

CW radars are not limited to LFM in order to obtain range information. A multiple frequency scheme allows CW radars to obtain range information as well [19]. In order to prove the ability of such radar to obtain range information, two CW signals are considered:

$$s_1(t) = A_1 \sin(2\pi f_1 t) \tag{46}$$

and

$$s_2(t) = A_2 \sin(2\pi f_2 t). \tag{47}$$

One example of two continuous signals of different frequencies and amplitudes are presented in Figure 8.

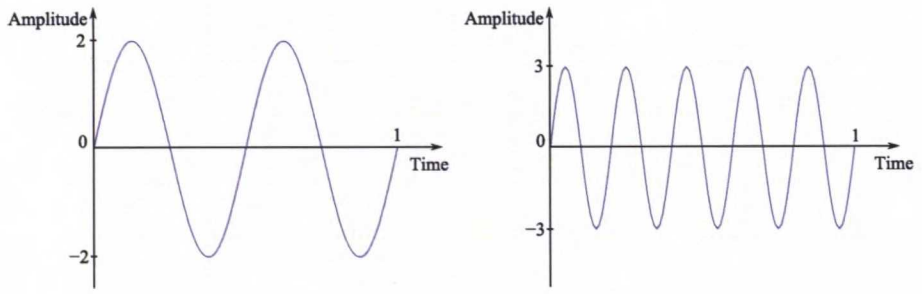

Figure 8: Example of two continuous signals with different frequencies and amplitudes

If these two signals are transmitted the received echoes will be:

$$s_{1r}(t) = A_{r1}\sin(2\pi f_1 t - \varphi_1) \tag{48}$$

and

$$s_{2r}(t) = A_{r2}\sin(2\pi f_2 t - \varphi_2), \tag{49}$$

where $\varphi_1 = \frac{4\pi f_1 R}{c}$ and $\varphi_2 = \frac{4\pi f_2 R}{c}$. After mixing with the carrier frequency, the phase difference between the two signals is:

$$\Delta\varphi = \varphi_2 - \varphi_1 = \frac{4\pi R}{c}(f_2 - f_1) = \frac{4\pi R}{c}\Delta f. \tag{50}$$

From the phase difference the range can be extracted as:

$$R = \frac{c\Delta\varphi}{4\pi\Delta f}, \tag{51}$$

which is maximum when $\Delta\varphi = 2\pi$. Thus, the maximum unambiguous range is [19]:

$$R = \frac{c}{2\Delta f}. \tag{52}$$

This equation shows that decreasing Δf increases the maximum range.

2.3.2 Pulsed Radar

The operating mode of a pulsed radar consists in the transmission of a train of modulated pulses and the reception of echoes as a train of pulses. The received echoes are processed in order to obtain range and Doppler information of the target. For range information the two-way time delay between transmitted and received pulses is utilized. For Doppler information there are two possibilities. First, if the range estimates between consecutive pulses is good enough, the range rate is utilized. Second, Doppler filter banks are utilized [19]. Pulsed radar waveforms can be completely defined by the following parameters:

- carrier frequency, which is chosen based on design requirements and radar purpose
- pulse width, which depends on the bandwidth and gives the radar range resolution
- modulation
- the pulse repetition frequency

The modulation techniques are chosen in order to improve the radar performance or enable capabilities. Choosing the PRF is done such as to avoid the Doppler and range ambiguities. Another consideration in choosing the PRF is the average transmitted power. The maximum range that can be detected depends on the amount of energy contained by the pulse. This energy is calculated as the peak transmitted power of the pulse multiplied by its width. Usually the power is measured over a longer period of time, which is longer than the pulse width. Thus, the average transmitted power is considered as a design parameter and not the peak transmitted power of one pulse.

In general, a radar can employ low, medium or high PRF, that bring their own advantages and disadvantages. For example, choosing a low PRF allows to unambiguous long range target detections, but has to deal with extreme Doppler ambiguities. A medium PRF deals with ambiguities in both range and Doppler, but provides a good level of average transmitted power. A high PRF provides a better level of average transmitted power and unambiguous Doppler, but it is extremely ambiguous in range. Radar systems utilizing high PRFs are often called Pulsed Doppler Radar (PDR). Distinction of a certain PRF as low, medium or high depends very much on the radar mode of operation [19].

It can be seen that the ambiguities in range or Doppler are the subject of a trade off in pulsed radar. Thus, the sources of these ambiguities need to be clear in order to design the best radar for a specific application. Range ambiguities occur when the echo arrives at the receiver after the PRI has passed. One or more pulses can be transmitted before the echo is received, so the radar thinks the echo belongs to the last transmitted pulse. This is called range aliasing and it means that the target has a range that exceeds the wavelength of the PRF. Doppler ambiguities occur when the Doppler frequency of a moving target exceeds the PRF.

To avoid Doppler ambiguities, radar systems require high PRF rates when detecting high speed targets. When a radar is required to detect a target situated at a long range, moving with high speed, it may not be possible to estimate both range and Doppler unambiguously. This problem can be solved using multiple PRFs. Multiple PRF schemes can be incorporated sequentially within each dwell interval or the radar can use single PRF in one scan and resolve ambiguity in the next. The latter technique may face problems due to changing target dynamics from one scan to the next [19].

The implementation of a two PRFs scheme is tested in order to see if it can solve the ambiguity problem stated above. The two PRFs are denoted as f_{r1} and

f_{r2} and the unambiguous corresponding ranges as R_{u1} and R_{u2}. These unambiguous ranges are relatively small and are shorter than the desired unambiguous range R_u ($R_u >> R_{u1}, R_{u2}$) corresponding to the desired PRF f_{rd}. Choosing the two PRFs is done such that the two are prime with respect to each other. This is in order to avoid obtaining the same aliases for specific ranges. If the true target range would be larger than both wavelengths of the PRFs, the alias would be the same. So it would not be possible to resolve the range ambiguity. One choice would be to select $f_{r1} = Nf_{rd}$ and $f_{r2} = (N+1)f_{rd}$ for some integer N. Within the desired PRI the range estimates for both PRFs would coincide at the true target position. This can be visualized in Figure 9. The time delays t_1 and t_2 correspond to the time between the transmit of a pulse on each PRF and the received echoes from the same pulse. The number of intervals between transmission of a pulse and reception of the true return for PRF1 and PRF2 respectively are denoted as M_1 and M_2. Before the true return is received, there are two possible situations $M_1 = M_2 = M$ or $M_1 + 1 = M_2$. The radar needs to measure only t_1 and t_2 [19].

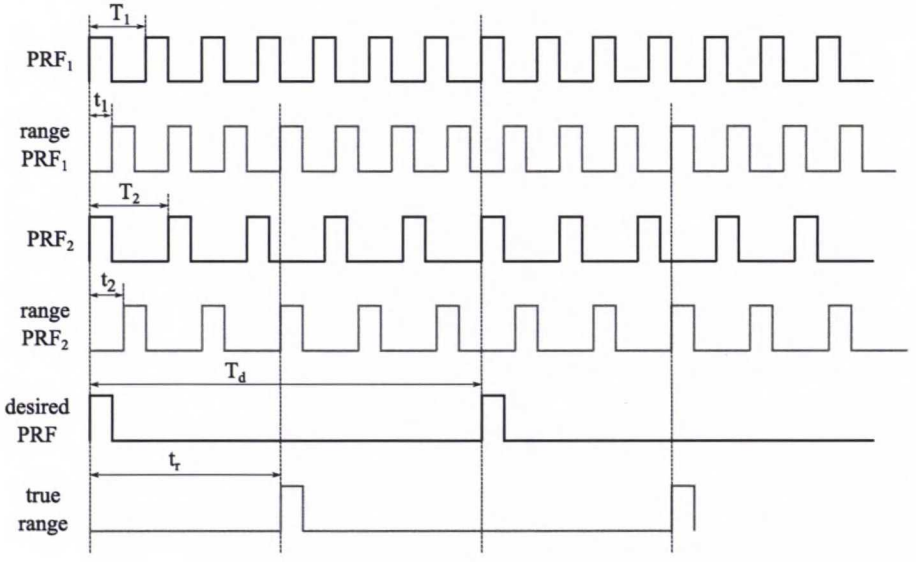

Figure 9: Resolving range ambiguity [19]

First it is considered that $t_1 < t_2$. In this case

$$t_1 + \frac{M}{f_{r1}} = t_2 + \frac{M}{f_{r2}}, \tag{53}$$

which means that

$$M = \frac{t_2 - t_1}{T_1 - T_2}, \tag{54}$$

where $T_1 = 1/f_{r1}$ and $T_2 = 1/f_{r2}$. It follows that the round trip time to the true target location is

$$t_r = MT_1 + t_1 = MT_2 + t_2 \tag{55}$$

and the true target range is:

$$R = \frac{ct_r}{2}. \tag{56}$$

When $t_1 > t_2$, the round-trip time to the true target location is

$$t_{r1} = MT_1 + t_1 \tag{57}$$

and the true target range is:

$$R = \frac{ct_{r1}}{2}. \tag{58}$$

Finally, if $t_1 = t_2$ then the true target range is:

$$R = \frac{ct_{r2}}{2}. \tag{59}$$

Since a pulse cannot be received while the following pulse is being transmitted, these transmission times correspond to blind ranges. This means that if the echo arrives at the radar when the transmission has started it will not be received. Consequently the target will not be detected. This problem can be solved by using a third PRF. Again, these have to be prime to each other.

For solving the Doppler ambiguity problem the same methodology can be used. In this case, the Doppler frequencies f_{d1} and f_{d2} are measured instead of t_1 and t_2. If $f_{d1} > f_{d2}$, then

$$M = \frac{(f_{d2} - f_{d1}) + f_{r2}}{f_{r1} - f_{r2}} \tag{60}$$

and if $f_{d1} < f_{d2}$, then

$$M = \frac{f_{d2} - f_{d1}}{f_{r1} - f_{r2}}. \tag{61}$$

Thus the true Doppler is:

$$\begin{aligned} f_d &= Mf_{r1} + f_{d1} \\ f_d &= Mf_{r2} + f_{d2}. \end{aligned} \tag{62}$$

Finally, if $f_{d1} = f_{d2}$, then

$$f_d = f_{d1} = f_{d2}. \tag{63}$$

When the Doppler frequency of the moving target is the same as the PRF the target appears to the radar as stationary. This is called blind Doppler. This can be resolved using a third PRF [19].

2.3.3 Pulse Compression Radar

Pulse compression is a technique that allows for better range resolution without sacrifice of the average transmitted power. Range resolution is improved if narrower pulses are utilized, but this has a bad impact on the average transmitted power. This affects the radar operation mode. In order to obtain a good level of average transmitted power the use of wider pulses is necessary. At the same time, a good level of average transmitted power is associated with a good SNR level at the receiver. The higher the SNR at the receiver the better the chances of target detection are. Hence, the purpose of pulse compression is to achieve the average transmitted power of a relatively long pulse and obtain the range resolution of a short pulse at the same time [19].

Pulse compression techniques can be classified into frequency and phase modulation methods. Phase modulation methods are further classified into binary and polyphase codes. Here are some examples of used compression techniques:

- Frequency modulation
  - Linear Frequency Modulation (LFM)
  - Non-Linear Frequency Modulation (NLFM)
  - Discrete frequency modulation (Costas-code)
- Binary phase codes
  - Barker-code
  - Minimum Peak Sequences (MPSs)
  - Pseudo Random Sequences (PRNs)
  - Quadratic Residue Sequences (QRSs)
  - Complementary codes
- Polyphase codes
  - Frank-code
  - P1–P4 codes

The bandwidth of the modulated pulse is larger compared to that of an unmodulated pulse with the same duration. The received echo is processed using a matched filter. The response of the matched filter is a narrow pulse with the mainlobe width of approximately $1/B$. The ratio of the transmitted pulse width to the compressed pulse mainlobe is defined as the pulse compression ratio. The pulse compression ratio is TB and is defined as the time bandwidth product of the waveform. The time bandwidth product for an unmodulated pulse approaches unity. Through the use of frequency modulation or phase modulation this product can be increased considerably [19, 27].

Ambiguity function is a tool widely used to evaluate the pulse compression techniques. It is a two dimensional function of time delay and Doppler frequency which shows the effect of the matched filter on the echo and the Doppler shift associated

with a moving target. Matched filter is a detector for known signals that maximizes the SNR at the output. The frequency response of the matched filter depends on the used waveform.

The linear frequency modulation waveform has a rectangular amplitude modulation with a pulse duration of T and a linear frequency modulation with a swept bandwidth B applied over the pulse [27]. Figure 10 presents an example of such waveforms. The change in frequency increases the pulse bandwidth and compression ratio.

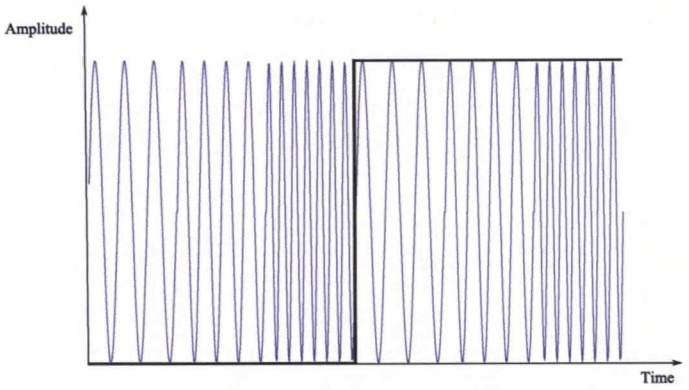

Figure 10: Linear Frequency Modulation pulses

The benefits of LFM include ease of generating such pulses as well as its robustness in the face of Doppler shifts because of its pulse shape and SNR. It also has its disadvantages, mainly because the instantaneous frequency changes linearly in time. As a result, it is hard to resolve between Doppler shift and delay in time domain if the differences are small. Also, LFM can employ weighting functions in order to lower the sidelobes. As a result there will be a SNR reduction.

Non-Linear Frequency Modulation (NLFM) brings few advantages over the LFM. First, there is no need for frequency weighting as the spectrum yields the required sidelobe level. This is achieved by increasing the rate of the frequency change near the ends of the pulse and decreasing it in the center. Thus, the loss in SNR does not take place here [27].

Discrete frequency modulation can be either linear or non-linear. One pulse is divided into a number of subpulses and for each subpulse a different frequency is used. From subpulse to subpulse, the frequency can be changed in a linear or a non-linear manner. The so-called Costas-codes are considered a class of frequency-coded waveforms. The ambiguity function of such waveform approaches the ideal thumbtack. Costas codes can be obtain by following the steps [11]:

1. Choose the number of subpulses as $N = q - 1$, where q is a prime number.
2. Let γ a primitive root of q, i.e. numbers $\gamma, \gamma^2, \gamma^3, \ldots, \gamma^{q-1}$ mod q generate all integer numbers from the interval $1 \ldots q - 1$.
3. Number of rows of $N \times N$-matrix as $i = 1 \ldots q - 1$ and the columns as $j = 0 \ldots q - 2$.

4. Choose the frequency $f_i = f_0 + i\Delta f$ for subpulse j if and only if $i = \gamma^j \mod q$.

A new Costas code is obtained by removing the first row and column of the matrix obtained by the above mentioned procedure. Table 3 illustrates the Costas codes for six subpulses, where the primitive root is $\gamma = 3$.

	0	1	2	3	4	5
1	×					
2			×			
3		×				
4					×	
5						×
6				×		

Table 3: Costas-code for six subpulses

It is known that there are $N = 6$ pulses and the primitive root is $\gamma = 3$. Thus, according to step 1, $q = 7$ and for every $j = 0 \ldots q-1$ $\gamma^j \mod q$ is calculated. In this case the results are $1, 3, 2, 6, 4, 5$. Step 4 is applied and Table 3 can be obtained. If another primitive root is chosen, for example $\gamma = 2$, the costas code would have different frequencies.

A phase coded waveform contains pulses that are divided into a number of subpulses. These waveforms are characterized by the phase modulation applied to each subpulse. A phase code can be either binary or polyphase. A binary code contains only two phase values of 0 or π radians. It can also be defined by a sequence of 0 and 1 or a sequence of $+1$ and -1. These are only different notations of the same codes. A well known binary phase code is Barker code that has a maximum autocorrelation of 1 when codes are not aligned. The compression rate is equal to the length of the code, which is maximum of 13 for Barker. All known barker codes are shown in Table 4 [18, 2].

Length N	**Subpulse phases**
2	$+-$
	$++$
3	$++-$
4	$++-+$
	$+++-$
5	$+++-+$
7	$+++--+-$
11	$+++---+--+-$
13	$++++$

Table 4: Known Barker codes

Each code can be given negated, reversed or both. In order to obtain larger codes, different Barker codes can be combined. For example, one can combine codes with

$N = 5$ and $N = 4$ to find a code with $N = 20$: $\{++++-+, +++--+, ----+-, +++-+-+\}$. When using this type of codes the sidelobe levels are not unity anymore.

The number of optimal binary codes is limited. So it would be preferable to find codes with best autocorrelation properties for the code length. These are called Minimum Peak Sidelobe (MPS) codes [22, 27]. The maximum code length that gives minimum sidelobe levels is 48. Maximum sidelobe level for autocorrelation function is 3 for these codes. Some examples of MPS codes are presented in Table 5.

Length N	**Sidelobe level**	**Subpulse phases**
8	2	+−−+−+++
12	2	+−−++−+−++++
17	2	−−+++−+++−+−−+−++
22	3	−−+++−−++−++−+−+−++++
28	2	+−−−+++−−−+−−−+−−−+−−+−++−+
30	3	+−−−++−−−+−+−+−−+−−+−−−−−−++++

Table 5: Examples of MPS codes

Pseudo Random Codes (PRCs) are binary codes that have similar properties to completely random binary sequences. They are also called maximum-length sequences or M-sequences [27]. Random sequences are characterized by the following properties:

1. The number of + and − in the sequence is almost equal.
2. If one takes a look at the runs of + and −, the length of such runs is equal to 1 in half cases, 2 in 1/2 cases, 3 in 1/8 and so on.
3. Autocorrelation function has a peak in the middle and otherwise it approaches zero.

Maximum Length Sequences (MLSs) are generated using shift registers and modulo 2 adders with appropriate feedback loops. They are periodic sequences of period $2^n - 1$, where $n \in \mathbb{N}$ is the length of the shift register. In practice these sequences are truncated and this leads to increased sidelobe levels. An important property of MLS codes is that a new, shifted version of the original code can be obtained if a shifted version is modulo 2 summed with the original code [27].

Gold codes can be generated using two MLS codes [9]. By choosing the right codes one can achieve desired correlation properties. A Gold code is obtained by modulo 2 summing the bits of selected MLS codes. A new code is always obtained by shifting one of the codes with respect to the other.

In a polyphase code each pulse is divided into subpulses and each subpulse phase can get many different values, not just 0 and π like in binary codes. Polyphase codes are complex sequences whose elements have a magnitude of one, but with variable phase [27]. In a Frank code, the pulse is first divided into N groups and then each group into N subpulses. The phase Φ_{ji} of the subpulse i in group j is selected as follows [27]:

$$\Phi_{ji} = \frac{2\pi}{N}(i-1)(j-1).$$

Frank code is based on quantized discrete frequency modulation. Commonly, Frank codes are represented in matrix form where the rows correspond to groups and columns correspond to subpulses. As an example, the code matrix of 5 phase Frank code is obtained as follows:

$$\Phi = \begin{bmatrix} 0 & 0 & 0 & 0 & 0 \\ 0 & \frac{2\pi}{5} & \frac{4\pi}{5} & \frac{6\pi}{5} & \frac{8\pi}{5} \\ 0 & \frac{4\pi}{5} & \frac{8\pi}{5} & \frac{2\pi}{5} & \frac{6\pi}{5} \\ 0 & \frac{6\pi}{5} & \frac{2\pi}{5} & \frac{8\pi}{5} & \frac{4\pi}{5} \\ 0 & \frac{8\pi}{5} & \frac{6\pi}{5} & \frac{4\pi}{5} & \frac{2\pi}{5} \end{bmatrix}.$$

The most significant phase changes in a Frank code take place in the middle of the pulse. This may be a drawback especially if there is a need to low-pass filter the signal in order to attenuate noise. So the middle of the pulse is attenuated the most.

Another class of codes has been developed to reduce the problems caused by Frank codes. These codes are called $P1$ and they present large changes in phase in the beginning and end of the code. The matrix used to form these codes is defined by [27]:

$$\Phi_{ji} = -\frac{\pi}{N}[N-(2j-1)][(j-1)N+(i-1)].$$

It can be seen from the matrix that the phases are the same as in the case of Frank codes, but the ordering of the row has changed. This is valid for all odd values of N. The matrix associated with 5-phase $P1$ codes is:

$$\Phi = \begin{bmatrix} 0 & \frac{6\pi}{5} & \frac{2\pi}{5} & \frac{8\pi}{5} & \frac{4\pi}{5} \\ 0 & \frac{8\pi}{5} & \frac{6\pi}{5} & \frac{4\pi}{5} & \frac{2\pi}{5} \\ 0 & 0 & 0 & 0 & 0 \\ 0 & \frac{2\pi}{5} & \frac{4\pi}{5} & \frac{6\pi}{5} & \frac{8\pi}{5} \\ 0 & \frac{4\pi}{5} & \frac{8\pi}{5} & \frac{2\pi}{5} & \frac{6\pi}{5} \end{bmatrix}.$$

$P2$ codes will produce low sidelobe level when N is even. The subpulse phases are obtained from the following matrix [27]:

$$\Phi_{ji} = \left[\frac{\pi}{2}\frac{N-1}{N} - \frac{\pi}{N}(i-1)\right](N+i-2j).$$

The matrix associated with $P2$ codes with $N=4$ is:

$$\Phi = \begin{bmatrix} \frac{9\pi}{8} & \frac{3\pi}{8} & \frac{-3\pi}{8} & \frac{-9\pi}{8} \\ \frac{3\pi}{8} & \frac{\pi}{8} & \frac{-\pi}{8} & \frac{-3\pi}{8} \\ \frac{-3\pi}{8} & \frac{-\pi}{8} & \frac{\pi}{8} & \frac{3\pi}{8} \\ \frac{-9\pi}{8} & \frac{-3\pi}{8} & \frac{3\pi}{8} & \frac{9\pi}{8} \end{bmatrix}.$$

$P2$ codes have the property that they are symmetric about the zero phase. Moreover, the code is palindromic, i.e. is the same when read in reverse order.

Two other codes called $P3$ and $P4$ are based on quantized linear frequency modulation. These codes are more robust against Doppler and have lower sidelobes, compared to the previous codes. These codes are given using phase vectors. In case of $P3$ code, the vector can be written as [27]:

$$\phi_i = \frac{\pi}{N^2}(i-1)^2.$$

In case of code length $N^2 = 16$, the $P3$ code is:

$$\boldsymbol{\phi} = \left[0, \frac{\pi}{16}, \frac{4\pi}{16}, \frac{9\pi}{16}, \pi, \frac{25\pi}{16}, \frac{4\pi}{16}, \frac{17\pi}{16}, 0, \frac{17\pi}{16}, \frac{4\pi}{16}, \frac{25\pi}{16}, \pi, \frac{9\pi}{16}, \frac{4\pi}{16}, \frac{\pi}{16}\right].$$

The phase vector for $P4$ code is [27]:

$$\phi_i = \frac{\pi}{N^2}(i-1)^2 - \pi(i-1).$$

In the case of sixteen subpulses $P4$ is:

$$\boldsymbol{\phi} = \left[0, \frac{17\pi}{16}, \frac{4\pi}{16}, \frac{25\pi}{16}, \pi, \frac{9\pi}{16}, \frac{4\pi}{16}, \frac{\pi}{16}, 0, \frac{\pi}{16}, \frac{4\pi}{16}, \frac{9\pi}{16}, \pi, \frac{25\pi}{16}, \frac{4\pi}{16}, \frac{17\pi}{16}\right].$$

3 Multicarrier radar

3.1 Motivation

The idea of multicarrier data transmission was introduced in 1960's [23, 35] but it raised significant interest in 1980's [5]. The increased interest was facilitated by the progress in digital circuit technology as well as single and multi-user communication systems. Wireless MC systems utilize multiple complex exponentials as information-bearing carriers. Nowadays, MC systems such as OFDM are included in the digital television systems (DVB [25]), digital radio systems (DAB [30]), local area mobile wireless networks (WLAN [6, 33]), wireless communications (WiMAX [8]) and cellular communications (LTE [12]) [34].

Multicarrier systems that employ spread spectrum have been proposed and are known as OFDM, Multicarrier CDMA (MC-CDMA), Multicarrier Direct Sequence CDMA (MC-DS-CDMA), Multitone CDMA (MT-CDMA) and others [7, 34]. A block diagram for multicarrier transmitter and receiver, employing OFDM modulation, is presented in Figure 11.

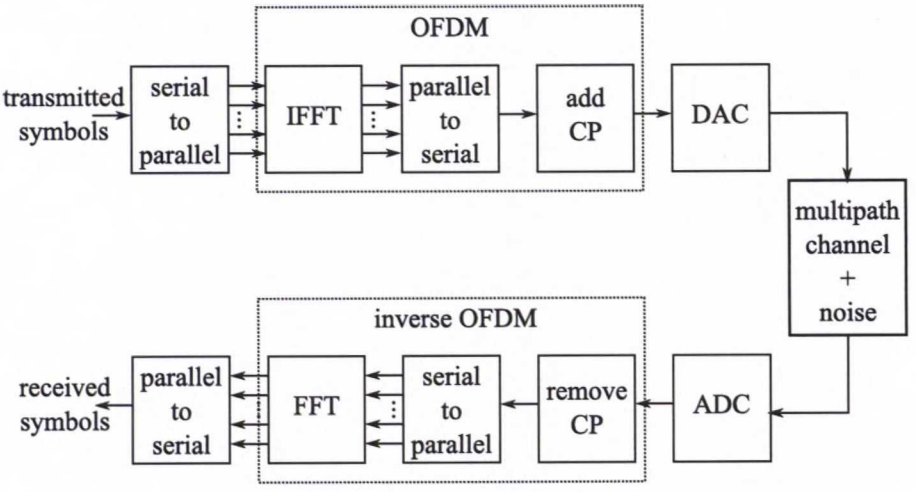

Figure 11: Transmitter and receiver block diagram employing OFDM

Multicarrier systems that have orthogonal subcarriers transmit information in symbols obtained through Inverse Fast Fourier Transform (IFFT). When their transmitted symbols propagate through Linear Time-Invariant (LTI) multipath channels, they experience Inter-Symbol Interference (ISI). This is because the underlying channel's impulse response combines contributions from more than one transmitted symbol at the receiver. To account for ISI, MC systems utilize a Cyclic Prefix (CP). This is redundant information obtained by replicating at the beginning of the symbol the ending part of the symbol. To remove ISI, the redundant part of the symbols is chosen greater than the channel length and is discarded at the receivers [34].

OFDM is the most commonly used multiplexing technique nowadays. It brings many great advantages such as high spectral efficiency, robustness against ISI and multipath propagation fading, efficient implementation and many others. In com-

munications, the major benefit is that the broadband channel is turned into many narrowband channels. This makes the implementation very attractive because each channel needs only one tap equalizer at the receiver. OFDM has some drawbacks also. Few of these are: sensitivity to Doppler shifts, loss of efficiency, caused by the use of CP, and high levels of Peak-to-Average Power Ratio (PAPR) caused by the varying envelope.

As in communication systems, multicarrier waveforms bring several major advantages over single carrier waveforms in radar systems, too. One of the major advantages, if not the most significant, is frequency diversity. As many carrier frequencies are available at the same time, it is easy to overcome problems like jamming, interference or attenuation by allocating power to subcarriers where the channel quality is high. These are very important aspects of radar that have to be taken into account when designing the utilized waveform and allocating power to different subcarriers. In the case of jamming, the multicarrier waveform forces the jammer to spread its power in a wide bandwidth of frequencies, thus being less efficient. Having multiple frequencies it is likely that not all will be equally attenuated or interfered at the same time, so most probably some of the frequencies will operate at a good level of performance. In the case of unintentional interference or attenuation, the power resources could be reallocated to the frequencies that are less affected, thus a better resource allocation for multicarrier waveforms.

A great advantage that multicarrier waveforms bring to radar is that the time on target is greatly reduced. Only one pulse is required to obtain range and Doppler information. Another advantage is the waveform diversity. Designing the waveforms both in time and frequency brings in additional degrees of freedom. Last but not least, the possibility to optimize the transmitted waveform is important for radar systems. Traditionally, only the receiver has been adaptive and optimized in radars. The hardware requirements are very similar to those in commercial communication systems which facilitates cost efficient implementation of multicarrier radars.

Of course, multicarrier systems have their disadvantages, too. The most significant is the time-varying envelope, i.e. the transmitted signal does not have a constant modulus. Multicarrier radar is subject to this problem as well. However, plenty of research has been done to mitigate this problem [15, 17, 21, 22].

Common multicarrier radar signal models employ OFDM [14, 13, 20, 26]. A special type of OFDM radar signals employ MCPC pulses [16, 15, 22]. In the following, these two signal models are described in more detail using chronological order.

3.2 Multi-Carrier Phase Coded pulses in Radar

The MCPC signal model is proposed by Levanon in [15, 16, 17, 21, 22]. A multifrequency radar signal is introduced, where each subcarrier is modulated by a code sequence of a specific length. The carriers have equal spacing in frequency domain. This carrier spacing is chosen such that the subcarriers are orthogonal to each other. Similar principle is used in OFDM-based communication systems. Figure 12 presents how an MCPC pulse is obtained. Each subcarrier is modulated by a code of length M. In this example, the codes that modulate the subcarriers are cyclic

shifts of each other.

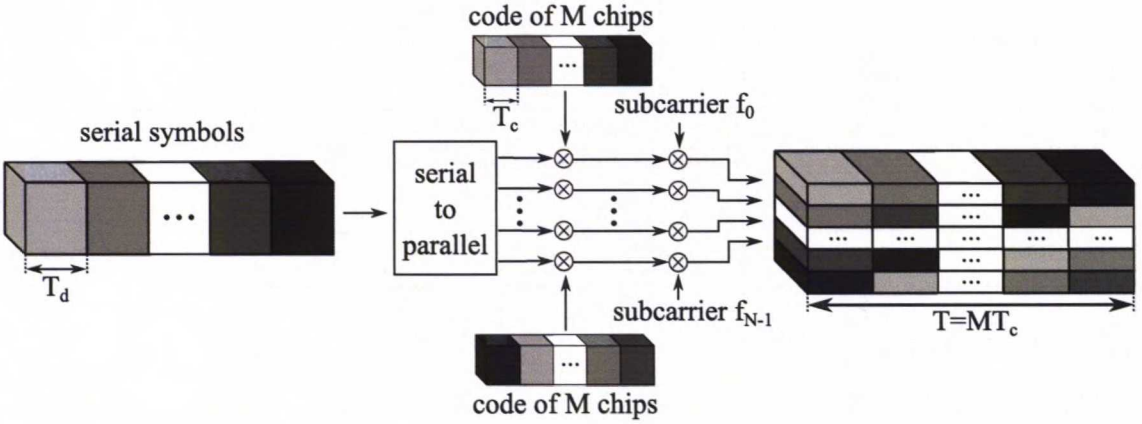

Figure 12: Generation of a $N \times M$ MCPC pulse

In Figure 13 the matrix of codes that modulate the subcarriers is presented together with the spectrum of the pulse.

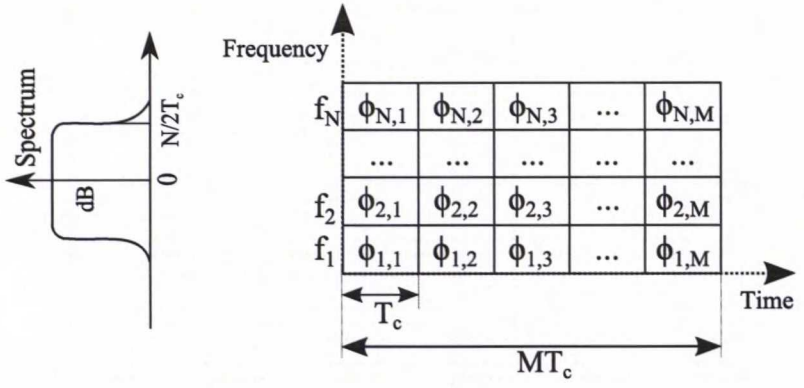

Figure 13: Scheme of a $N \times M$ MCPC pulse and its spectrum [15]

The modulating sequences on each subcarrier, denoted as $\boldsymbol{\phi}_n = [\phi_{n,1}\phi_{n,2} \ldots \phi_{n,M}]$, where n is the subcarrier index, were first considered to be $P3$ and $P4$ pulse compression codes [16, 15]. These code sequences are ideal sequences and represent the samples of a discretized analog LFM signal. An ideal sequence is a sequence that has zero autocorrelation sidelobes. The modulating sequences $\boldsymbol{\phi}_n$ can be identical on each subcarrier or can be different cyclic shifts of the same sequence. For example, Table 6 shows how a number of M different sequences can be obtained from an ideal sequence by using cyclic shifts. The first sequence is the ideal sequence and the rest of the sequences are cyclic shifted versions of the previous one. All these sequences form a complementary set. This is based on Popovic's theorem in [24] which states that if the sequences in the set are all the different cyclic time shifted versions of an ideal sequence, the set is complementary. A complementary set achieves the same low autocorrelation sidelobes as an ideal sequence. This is the reason for which the use of such set in a MCPC pulse is desirable.

Sequence Number	Sequence
1	$\phi_1 \quad \phi_2 \quad \cdots \quad \phi_k \quad \phi_{k+1} \quad \cdots \quad \phi_{M-1} \quad \phi_M$
2	$\phi_2 \quad \phi_3 \quad \cdots \quad \phi_k \quad \phi_{k+1} \quad \cdots \quad \phi_M \quad \phi_1$
$\vdots$	
k	$\phi_k \quad \phi_{k+1} \quad \cdots \quad \phi_M \quad \phi_1 \quad \cdots \quad \phi_{k-2} \quad \phi_{k-1}$
$\vdots$	
M-1	$\phi_{M-1} \quad \phi_M \quad \cdots \quad \phi_k \quad \phi_{k+1} \quad \cdots \quad \phi_{M-3} \quad \phi_{M-2}$
M	$\phi_M \quad \phi_1 \quad \cdots \quad \phi_k \quad \phi_{k+1} \quad \cdots \quad \phi_{M-2} \quad \phi_{M-1}$

Table 6: Complementary set of phase coded sequences

The example in Table 6 is valid as a complementary set because the number of sequences is equal to the number of the code elements in the ideal sequence ($N = M$). When the set does not contain all the different cyclic shifts of the ideal sequence ($N \neq M$), the set is complementary only if the following definition is met: *A complex valued sequence X_i, whose kth element is $x_i(k)$, forms a complementary set if the sum of the aperiodic autocorrelation functions of all sequences from the set is equal to zero for all non-zero shifts* [24]. This can be mathematically stated as:

$$Z(p) = \sum_{i=0}^{M-1} \sum_{k=0}^{M-1-p} x_i(k) x_i^*(k+p) = \begin{cases} \sum_{i=0}^{M-1} R_i(0), & p = 0 \\ 0, & p \neq 0 \end{cases}, \tag{64}$$

where * denotes the complex conjugate, p is the positive time shift and $R_i(0)$ is the energy of the sequence X_i [24].

Other codes are proposed in [15]. These codes are based on Barker codes that also have ideal periodic autocorrelation function. While a Barker code has two phases 0° and 180°, the proposed codes have phases 0° and 138.59°(= $\arccos(-3/4)$) [10]. The phases are chosen such that the out of phase autocorrelation is zero. The different ways of achieving this are presented in [10].

The complex envelope of a $N \times M$ MCPC is given by [22]:

$$g(t) = \sum_{n=1}^{N} \sum_{m=1}^{M} w_n a_{n,m} s[t - (m-1)T_c] \exp\left[2\pi j \left(n - \frac{N+1}{2}\right) \frac{t}{T_c}\right], \quad 0 \leq t \leq MT_c \tag{65}$$

where $a_{n,m}$ is the mth element of the sequence modulating the nth subcarrier, w_n is the complex weight associated with the nth subcarrier and $s(t) \equiv 1$ for $0 \leq t \leq T_c$ and zero elsewhere. The overall duration of such MCPC pulse is MT_c, if the modulating code sequence has M components. The duration of one code component or phase element is T_c. In order to have orthogonality between the subcarriers the intercarrier spacing has to be $1/T_c$. In a system with N subcarriers the effective bandwidth is N/T_c (without weighting). As can be seen in Figure 13, the spectrum of a MCPC pulse is relatively flat.

The autocorrelation main lobe width of such signal is T_c/M. Figure 14 presents the autocorrelation plot for a 8×8 MCPC pulse.

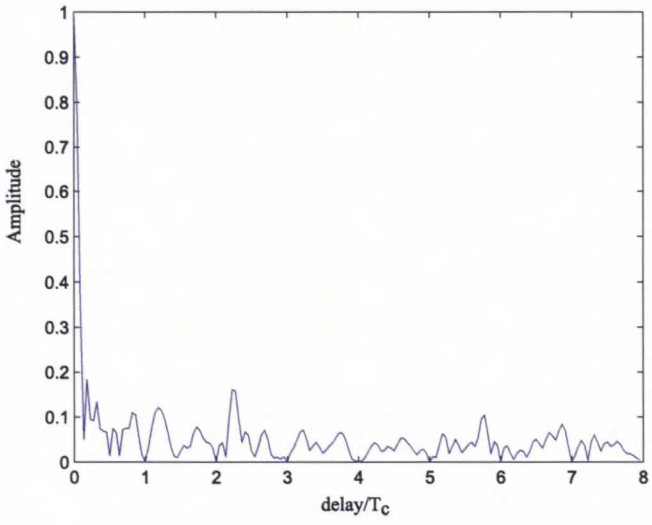

Figure 14: Autocorrelation of a 8×8 MCPC pulse based on $P3$ sequence

The main lobe width is comparable to the main lobe width of a single-frequency pulse-compression radar signal, for example $P4$ waveform with M^2 elements and the same overall pulse duration [16, 15]. Also the nulls at multiples of phase element duration T_c can be observed in Figure 14. These are a result of the orthogonality of the subcarriers with $1/T_c$ spacing and the utilized complementary set.

The major drawback of a MCPC signal is its varying envelope. This is a common characteristic of multicarrier systems in general and the MCPC signal makes no exception. Usually, the interest lies in knowing the Peak-to-Average Power Ratio (PAPR) level, which can be lower than Peak-to-Mean Envelope Power Ratio (PMEPR) level. The difference between the two is that the PAPR is used when the signal is passband, while the PMEPR is used when the signal is baseband. However, for low-bandwidth signals ($f_c \gg N/T_c$) the PMEPR is a good approximation of PAPR [22]. The performance of radars using MCPC signals can be improved by controlling the PMEPR. Two solutions are proposed for this. One is based on the use of so called Consecutive Ordered Cyclic Shifts (COCSs) of an ideal sequence [15, 17, 22] and the other is based on the use of Identical Sequences (ISs) [21, 22]. These two methods of lowering the PMEPR are presented next in more detail.

The first method uses as modulating sequence for each subcarrier consecutive order cyclic shifts of an ideal code sequence. This can be any ideal code sequence, but commonly the ideal $P3$ and $P4$ sequences are used. The PMEPR level depends on the variant of the ideal sequence used, direction of the consecutive order cyclic shift (upward or downward) and the initial phase (or cyclic shift) of the ideal sequence [22]. It also depends on the relation between N and M. When $N = M$, the N sequences form a complementary set. The best results are obtained when a $P4$ sequence is used, whith a PMEPR level that aproaches 1.825, for large values of N and M. Still, for $N = M > 4$, the PMEPR level is lower than 2.04 [22]. Similar results are reported by Boyd in [3] when using cyclic shifts of a $P3$ sequence. These are called Newmann phases in [3]. When $N \neq M$, the PMEPR has lower level for

$N \cong M$ in general than for $N \ll M$ or $N \gg M$. On the other hand, if N is low, the PMEPR level can be even lower than when $N = M$. If amplitude modulation is introduced on the carriers, the PMEPR level can be further reduced. When $N = M$, the PMEPR level can be as low as 1.5 [22].

The second method uses the same sequence to modulate all subcarriers. When using identical sequences, the magnitude of the complex envelope is a function of only the carriers' initial phase and amplitude. So, minimizing the PMEPR in this case becomes a problem of minimizing the PMEPR of a multitone signal. The complex envelope of a single MCPC pulse where all N carriers are modulated by the same sequence is obtained from (65):

$$g(t) = \sum_{n=1}^{N} \sum_{m=1}^{M} w_n a_m s[t - (m-1)T_c] \exp\left[2\pi j \left(n - \frac{N+1}{2}\right) \frac{t}{T_c}\right], \quad 0 \leq t \leq MT_c \tag{66}$$

where a_m is the mth element of the sequence modulating all carriers [21, 22].

Closed form solutions of carrier initial phase that lower the level of PMEPR are given in [21, 22]. These closed form solutions can be found for any N, but they do not always offer the best possible level of PMEPR. A carrier phasing scheme that takes into account carrier weighting achieves a PMEPR of 1.55 in an example presented in [22]. The example is for a 15 carrier setup with amplitude modulation over the carriers that follow a square root of Hamming window rule. Further reduction of PMEPR is possible through iterative algorithms. An example of such algorithm is the time-frequency switching and clipping approach described in [32]. This offers a PMEPR level of 1.22 for an example presented in [22]. More such iterative algorithms are presented in [21] which offer even lower PMEPR levels.

The radar performance in Doppler estimation is related to the duration of time the target is illuminated. The duration of one MCPC pulse might not be enough for Doppler processing so the use of multiple pulses can solve this problems. The use of multiple pulses is divided in two categories. In the first category the MCPC pulses are transmitted in a continuous manner, with no time separation between the pulses. Such type of signal is called CW MCPC signal. In the second category there is a constant time interval between the MCPC pulses. This is called train of diverse MCPC pulses. These two categories are presented in Figure 15. Each MCPC pulse in a CW signal is considered to be a period of the signal. This period repeats itself, so the autocorrelation function of such signal is called Periodic Autocorrelation Function (PACF). For example, in Figure 15, there are 6 visible periods of the signal. Different complementary sets modulate the MCPC pulses in a CW signal or train of pulses. These can be Identical Complementary Sets (ICSs), when the same ideal sequence modulates all subcarriers, or COCS of an ideal sequence [15, 17, 21, 22]. However, for the train of pulses only, there is another type of sets called Mutually Orthogonal Complementary Sets (MOCSs) [21, 22]. Two sets are mutually orthogonal when the sum of the cross-correlation between the sequences in one complementary set with the corresponding sequences in the second set is zero for all shifts [22]. For the CW signal, the N sequences modulating the subcarriers

do not have to constitute a complementary set. This allows repeating the same sequence at several carriers. The only constraint is that the product $M(N+1)$ must be even [17].

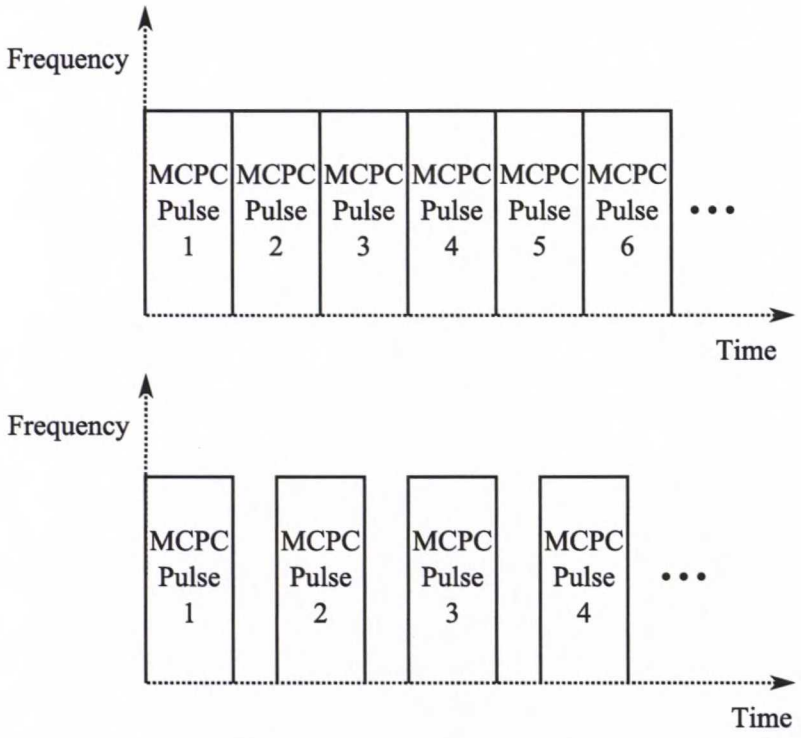

Figure 15: CW multicarrier signal and train of MCPC pulses

A train of M MCPC pulses of dimension $M \times M$ can be complementary in time as well as in frequency [17]. This happens when each pulse in the train is a different one-way cyclic frequency shift of the pulse. For example, one cyclic shift is used to generate the first pulse, two shifts create the fifth pulse and so on. There are $M!$ different ways to order the basic pulse along frequencies, and for each choice of a basic pulse there are $M!$ different ways to order the pulses in time.

Efforts for both CW and train of pulses aim at the reduction of PMEPR and Peak Sidelobe Level (PSLL) of the autocorrelation function. The reduction methods for one pulse are also proposed for these two types of signals. Examples of how desirable levels for PMEPR and PSLL can be achieved are presented in [17, 21, 22] and are not discussed here in more detail. Few observations are made though.

In the CW case, the PACF is independent of the type of used sequence as long as the sequence is ideal. This happens when using either ICS or COCS [21, 22]. However, when using COCS the signal magnitude depends on the type of sequence used. Choosing ICS, the PACF exhibits zero sidelobes over the delay range $T_c < \tau < (M-1)T_c$, i.e. everywhere except the first and the last code bit. In order to reduce the PACF's sidelobes in the remaining first and last bit, the polarity of the weights should alternate between consecutive carriers.

For a train of pulses the use of COCS implies a reduction of the PSLL on the

duration $T_c < \tau < MT_c$ (the autocorrelation function is considered for the duration of one pulse only). For the rest of the pulse duration, the use of COCS is combined with the use of frequency weighting. The use of frequency weighting is presented in [15, 17, 22] where it is shown that the reduction is valid for the duration of the first bit only $\tau < T_c$. Different windows like general cosine window, Kaiser window and the Chebyshev family of windows are considered in [15, 17, 22].

3.3 OFDM in Radar

Orthogonal Frequency Division Multiplexing (OFDM) is used in many widely used and emerging wireless communication standards such as LTE, WiMAX and WLAN. The OFDM signal structure is very similar to the structure of the MCPC signal that was presented earlier. In fact, the MCPC signal is a particular case of OFDM. The MCPC signal is obtained when coding is applied on each subcarrier of an OFDM signal without the loss of orthogonality. The spectrum of an OFDM signal with N subcarriers can be visualized in Figure 16. The spectrum is relatively flat and the subcarriers are orthogonal to each other.

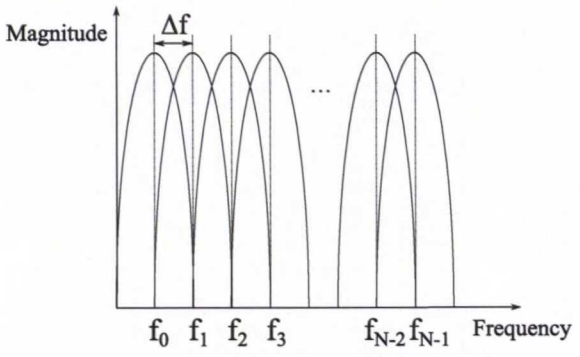

Figure 16: Spectrum of an OFDM symbol

The OFDM modulation is a multicarrier modulation technique that satisfies the orthogonality condition between the subcarriers. Figure 17 presents an example of multicarrier modulation with N subcarriers. The orthogonality condition is satisfied when $\Delta f = 1/T_s$, where Δf is the intercarrier spacing and T_s is the OFDM symbol duration. The OFDM modulation can be implemented very easily by using the IFFT operation.

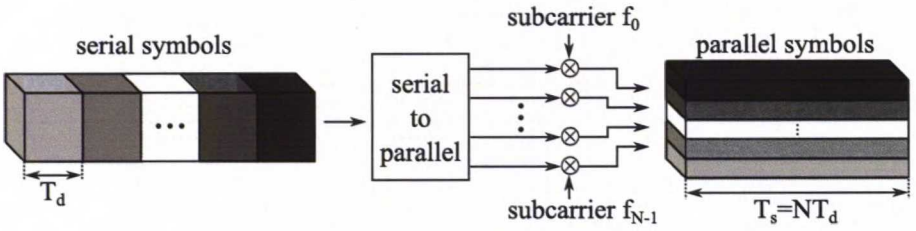

Figure 17: Multicarrier modulation with N subcarriers

The duration of an OFDM symbol is $T_s = NT_d$, where T_d is the duration of a serial symbol. The complex envelope of an OFDM symbol is described by the equation:

$$x(t) = \text{rect}(t) \sum_{n=0}^{N-1} d_n \exp(j2\pi f_n t), \tag{67}$$

where d_n represents the source symbol on the nth subcarrier and f_n are obtained from:

$$f_n = \frac{n}{T_s} = n\Delta f. \tag{68}$$

The rect(t) function is defined as:

$$\text{rect}(t) = \begin{cases} 1 & \text{if } 0 \leq t \leq T_s \\ 0 & \text{elsewhere} \end{cases} \tag{69}$$

and has the purpose to limit the duration of one symbol.

In order to avoid the ISI, at OFDM receiver, a Cyclic Prefix (CP) can be added to the beginning of the symbol. This represents a copy of the ending part of the OFDM symbol and can have different length. Its length is chosen to be larger than the maximum delay in the channel. The resulting OFDM symbol duration becomes $T_s' = T_s + T_{CP}$, where T_{CP} is the length of the CP.

The success of OFDM in communication systems has motivated for applications in radar [14]. Several waveform designs are proposed for OFDM radar signals in the literature. The first proposed design is a pulse-to-pulse agile waveform that allows for Doppler processing [14]. Pulse-to-pulse frequency agility or frequency hopping forces the jammer to spread its power over a wide bandwidth. This leads to the reduction of the jammer's power density that the radar has to face. Frequency agility is easy to be implemented for MC waveforms due to its structure which is a linear combination of narrowband signals [14]. In order to generate agile patterns based on OFDM, IFFT is applied over a phase code matrix. When this matrix contains a null, then the respective subcarrier/chip pair is inactive [14]. This is visualized in Figure 18 where two pulses of a train are illustrated. The first one has half of the subcarriers inactive and the second one has the other half of the subcarriers inactive. Each of the pulse resembles the structure of a MCPC pulse where the subcarriers are code modulated. Each subcarrier is represented by a row of chips which are marked by different colours.

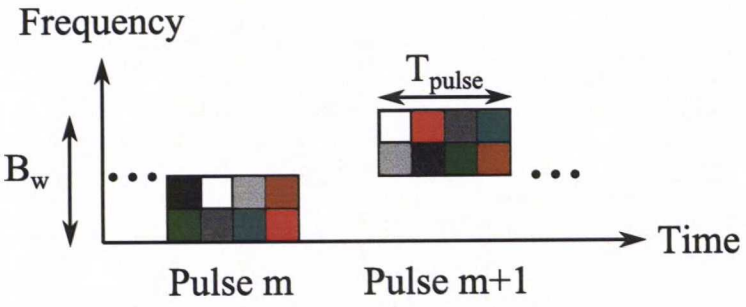

Figure 18: Train of frequency agile pulses where the mth pulse has half of the subcarriers inactive and the $m+1$th pulse has the other half of subcarriers inactive [14]

This simple example can be extended such that more complex patterns are generated. For example, the available bandwidth can be divided in more than two groups and these groups can hop randomly over the available bandwidth [14]. Also individual subcarriers can hop randomly over the available bandwidth and be inactive at different time instances [14].

For the waveform proposed in [14], Doppler processing techniques are investigated in [13]. The chosen processing techniques are based on classical matched filter and Fast Fourier Transform (FFT) approach. Another Doppler processing method is also proposed in [14] and mentioned in [13]. This method first transforms the received OFDM symbols from frequency to time domain by using FFT and then observes the same subcarrier over a number of symbols. The Doppler frequency is obtained by using another FFT operation over the observations in the considered pulses. The signals considered in [14, 13] are all wideband. This means that the Doppler effect is considered to be different for each individual subcarrier.

Another waveform design is proposed in [26] where the emphasis is on the scattering parameters of the target. It is shown that taking target properties into consideration the waveform can be adaptively computed in order to obtain the desired ambiguity function. The signal considered in [26] is wideband and for its performance analysis the Wideband Ambiguity Function (WAF) is utilized. A different coefficient is considered for every direction and/or frequency in [26]. The adaptive design of OFDM signal emphasizes that the received signal and hence the corresponding WAF at the output of the matched filter depend on the scattering parameters of the target. It is also shown in [26] that in order to obtain the desired ambiguity function, carrier weights have to be taken into account. The results show that for best performance the sum of the complex weights over different subcarriers has to be 1 ($\sum_{n=0}^{N-1} |w_n|^2 = 1$, where w_n is the weight of the nth subcarrier) [26].

A technique to resolve range and radial velocity information, that is independent of the phase coding, is proposed in [31]. This allows for employing communication and radar waveforms simultaneously. The processing scheme is based on the decoding of the received OFDM waveform by an FFT. Figure 19 presents the processing scheme block diagram [31].

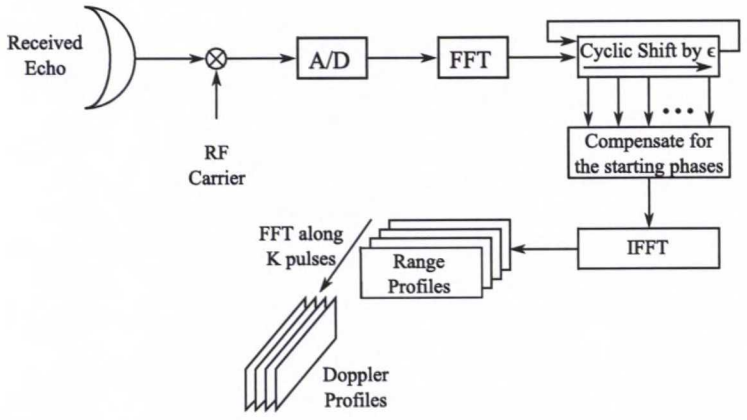

Figure 19: Range and Doppler processing through starting phase compensation and FFT [31]

Pulse compression is achieved by compensating for all the starting phases of the carriers. This well-known operation is matched filtering. The received echoes are de-modulated through FFT and recovered phases are compensated by multiplying with complex conjugates of the transmitted phases. Doppler effect on OFDM waveform is considered as the shift of the carriers by an amount determined by the radial velocity component of the target. Doppler compensation is done by implementing a cyclic shift of the FFT output in the receiver. The amount of cyclic shift is obtained by considering the maximum radial velocity of the target. This Doppler processing technique is similar to the one presented in [14]. For the OFDM signal utilized in [31] a CP is considered. In a multipath scenario the transmitted symbols arrive at the receiver as a sum of delayed replicas. Each path in the channel introduces a different delay. If the delay introduced by at least one path is longer than the transmission interval between the symbols ISI is created. The use of CP, whose duration is usually longer than the maximum delay in the channel, allows the receiver to select the useful part of the symbol that does not contain samples from other symbols. The presence of ISI is equivalent to noise at the receiver, which causes a lower SNR. As the radar performance is directly proportional with the SNR at the receiver it is desirable to have no ISI. Thus, the use of CP prevents the radar performance deterioration in a multipath channel.

Another OFDM radar processing technique is proposed in [28] and tested in [29]. This method allows for both radar and communication operations simultaneously, similarly to the method proposed in [31]. The novel approach to OFDM radar processing in [28] consists of using the transmitted information and received information at the output of the OFDM de-multiplexer before the channel equalization and decoding. At this point the distortion from the channel is fully contained in the complex modulation symbols of received data. Since all information symbols in one OFDM symbol are transmitted through the channel at different frequencies separated by Δf, the received information symbols can be used to perform channel estimation at discrete frequencies like in stepped frequency radar. The samples of the frequency domain channel transfer function can be easily obtained through an element-wise division:

$$I_{div}(n) = \frac{I_r(n)}{I(n)}, \tag{70}$$

where $I_r(n)$ is the received information and $I(n)$ is the transmitted information. $I(n)$ and $I_r(n)$ can be retrieved from the beginning and the end of the transmission-reception chain presented in Figure 11. The sampled channel impulse response, which corresponds to the radar range profile, is obtained as in the IDFT of $I_{div}(n)$. As a consequence, the resulting radar range profile is periodic in time. The novel processing approach in [28] is completely independent of the transmitted information, since it relates every received modulation symbol to a transmitted one. The only minor disadvantage is the periodicity of the radar range profile, which can cause ambiguities if improper subcarrier spacing is considered. In order to avoid ISI between subsequent OFDM signals a CP is utilized. The duration of the CP must correspond to the maximum time difference of the received signal components. For the radar application there is a factor of 2 involved, since the signal travels the distance between platform and scatterer twice.

The performance of the method in [28] is evaluated in [4]. The evaluation is done by analyzing the effect of the SNR at the receiver on the radar system. It is found that the estimation of target parameters in OFDM radar works very well above a SNR threshold, but rapidly degrades under this threshold [4]. The SNR threshold is found through simulations that utilize the same target at different distances. Above the threshold the range estimates contain very little or no error, while under the threshold the range estimates are mostly erroneous. This is valid for the processing method in [28] and also for classical processing methods that involve matched filtering [4].

3.4 Discussion on MCPC and OFDM Radar

MCPC is a particular case of OFDM which is illustrated in Figures 16 and 12. The MCPC signal is obtained from an OFDM signal for which coding is applied on each subcarrier. As a result of the relation between the two it can be stated that the proprieties of OFDM are valid also for MCPC.

The key advantages that OFDM and MCPC bring to radar are:

- Spectral efficiency
- Waveform and frequency diversity
- Robustness against multipath propagation
- Easy implementation in digital domain
- Easily available hardware

Some of the drawbacks are:

- The variable envelope that results in a high PAPR level

- Doppler sensitivity that might spoil the orthogonality of the subcarriers

When MCPC is employed, several OFDM symbols are transmitted sequentially. The first symbol contains the first chips on each subcarrier, the second symbol contains the second chip on each subcarrier and so on. The duration of each symbol is T_c and the duration of the MCPC symbol will be MT_c. Thus, the MCPC symbol will contain M OFDM symbols. This process is visible in Figure 20, which can be considered as a continuation of Figure 12.

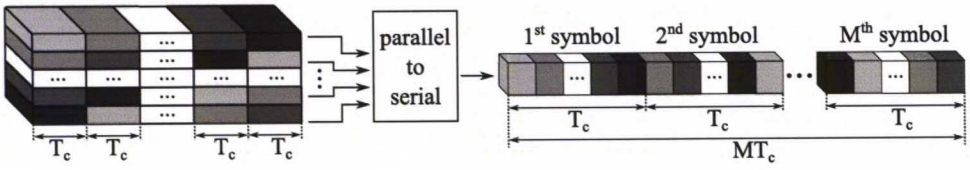

Figure 20: The result of a MCPC pulse modulation is represented by serial OFDM symbols

When no coding on the subcarriers is done, one long OFDM symbol is obtained. More specific of a duration $T_s = MT_c$. If this is the case, the intercarrier spacing is $\Delta f = 1/T_s = 1/MT_c$, so M times smaller than when coding on each subcarrier is employed. The bandwidth is the same in both cases, with coding on the subcarriers (MCPC case) and without coding on the subcarriers (OFDM case), and equal to $B = N\Delta f$. Thus, the following relation is obtained:

$$N_{OFDM}\Delta f_{OFDM} = N_{MCPC}\Delta f_{MCPC}, \tag{71}$$

which is further written as:

$$N_{OFDM}\frac{1}{MT_c} = N_{MCPC}\frac{1}{T_c} \tag{72}$$

and finally it is obtained that:

$$N_{OFDM} = MN_{MCPC}. \tag{73}$$

Thus, the number of subcarriers, when coding on each subcarrier is employed, is reduced by the number of chips in the code. This does not influence the radar performance as the range resolution depends on the utilized total bandwidth.

Nevertheless, coding can be done in frequency domain for OFDM, while coding in time domain is done for MCPC. The coding in frequency domain does not influence the relation between the number of subcarriers as it was derived above.

The above mentioned coding in time domain on the subcarriers is a technique known in communication systems as MC-DS-CDMA. This is a combination of multicarrier modulation and the spread spectrum technique for single carrier systems Direct Sequence CDMA (DS-CDMA). The DS-CDMA is a technique proposed for multiple access, where each user would have its own code that would spread the data with. The key relation between the codes is that these are orthogonal, which allows the users to utilize the same time and frequency resources while being separated

from each other in the code domain. The MC-DS-CDMA scheme is presented in Figure 21 where the waveform time diversity can also be observed. This technique is employed when a MCPC signal is desired.

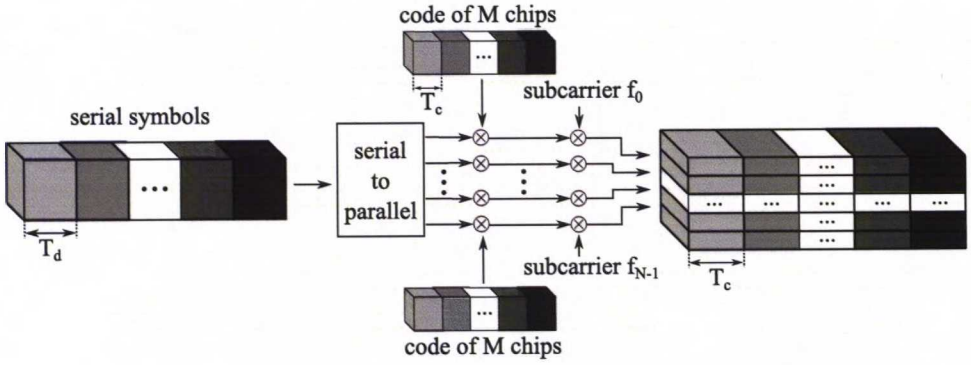

Figure 21: MC-DS-CDMA scheme (each subcarrier is modulated by a code sequence)

A technique that involves coding in frequency domain is known in communication systems as MC-CDMA. This technique uses a single code which contains a number of chips no larger than the number of subcarriers. In MC-CDMA each chip in the code modulates one subcarrier, while in MC-DS-CDMA all the chips in the code modulate one subcarrier. The MC-CDMA scheme is presented in Figure 22, where the waveform frequency diversity can be observed.

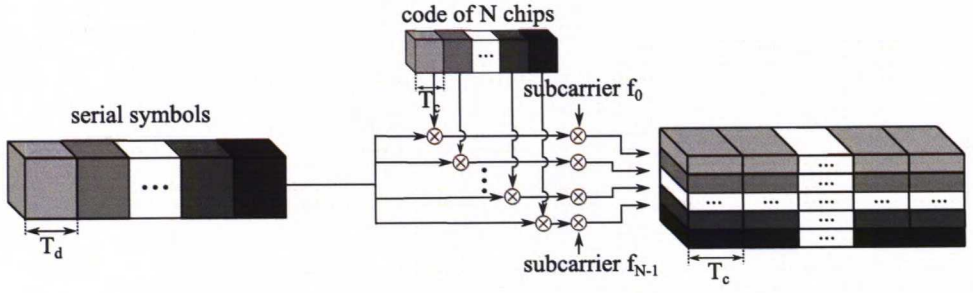

Figure 22: MC-CDMA scheme (each subcarrier is modulated by one chip of a code sequence)

The two techniques, MC-DS-CDMA and MC-CDMA, applied in a radar system bring the benefit of time and frequency diversity respectively. The time and frequency waveform diversity can be observed in Figures 21 and 22 by looking at the different shades of gray that correspond to different chips in the code.

A similar structure to MCPC is sometimes proposed and referred to as OFDM, see for example in [14, 13]. In fact the signal has the same structure as a MCPC signal but it is not denoted as such. When MCPC is employed, or OFDM as proposed in [14, 13], there is no CP involved. Other sources, for example [31, 28], mention the use of a CP. The reasons for using a CP is to remove the ISI and to allow the modeling of the linear convolution of a frequency selective multipath channel as a

circular convolution. The latter would facilitate the use of a Discrete Fourier Transform (DFT) at the receiver.

One of the advantages of OFDM in general and MCPC in particular is that the spectrum is efficiently utilized. This comes from the fact that spacing between the subcarriers is just enough to make sure they remain orthogonal, so no bandwidth is wasted with guard bands in frequency domain. Other advantages of OFDM are robustness against multipath fading, easy synchronization and equalization and high flexibility in system design. Also, given the wide spread use of OFDM in communication systems, the hardware is easily available.

Multicarrier signals facilitate for easy generation of frequency agile waveforms, implemented in the digital domain. Thus, no extra oscillators are required to implement such waveforms. Frequency agile waveforms bring important benefits to radar. In the face of jammers the radar receives less jamming power as the jammer is forced to spread its power in a larger bandwidth. Also some frequencies could be highly attenuated in certain conditions and the radar can deactivate these subcarriers and allocate the power for the ones that experience lower attenuation. It was mentioned in [21] that the spectral sidelobes of MCPC signals are very low compared to the the sinc-squared spectrum of single carrier phase-coded radar signals. Thus MCPC has better performance in radar application.

The varying envelope is the main disadvantage of multicarrier signals and OFDM and MCPC in particular. This translates in high levels of PMEPR. However, solutions to lower the levels of PMEPR have been found [15, 17, 21, 22].

4 Generalized Multicarrier Radar

There are many proposed concepts of multicarrier radar and different waveform designs in the literature [16, 14, 20, 26]. A general model that could describe all these concepts in an easy and intuitive way is desirable. In the following, such general model is derived and proposed using a matrix representation. This would allow the implementation of different multicarrier radar concepts by simply filling in the elements to corresponding matrices appropriately. After the model is derived, a few waveform design examples are provided along with the corresponding matrices that need to be tailored.

4.1 Generalized Model

First the equation for the transmitted signal is derived. Then the equation of the received signal which contains the target information is derived as well. The equations are then transformed into matrix form for an easier implementation and more compact notation.

The equation of a multicarrier signal with N subcarriers is the starting point for this model. The equation of the passband MC signal is:

$$p_t(t) = \text{rect}(t) \sum_{n=0}^{N-1} \exp(j2\pi f_n t), \tag{74}$$

where f_n are the subcarrier frequencies and rect(t) has the following formula:

$$\text{rect}(t) = \begin{cases} 1 & \text{if } 0 \leq t \leq T \\ 0 & \text{elsewhere} \end{cases}, \tag{75}$$

which is used to limit the duration of the signal to T. It is possible to carry information on these subcarriers by modulating them and then (74) will become:

$$p_t(t) = \text{rect}(t) \sum_{n=0}^{N-1} d_n \exp(j2\pi f_n t), \tag{76}$$

where symbol d_n is chosen in accordance with the selected constellation. For example, for each subcarrier, the modulation could be: BPSK, QPSK, or M-ary QAM. If the selected modulation is BPSK, then d_n are selected from the set {-1,1}. These specific data symbols are of no interest to pure radar applications. However, these come into use when joint radar and communication purposes are considered [28]. Known waveform is needed in matched filter at the receiver. What this specific waveform is does not matter much as long as it is known and has desirable properties. In order to keep the model as general as possible, the data symbols are considered in the following.

The advantages of pulse compression were stated earlier in this work. The pulse compression techniques can also be performed for multicarrier radar waveforms. For

a multicarrier waveform pulse compression can be achieved through coding in time or frequency domain. These coding options, presented in Figures 21 and 22, were first introduced in communication systems as MC-DS-CDMA and MC-CDMA respectively. These will be further referred to as Time Diversity Radar Waveform (TDRW) and Frequency Diversity Radar Waveform (FDRW) in radar systems. The pulse compression gain or ratio depends on the length of the modulating code. This length is denoted as M. The implementation of such coding can be done as a product of matrices. The rows of the matrices represent the codes in time domain, while the columns represent the codes in frequency domain. A series of data symbols $\mathbf{d} = [d_0 \quad d_1 \quad \cdots \quad d_{N-1}]$ is considered for the transmission. The code used for modulation is denoted by $\mathbf{c} = [c_0 \quad c_1 \quad \cdots \quad c_{M-1}]$. It is assumed that when coding in frequency domain is employed, the relation $M \leq N$ is satisfied, where N is the number of subcarriers. The case where $M = N$ is considered in the following, so that all subcarriers are utilized. The coding operations in frequency or time domain are defined by the following equations:

$$\mathbf{X}_{FDC} = \mathbf{c}^T\mathbf{d} \tag{77}$$

and

$$\mathbf{X}_{TDC} = \mathbf{d}^T\mathbf{c}, \tag{78}$$

with dimensions $1 \times N$ and $1 \times M$ for $\mathbf{d}$ and $\mathbf{c}$ respectively. FDC and TDC stand for Frequency Domain Coding and Time Domain Coding respectively. The result of such operations are the following matrices:

$$\mathbf{X}_{FDC} = \begin{bmatrix} d_0c_0 & d_1c_0 & d_2c_0 & \cdots & d_{N-1}c_0 \\ d_0c_1 & d_1c_1 & d_2c_1 & \cdots & d_{N-1}c_1 \\ d_0c_2 & d_1c_2 & d_2c_2 & \cdots & d_{N-1}c_2 \\ \vdots & \vdots & \vdots & \ddots & \vdots \\ d_0c_{M-1} & d_1c_{M-1} & d_2c_{M-1} & \cdots & d_{N-1}c_{M-1} \end{bmatrix}_{[M\times N]} \tag{79}$$

and

$$\mathbf{X}_{TDC} = \begin{bmatrix} d_0c_0 & d_0c_1 & d_0c_2 & \cdots & d_0c_{M-1} \\ d_1c_0 & d_1c_1 & d_1c_2 & \cdots & d_1c_{M-1} \\ d_2c_0 & d_2c_1 & d_2c_2 & \cdots & d_2c_{M-1} \\ \vdots & \vdots & \vdots & \ddots & \vdots \\ d_{N-1}c_0 & d_{N-1}c_1 & d_{N-1}c_2 & \cdots & d_{N-1}c_{M-1} \end{bmatrix}_{[N\times M]} . \tag{80}$$

If the code chips on the columns in matrix $\mathbf{X}_{FDC}$ and the code chips on the rows of matrix $\mathbf{X}_{TDC}$ are investigated, one can see that these resemble the shades of gray in Figures 22 and 21. These show the waveform diversity that this type of multicarrier waveforms brings to radar. For the case when coding in frequency domain is employed and the length of the code is smaller than the number of subcarriers, $M < N$, the matrix could have the following structure:

$$\mathbf{X}_{FDC} = \begin{bmatrix} d_0c_0 & d_1c_0 & d_2c_0 & \cdots & d_{N-1}c_0 \\ d_0c_1 & d_1c_1 & d_2c_1 & \cdots & d_{N-1}c_1 \\ \vdots & \vdots & \vdots & \ddots & \vdots \\ d_0c_{M-1} & d_1c_{M-1} & d_2c_{M-1} & \cdots & d_{N-1}c_{M-1} \\ 0 & 0 & 0 & \cdots & 0 \\ \vdots & \vdots & \vdots & \ddots & \vdots \\ 0 & 0 & 0 & \cdots & 0 \end{bmatrix}_{[N\times N]}, \tag{81}$$

so that the number of rows equals the number of subcarriers. Different positions for the rows containing null elements can be considered also. One possibility is to have these as the first rows in the matrix. Another possibility is to have half of them as the first rows in the matrix and the other half as the last rows. Other variations can also be implemented based on the fact that the matrix has to have $N - M$ rows that contain null elements.

The two matrices that describe the coding in frequency and time domain can be generalized under the code matrix which has the following structure:

$$\mathbf{X} = \begin{bmatrix} c_{0,0} & c_{0,1} & c_{0,2} & \cdots & c_{0,M-1} \\ c_{1,0} & c_{1,1} & c_{1,2} & \cdots & c_{1,M-1} \\ c_{2,0} & c_{2,1} & c_{2,2} & \cdots & c_{2,M-1} \\ \vdots & \vdots & \vdots & \ddots & \vdots \\ c_{N-1,0} & c_{N-1,1} & c_{N-1,2} & \cdots & c_{N-1,M-1} \end{bmatrix}_{[N\times M]} \tag{82}$$

and its elements $c_{n,m}$ can be used in the signal equation for the general model.

Taking coding into account, (76) can be updated to:

$$p_t(t) = \text{rect}(t) \sum_{n=0}^{N-1} \sum_{m=0}^{M-1} \text{rect2}(t - mT_c) c_{n,m} \exp(j2\pi(f_c + n\Delta f)t), \tag{83}$$

where $\text{rect2}(t)$ has the following formula:

$$\text{rect2}(t) = \begin{cases} 1 & \text{if } 0 \le t \le T_c \\ 0 & \text{elsewhere} \end{cases}, \tag{84}$$

with T_c being the duration of the modulating chip.

Frequency diversity is another advantage of multicarrier radar that is included in the developed model. This is obtained by introducing weights on each subcarrier. These weights can be used to set some subcarriers inactive if they are experiencing interference or high attenuation, for example. Another use for this weights could be as a power allocation tool. A new term w_n that accounts for the weight on the nth subcarrier is introduced in (83). Also another term $u_{n,m}$ is introduced, which has the role of deactivating each of the subcarriers at different time instances. Thus, the updated equation of the transmitted signal is:

$$p_t(t) = \text{rect}(t) \sum_{n=0}^{N-1} \sum_{m=0}^{M-1} \text{rect2}(t - mT_c) w_n u_{n,m} c_{n,m} \exp(j2\pi(f_c + n\Delta f)t), \tag{85}$$

which is the final equation for the transmitted signal. The baseband version of (85) is obtained as follows:

$$p_t(t) = \text{rect}(t) \sum_{n=0}^{N-1} \sum_{m=0}^{M-1} \text{rect2}(t - mT_c) w_n u_{n,m} c_{n,m} \exp(j2\pi n \Delta f t). \tag{86}$$

In order to be able to formulate this in a matrix form, discretization of (86) is required. The critical sampling rate is chosen such that one sample would be acquired for each modulating chip. This is given by:

$$f_{sampling} = \frac{M}{T}, \tag{87}$$

where T is the symbol duration and M is the length of the spreading code. The sampling interval will be:

$$t_{sampling} = \frac{T}{M}. \tag{88}$$

The discrete time version of (86) is:

$$s_t\left(\frac{kT}{M}\right) = \sum_{n=0}^{N-1} \sum_{m=0}^{M-1} w_n u_{n,m} c_{n,m} \exp\left(j2\pi n \Delta f \frac{kT}{M}\right), \tag{89}$$

where $k = 0 \ldots M-1$.
A more compact form can be obtained and the following notation is made:

$$i = \frac{kT}{M}, \tag{90}$$

where $i = 0 \ldots M-1$. Thus, the compact version of (89) is:

$$s_t(i) = \sum_{n=0}^{N-1} \sum_{m=0}^{M-1} w_n u_{n,m} c_{n,m} \exp(j2\pi n \Delta f i). \tag{91}$$

To be able to write (89) in a matrix form the following shorthand notation is employed:

$$\beta = \exp\left(j2\pi \Delta f \frac{T}{M}\right), \tag{92}$$

which will help construct the following matrix:

$$\mathbf{B} = \begin{bmatrix} 1 & 1 & 1 & \cdots & 1 \\ 1 & \beta & \beta^2 & \cdots & \beta^{M-1} \\ 1 & \beta^2 & \beta^4 & \cdots & \beta^{2(M-1)} \\ \vdots & \vdots & \vdots & \ddots & \vdots \\ 1 & \beta^{(N-1)} & \beta^{(N-1)2} & \cdots & \beta^{(N-1)(M-1)} \end{bmatrix}_{[N \times M]} \tag{93}$$

of dimension $N \times M$. The equation of the transmitted signal may be written as:

$$\mathbf{s}_t = \mathbf{q}\mathbf{W}(\mathbf{U} \circ \mathbf{B} \circ \mathbf{X}), \tag{94}$$

where $\circ$ is the Hadamard (entry-wise) product and $\mathbf{X}$ was presented in (82). Matrix $\mathbf{W}$ is a $N \times N$ diagonal matrix that contains the weights of each subcarrier on the main diagonal:

$$\mathbf{W} = \begin{bmatrix} w_0 & 0 & 0 & \cdots & 0 \\ 0 & w_1 & 0 & \cdots & 0 \\ 0 & 0 & w_2 & \cdots & 0 \\ \vdots & \vdots & \vdots & \ddots & \vdots \\ 0 & 0 & 0 & \cdots & w_{N-1} \end{bmatrix}_{[N \times N]}. \tag{95}$$

Matrix $\mathbf{U}$ is a $N \times M$ matrix that contains elements of 1 and 0 for active and inactive subcarriers respectively. For the element $u_{n,m}$ n is the subcarrier number while m is the sampling instant. If all the subcarriers are active for all the sampling instances this is a matrix of ones. Its general form is:

$$\mathbf{U} = \begin{bmatrix} u_{0,0} & u_{0,1} & u_{0,2} & \cdots & u_{0,M-1} \\ u_{1,0} & u_{1,1} & u_{1,2} & \cdots & u_{1,M-1} \\ u_{2,0} & u_{2,1} & u_{2,2} & \cdots & u_{2,M-1} \\ \vdots & \vdots & \vdots & \ddots & \vdots \\ u_{N-1,0} & u_{N-1,1} & u_{N-1,2} & \cdots & u_{N-1,M-1} \end{bmatrix}_{[N \times M]}. \tag{96}$$

Vector $\mathbf{q}$ is a vector of ones that accounts for the sum of the subcarriers in obtaining the transmitted signal:

$$\mathbf{q} = [1 \quad 1 \quad \cdots \quad 1]_{[1 \times N]}. \tag{97}$$

For the received signal equation, a delay and a Doppler shift caused by the radial velocity of the target are taken into account. The wideband case is considered where each individual subcarrier experiences its own Doppler shift. Considering a target at range R from the radar, moving with the radial velocity v, the equation of the received signal can be written as follows (in the absence of noise):

$$p_r(t) = \text{rect}(t\xi - \tau)\mu \sum_{n=0}^{N-1} \sum_{m=0}^{M-1} \text{rect2}(t\xi - mT_c) w_n u_{n,m} c_{n,m} \exp(j2\pi(f_c + n\Delta f)(t\xi - \tau)), \tag{98}$$

where $\tau = 2R/c$ is the delay, $\xi = \frac{c-v}{c+v}$ is the scaling factor which accounts for the Doppler shift and μ is the complex amplitude introduced by the target. The scaling factor can be approximated to $\xi = 1 - \frac{2v}{c}$, by assuming that $v << c$, where c is the speed of light.

It is desired to obtain the equations in matrix form, so the previous equation may be further factorized as:

$$p_r(t) = \text{rect}\left(t\left(1-\frac{2v}{c}\right)-\frac{2R}{c}\right)\mu\sum_{n=0}^{N-1}\sum_{m=0}^{M-1}\text{rect2}\left(t\left(1-\frac{2v}{c}\right)-mT_c\right) \\ w_n u_{n,m} c_{n,m}\exp\left(j2\pi(f_c+n\Delta f)\left(t\left(1-\frac{2v}{c}\right)-\frac{2R}{c}\right)\right) \tag{99}$$

and finally as:

$$p_r(t) = \text{rect}\left(t\left(1-\frac{2v}{c}\right)-\frac{2R}{c}\right)\mu\sum_{n=0}^{N-1}\sum_{m=0}^{M-1}\text{rect2}\left(t\left(1-\frac{2v}{c}\right)-mT_c\right) \\ w_n u_{n,m} c_{n,m}\exp\left(j2\pi f_c t\left(1-\frac{2v}{c}\right)\right)\exp\left(j2\pi n\Delta f t\left(1-\frac{2v}{c}\right)\right) \\ \exp\left(-j2\pi f_c\frac{2R}{c}\right)\exp\left(-j2\pi n\Delta f\frac{2R}{c}\right). \tag{100}$$

The baseband signal is obtained through downconversion as follows:

$$p_r(t) = \text{rect}\left(t\left(1-\frac{2v}{c}\right)-\frac{2R}{c}\right)\mu\sum_{n=0}^{N-1}\sum_{m=0}^{M-1}\text{rect2}\left(t\left(1-\frac{2v}{c}\right)-mT_c\right) \\ w_n u_{n,m} c_{n,m}\exp\left(-j2\pi f_c t\frac{2v}{c}\right)\exp\left(j2\pi n\Delta f t\left(1-\frac{2v}{c}\right)\right) \\ \exp\left(-j2\pi n\Delta f\frac{2R}{c}\right)\exp\left(-j2\pi f_c\frac{2R}{c}\right). \tag{101}$$

This can be rewritten as:

$$p_r(t) = \text{rect}\left(t\left(1-\frac{2v}{c}\right)-\frac{2R}{c}\right)\mu\exp\left(-j2\pi f_c t\frac{2v}{c}\right)\exp\left(-j2\pi f_c\frac{2R}{c}\right) \\ \sum_{n=0}^{N-1}\sum_{m=0}^{M-1}\text{rect2}\left(t\left(1-\frac{2v}{c}\right)-mT_c\right)w_n u_{n,m} c_{n,m} \\ \exp\left(j2\pi n\Delta f t\left(1-\frac{2v}{c}\right)\right)\exp\left(-j2\pi n\Delta f\frac{2R}{c}\right). \tag{102}$$

Equation (102) gives the continuous time received signal in baseband representation. In order to be able to formulate this in a matrix form, discretization of (102) is required. The critical sampling rate is chosen such that one sample is acquired for each modulating chip. This is given by:

$$f_{sampling} = \frac{M}{T}, \tag{103}$$

where T is the symbol duration and M is the length of the spreading code. However, oversampling is recommended, so the sampling frequency is increased by a factor of P. Thus, the sampling frequency is chosen as:

$$f_{sampling} = P\frac{M}{T}, \tag{104}$$

while the sampling interval will be:

$$t_{sampling} = \frac{T}{PM}. \tag{105}$$

The discrete time version of (102) is:

$$\begin{aligned} s_r\left(\frac{kT}{PM}\right) =& \text{rect}\left(\frac{kT}{PM}\left(1-\frac{2v}{c}\right)-\frac{2R}{c}\right)\mu\exp\left(-j2\pi f_c\frac{kT}{PM}\frac{2v}{c}\right)\exp\left(-j2\pi f_c\frac{2R}{c}\right) \\ & \sum_{n=0}^{N-1}\sum_{m=0}^{M-1}\text{rect2}\left(\frac{kT}{PM}\left(1-\frac{2v}{c}\right)-mT_c\right)w_n u_{n,m}c_{n,m} \\ & \exp\left(j2\pi n\Delta f\frac{kT}{PM}\left(1-\frac{2v}{c}\right)\right)\exp\left(-j2\pi n\Delta f\frac{2R}{c}\right), \end{aligned} \tag{106}$$

where $k = 0 \ldots PM-1$. The equation describes the discrete time version of the complex baseband signal echo where PM samples correspond to one transmitted pulse. A more compact form can be obtained and same notation as (90) is made:

$$i = \frac{kT}{PM}, \tag{107}$$

where $i = 0 \ldots PM-1$. Thus, the compact version of (106) is:

$$\begin{aligned} s(i) =& \text{rect}\left(i\left(1-\frac{2v}{c}\right)-\frac{2R}{c}\right)\mu\exp\left(-j2\pi f_c i\frac{2v}{c}\right)\exp\left(-j2\pi f_c\frac{2R}{c}\right) \\ & \sum_{n=0}^{N-1}\sum_{m=0}^{M-1}\text{rect2}\left(i\left(1-\frac{2v}{c}\right)-mT_c\right)w_n u_{n,m}c_{n,m} \\ & \exp\left(j2\pi n\Delta f i\left(1-\frac{2v}{c}\right)\right)\exp\left(-j2\pi n\Delta f\frac{2R}{c}\right). \end{aligned} \tag{108}$$

To be able to write (108) in a compact matrix form the following shorthand notations are employed:

$$\psi = \exp\left(-j2\pi f_c\frac{2R}{c}\right), \tag{109}$$

$$\gamma = \exp\left(-j2\pi f_c\frac{T}{PM}\frac{2v}{c}\right), \tag{110}$$

$$\beta = \exp\left(j2\pi\Delta f \frac{T}{PM}\left(1 - \frac{2v}{c}\right)\right), \tag{111}$$

$$a = \exp\left(-j2\pi\Delta f \frac{2R}{c}\right), \tag{112}$$

which will allow us to construct the following matrices:

$$\mathbf{\Gamma} = \begin{bmatrix} 1 & \gamma & \gamma^2 & \cdots & \gamma^{PM-1} \\ 1 & \gamma & \gamma^2 & \cdots & \gamma^{PM-1} \\ \vdots & \vdots & \vdots & \ddots & \vdots \\ 1 & \gamma & \gamma^2 & \cdots & \gamma^{PM-1} \end{bmatrix}_{[N\times PM]}, \tag{113}$$

$$\mathbf{B} = \begin{bmatrix} 1 & 1 & 1 & \cdots & 1 \\ 1 & \beta & \beta^2 & \cdots & \beta^{PM-1} \\ 1 & \beta^2 & \beta^4 & \cdots & \beta^{2(PM-1)} \\ \vdots & \vdots & \vdots & \ddots & \vdots \\ 1 & \beta^{(N-1)} & \beta^{(N-1)2} & \cdots & \beta^{(N-1)(PM-1)} \end{bmatrix}_{[N\times PM]} \tag{114}$$

and vector

$$\mathbf{a} = [1 \quad a \quad a^2 \quad \cdots \quad a^{N-1}]_{[1\times N]}. \tag{115}$$

Finally the matrix formulation for the baseband received signal echo in the absence of noise is:

$$\mathbf{s}_r = \mu\psi\mathbf{a}\mathbf{W}(\mathbf{\Gamma} \circ \mathbf{U} \circ \mathbf{B} \circ \mathbf{X}_{ovs}), \tag{116}$$

where matrix $\mathbf{X}_{ovs}$ is obtained as:

$$\mathbf{X}_{ovs} = \mathbf{X} \otimes [1 \quad 1 \quad \cdots \quad 1]_{[1\times P]}, \tag{117}$$

where $\otimes$ is the Kronecker product and the length of the vector of ones is equal to the oversampling factor P.

The equation in (116) contains only the effect of the target, assuming that the channel has no effect on the signal. If the velocity and distance parameters of the target, v and R, are set to zero, corresponding to a no target case, the transmitted signal in the absence of noise would be obtained. In such case the terms μ, ψ, $\mathbf{a}$ and $\mathbf{\Gamma}$ can be removed from (116), while elements of $\mathbf{B}$ become:

$$\beta = \exp\left(j2\pi\Delta f \frac{T}{PM}\right). \tag{118}$$

The exact equation of the transmitted signal in (94) is obtained.

4.2 Multicarrier Radar Waveform Design Examples

The purpose of the general model derived in the previous section is to enable the generation of various waveforms in an easy way, by modifying the elements of appropriate matrices in the general model. This would facilitate generating and programming many commonly used and new radar waveforms using simple matrix formulation. The MCPC and OFDM signals are generated using the derived model first. Few other waveforms that can be implemented using the developed model are also presented.

Recall that the equation for the transmitted signal is:

$$\mathbf{s}_t = \mathbf{q}\mathbf{W}(\mathbf{U} \circ \mathbf{B} \circ \mathbf{X}). \tag{119}$$

This equation will be used to generate all the following examples. For both MCPC and OFDM all the subcarriers are active. Thus, weighting matrix $\mathbf{W}$ is the $N \times N$ identity matrix:
Also the $\mathbf{U}$ matrix has only elements of one:

$$\mathbf{U} = \begin{bmatrix} 1 & 1 & 1 & \cdots & 1 \\ 1 & 1 & 1 & \cdots & 1 \\ 1 & 1 & 1 & \cdots & 1 \\ \vdots & \vdots & \vdots & \ddots & \vdots \\ 1 & 1 & 1 & \cdots & 1 \end{bmatrix}_{[N \times M]}, \tag{120}$$

as all subcarriers are active at all sampling instances. Vector $\mathbf{q}$ is a vector of ones of length N as presented in the derivation of the general model. Orthogonality between the subcarriers is required, so the carrier frequencies have to be chosen accordingly. For MCPC the intercarrier spacing has to be $\Delta f = 1/T_c$ and for OFDM $\Delta f = 1/T$, where $T = MT_c$. This will affect the elements of matrix $\mathbf{B}$ that will be:

$$\beta_{MCPC} = \exp\left(j2\pi\Delta f_{MCPC}\frac{T}{PM}\right) \tag{121}$$

and

$$\beta_{OFDM} = \exp\left(j2\pi\Delta f_{OFDM}\frac{T}{PM}\right). \tag{122}$$

After the corresponding values of the intercarrier spacing for MCPC and OFDM respectively are replaced in (121) and (122), the final form of the elements of matrix $\mathbf{B}$ is as follows:

$$\beta_{MCPC} = \exp\left(j2\pi\frac{1}{P}\right) \tag{123}$$

and

$$\beta_{OFDM} = \exp\left(j2\pi\frac{1}{PM}\right). \tag{124}$$

Matrix $\mathbf{B}$ is obtained as in (114) by filling in the corresponding β elements. The coding matrix $\mathbf{X}_{ovs}$ will also be different for the two implementations. This is because the matrix $\mathbf{X}$ is obtained as:

$$\mathbf{X}_{MCPC} = \begin{bmatrix} d_0c_0 & d_0c_1 & d_0c_2 & \cdots & d_0c_{M-1} \\ d_1c_0 & d_1c_1 & d_1c_2 & \cdots & d_1c_{M-1} \\ d_2c_0 & d_2c_1 & d_2c_2 & \cdots & d_2c_{M-1} \\ \vdots & \vdots & \vdots & \ddots & \vdots \\ d_{N-1}c_0 & d_{N-1}c_1 & d_{N-1}c_2 & \cdots & d_{N-1}c_{M-1} \end{bmatrix}_{[N\times M]}, \tag{125}$$

for MCPC, or

$$\mathbf{X}_{OFDM} = \begin{bmatrix} d_0c_0 & d_1c_0 & d_2c_0 & \cdots & d_{N-1}c_0 \\ d_0c_1 & d_1c_1 & d_2c_1 & \cdots & d_{N-1}c_1 \\ d_0c_2 & d_1c_2 & d_2c_2 & \cdots & d_{N-1}c_2 \\ \vdots & \vdots & \vdots & \ddots & \vdots \\ d_0c_{M-1} & d_1c_{M-1} & d_2c_{M-1} & \cdots & d_{N-1}c_{M-1} \end{bmatrix}_{[M\times N]}, \tag{126}$$

for OFDM, if coding is employed, and

$$\mathbf{X}_{OFDM} = \begin{bmatrix} d_1 & d_1 & d_1 & \cdots & d_1 \\ d_2 & d_2 & d_2 & \cdots & d_2 \\ d_3 & d_3 & d_3 & \cdots & d_3 \\ \vdots & \vdots & \vdots & \ddots & \vdots \\ d_{N-1} & d_{N-1} & d_{N-1} & \cdots & d_{N-1} \end{bmatrix}_{[N\times M]}, \tag{127}$$

if no coding is employed. The ideal signal at the receiver follows the equation:

$$\mathbf{s}_r = \mu\psi\mathbf{a}\mathbf{W}(\mathbf{\Gamma} \circ \mathbf{U} \circ \mathbf{B} \circ \mathbf{X}_{ovs}), \tag{128}$$

where the elements μ, ψ, $\mathbf{a}$, $\mathbf{\Gamma}$ and $\mathbf{B}$ contain the target effect. From these terms the target parameters of interest are obtained.

Another waveform example is based on discrete step approximation of LFM waveform, but particularized for the multicarrier radar model proposed in this work. A so-called up-chirp is presented in Figure 23. The frequency is changed in an ascending manner in a given bandwidth.

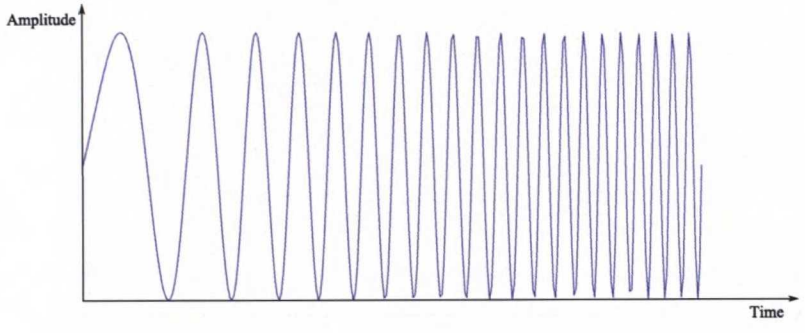

Figure 23: Example of up-chirp pulse

For the multicarrier radar this can be adopted by exciting each subcarrier on a different frequency, one higher than the previous, and increasing these frequencies as much as the available bandwidth allows it. This is illustrated in Figure 24, where only three subcarriers are considered. This is a stepwise approximation of a chirp pulse and can be considered to be a frequency hopping technique which follows a certain simple hopping pattern.

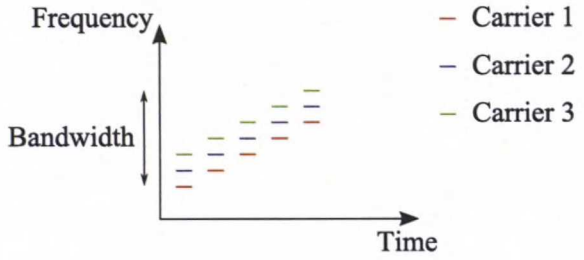

Figure 24: Example of stepwise approximation of up-chirp pulse using three subcarriers

The implementation of such a waveform involves the matrix $\mathbf{U}$. Its structure, corresponding to the pattern in Figure 24, is the following:

$$\mathbf{U} = \begin{bmatrix} 1 & 0 & 0 & 0 & \cdots & 0 \\ 1 & 1 & 0 & 0 & \cdots & 0 \\ 1 & 1 & 1 & 0 & \cdots & 0 \\ 0 & 1 & 1 & 1 & \cdots & 0 \\ \vdots & \vdots & \vdots & \vdots & \ddots & \vdots \\ 0 & 0 & 0 & 0 & \cdots & 1 \\ 0 & 0 & 0 & 0 & \cdots & 1 \\ 0 & 0 & 0 & 0 & \cdots & 1 \end{bmatrix}_{[N \times M]} . \tag{129}$$

Of course the three carriers can take values starting from anywhere in the whole employed band, not only from the lower end. These were chosen such that they follow the pattern in Figure 24. Also in the presented example, consecutive subcarriers are employed, but any subcarrier can be chosen to be active. Moreover, the number of active subcarriers can be different. All of these lead to multiple design possibilities.

The weighting matrix $\mathbf{W}$ is in this case the identity matrix:

$$\mathbf{W} = \begin{bmatrix} 1 & 0 & 0 & \cdots & 0 \\ 0 & 1 & 0 & \cdots & 0 \\ 0 & 0 & 1 & \cdots & 0 \\ \vdots & \vdots & \vdots & \ddots & \vdots \\ 0 & 0 & 0 & \cdots & 1 \end{bmatrix}_{[N \times N]} . \tag{130}$$

The elements of matrix $\mathbf{B}$ are now as follows:

$$\beta = \exp\left(j2\pi\Delta f \frac{T}{PM}\right), \tag{131}$$

where the intercarrier spacing is chosen as desired. If the subcarriers are orthogonal the elements simplify as:

$$\beta = \exp\left(j2\pi\frac{1}{PM}\right). \tag{132}$$

Another waveform example that can be generated in a similar way to the previous example is described next. In this example, the carrier frequency of the subcarriers is hopping in the available bandwidth, as presented in Figure 25.

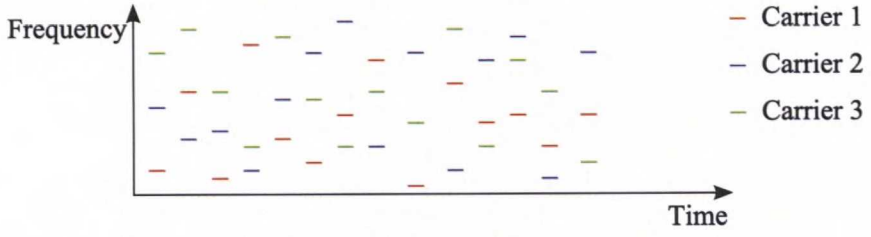

Figure 25: Pseudo-Random frequency hopping in multicarrier radar

Matrix **U** is again involved in the generation of such signal. It is used to select the active subcarriers so that it follows the desired pattern. These could follow, for example, the Costas-codes [1]. These codes offer an almost ideal ambiguity function and are obtained through a specific algorithm that was earlier presented in Pulse Compression Radar Section. Usually these codes are used for single carrier waveforms but can be adapted for multicarrier waveforms as well. If the Costas codes in Table 3 are taken as example, there will be six hops for each subcarrier. If only one subcarrier is active, this will hop in the available bandwidth on positions $1, 3, 2, 6, 4, 5$. This means that the structure of matrix **U** for six sample instants is:

$$\mathbf{U} = \begin{bmatrix} 1 & 0 & 0 & 0 & 0 & 0 \\ 0 & 0 & 1 & 0 & 0 & 0 \\ 0 & 1 & 0 & 0 & 0 & 0 \\ 0 & 0 & 0 & 0 & 1 & 0 \\ 0 & 0 & 0 & 0 & 0 & 1 \\ 0 & 0 & 0 & 1 & 0 & 0 \end{bmatrix}_{[6\times 6]}. \tag{133}$$

If other subcarriers are active, these follow the same pattern with the corresponding distance in carrier frequency. The elements of matrix **B** are the same as in the previous example:

$$\beta = \exp\left(j2\pi\Delta f\frac{T}{PM}\right), \tag{134}$$

that simplifies to:

$$\beta = \exp\left(j2\pi\frac{1}{PM}\right), \tag{135}$$

when the subcarriers are orthogonal.

Other examples are the waveforms described by TDRW and FDRW. For such waveforms all subcarriers are active, thus weighting matrix $\mathbf{W}$ is an identity matrix and matrix $\mathbf{U}$ is a matrix of ones. None of the techniques presumes orthogonality of the subcarriers. If orthogonality is the case, the two examples of MCPC and OFDM respectively, that are presented in the beginning of this section, are obtained. For the case when the subcarriers are not orthogonal, the elements of matrix $\mathbf{B}$ are given by:

$$\beta = \exp\left(j2\pi\Delta f \frac{T}{PM}\right). \tag{136}$$

The $\mathbf{X}$ matrix, utilized to generate the $\mathbf{X}_{ovs}$ matrix, has two structures. One for the TDRW case:

$$\mathbf{X} = \begin{bmatrix} d_0c_0 & d_0c_1 & d_0c_2 & \cdots & d_0c_{M-1} \\ d_1c_0 & d_1c_1 & d_1c_2 & \cdots & d_1c_{M-1} \\ d_2c_0 & d_2c_1 & d_2c_2 & \cdots & d_2c_{M-1} \\ \vdots & \vdots & \vdots & \ddots & \vdots \\ d_{N-1}c_0 & d_{N-1}c_1 & d_{N-1}c_2 & \cdots & d_{N-1}c_{M-1} \end{bmatrix}_{[N\times M]}, \tag{137}$$

and one for FDRW case:

$$\mathbf{X} = \begin{bmatrix} d_0c_0 & d_1c_0 & d_2c_0 & \cdots & d_{N-1}c_0 \\ d_0c_1 & d_1c_1 & d_2c_1 & \cdots & d_{N-1}c_1 \\ d_0c_2 & d_1c_2 & d_2c_2 & \cdots & d_{N-1}c_2 \\ \vdots & \vdots & \vdots & \ddots & \vdots \\ d_0c_{M-1} & d_1c_{M-1} & d_2c_{M-1} & \cdots & d_{N-1}c_{M-1} \end{bmatrix}_{[M\times N]}. \tag{138}$$

Given the flexibility that multicarrier systems offer, many other waveforms can be generated to meet the needs for a particular radar application. Providing examples for all these radar applications is beyond the scope of this work and further examples are not provided here.

5 Radar performance of TDRWs in comparison with MCPC signal

The radar performance of TDRWs, generated using the model derived in Section 4.1, is investigated in the following. The performance is assessed by comparison with an already proposed MCPC waveform in the literature [16, 15, 22]. The ambiguity function plots of the reference and generated signals are first generated. From the ambiguity function plots, the zero Doppler and the zero delay cuts are further evaluated in order to obtain the delay and the Doppler resolution respectively. The resolution is defined by the first null of the main lobe in the respective cut. The closer to zero the null is, the better the resolution. Another performance criterion is the sidelobe level of the Doppler and the delay cut plots. This is considered to be the level of the highest sidelobe in the respective cut plot. The lower the sidelobe level is, the better radar performance is obtained.

In the performed simulations no noise is considered to affect the signals. For a fair comparison both the reference signals and the generated TDRWs occupy the same bandwidth and have the same duration. The axes for the ambiguity plots are expressed in chip duration and inverse of the signal duration for the delay and the Doppler axes respectively. These axes are maintained for the zero Doppler and the zero delay cut plots, respectively. This allows for direct comparison of the plots.

The MCPC signals proposed in [15, 17] are considered in this section as the reference signals. The first considered MCPC signal has $N = 8$ subcarriers, each modulated by codes of length $M = 8$ [17]. These codes are obtained through cyclic shifts of an ideal sequence based on $P3$ codes. Each code is shifted according to the sequence [4 7 2 1 8 3 6 5] similarly to [17]. Every entry in the shift sequence represents the number of cyclic shifts that are applied to the ideal sequence.

The parameters of the TDRWs are chosen in order to make the bandwidth and duration equal with the MCPC reference signal. Based on these constraints the following three cases are considered:

- the TDRW has the same number of subcarriers and same intercarrier spacing as the MCPC signal
- the TDRW has larger number of subcarriers and smaller intercarrier spacing than the MCPC signal
- the TDRW has lower number of subcarriers and larger intercarrier spacing than the MCPC signal

Different values for code length M are chosen for each case such that it can be smaller, equal or larger than the one considered for the MCPC signal. The ideal sequence utilized to obtain the modulating codes for each subcarrier of the TDRW is from the same family as the ideal sequence utilized for MCPC. For example, $P3$ and $P4$ codes are used in this work. However, the sequence of the cyclic shifts is not the same as for MCPC. For the TDRW the shifts are chosen in a random manner, while ensuring that the codes are orthogonal to each other. Orthogonality of the

codes modulating each subcarrier is the main concern. Whether these are optimal or not is outside of the scope of this work.

For the first case, when the two signals use modulating codes of equal length, the spectrum of each channel of the two signals looks like this:

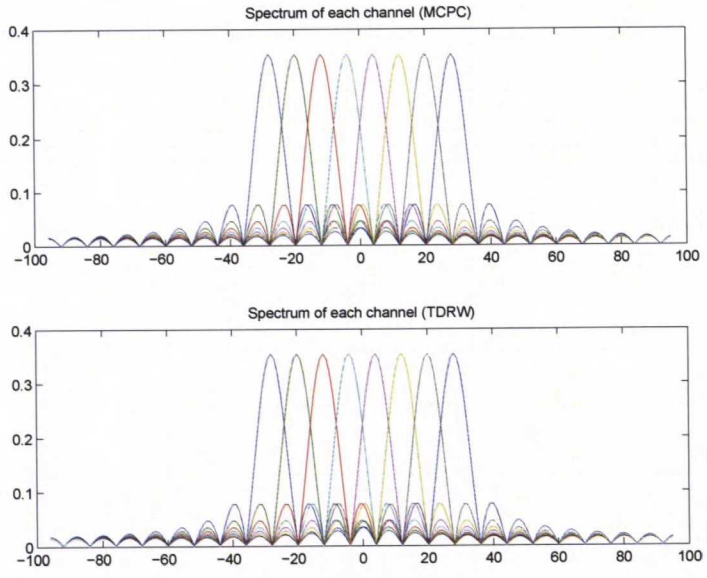

Figure 26: Spectrum of each subchannel for MCPC ($N = 8$, $M = 8$, P3 code) and TDRW ($N = 8$, $M = 8$, P3 code) signals. In this case the TDRW is a MCPC signal.

In this case the TDRW is a MCPC signal. The only difference between the signals is the code matrix that is utilized. The radar performance of the two signals is investigated in the following ambiguity plots:

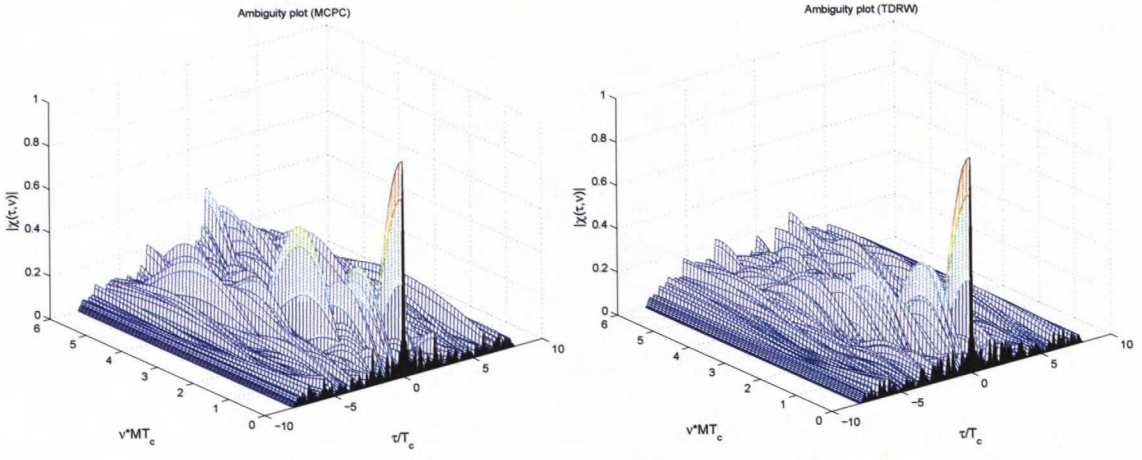

(a) MCPC (b) TDRW

Figure 27: Ambiguity plots for MCPC ($N = 8$, $M = 8$, P3 code) and TDRW ($N = 8$, $M = 8$, P3 code) signals. The sidelobes corresponding to the TDRW are lower.

It is observed that the ambiguity plot of the TDRW has lower sidelobes than the ambiguity plot of the MCPC signal. This means it is closer to the ideal ambiguity plot. This is a consequence of choosing a better coding matrix for the TDRW. In order to compare the Doppler and the delay resolutions of the two signals, the zero delay cut and the zero Doppler cut plots respectively are produced. The zero delay cut plots reveal that the two signals have equal Doppler resolution. This is visualized in the following plots:

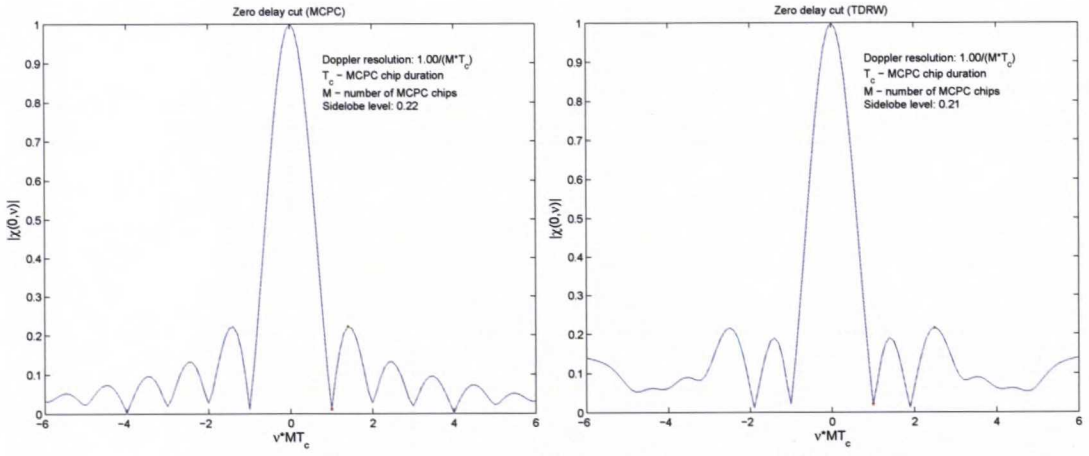

(a) MCPC (b) TDRW

Figure 28: Zero delay cut plots for MCPC ($N = 8$, $M = 8$, P3 code) and TDRW ($N = 8$, $M = 8$, P3 code) signals. The TDRW shows lower sidelobe level.

It is observed that the TDRW has a lower sidelobe level than the MCPC signal. This is also the case for the zero Doppler cut plots:

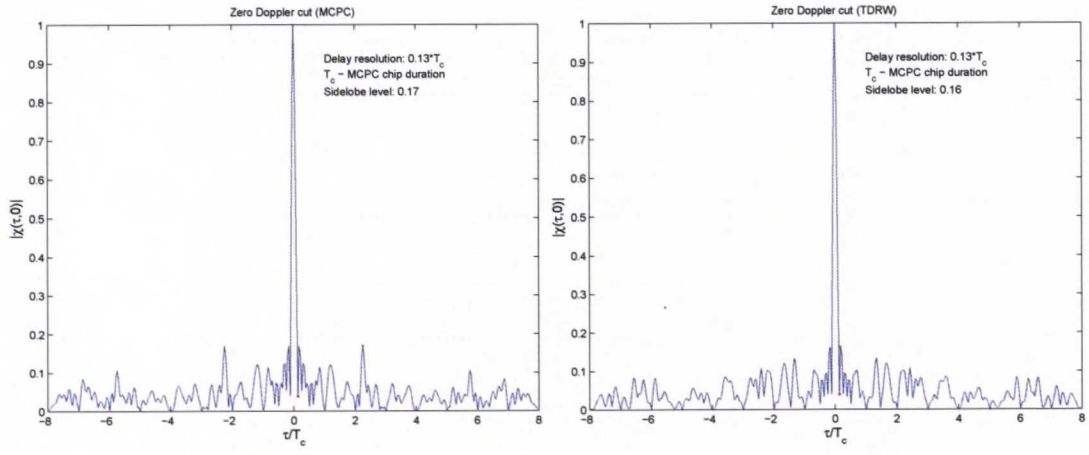

(a) MCPC (b) TDRW

Figure 29: Zero Doppler cut plots for MCPC ($N = 8$, $M = 8$, P3 code) and TDRW ($N = 8$, $M = 8$, P3 code) signals. The TDRW shows lower sidelobe level.

Again, none of the employed signal offers a better delay resolution than the others. As the TDRW exhibits lower sidelobe levels in both delay and Doppler domain, it can be concluded that this is influenced by the code choice.

A different length ($M = 16$) of the modulating code for the TDRW is considered next. The spectrum of each channel for this signal and the MCPC reference is presented in Figure 30.

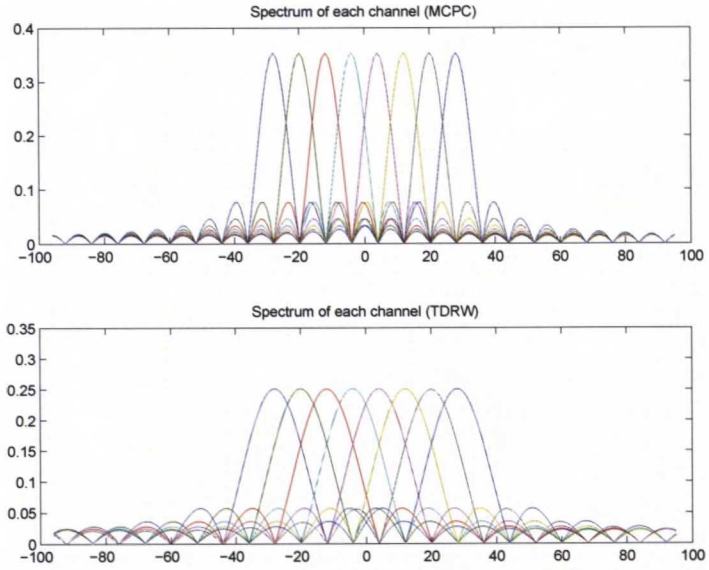

Figure 30: Spectrum of each subchannel for MCPC ($N = 8$, $M = 8$, P3 code) and TDRW ($N = 8$, $M = 16$, P3 code) signals. In this case the TDRW is different from a MCPC signal. The longer code ($M = 16$) cancels the orthogonality of the subcarriers.

By choosing a longer modulation code the TDRW is different from a MCPC signal. This is because the subchannels are not orthogonal and this does not meet the requirements of a MCPC signal. The radar performance of the new TDRW and the reference MCPC signal is investigated in the ambiguity functions in Figure 31.

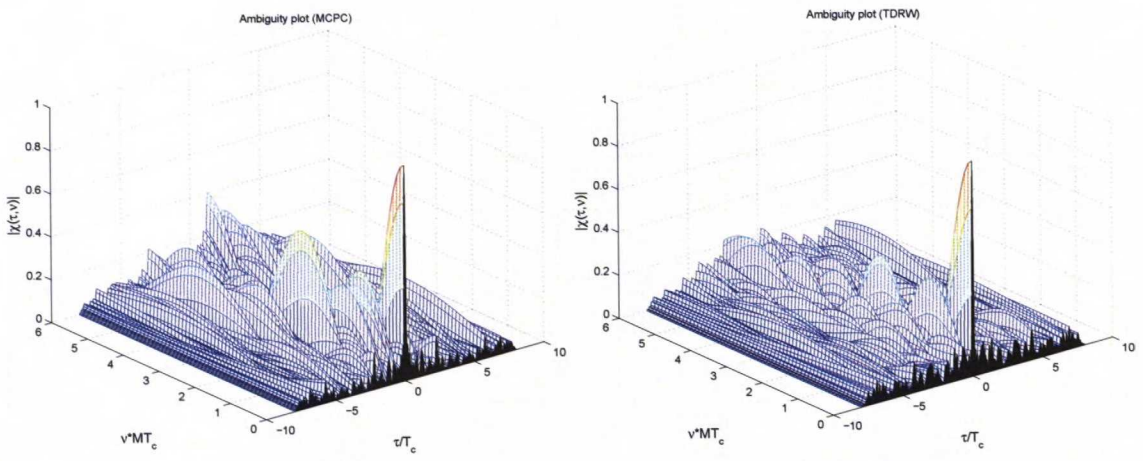

(a) MCPC (b) TDRW

Figure 31: Ambiguity plots for MCPC ($N = 8$, $M = 8$, P3 code) and TDRW ($N = 8$, $M = 16$, P3 code) signals. The sidelobes corresponding to the TDRW are lower.

Again, the ambiguity plot of the TDRW exhibits lower sidelobes than the ambiguity plot of the MCPC signal. For the Doppler resolution the zero delay cuts are compared in Figure 32.

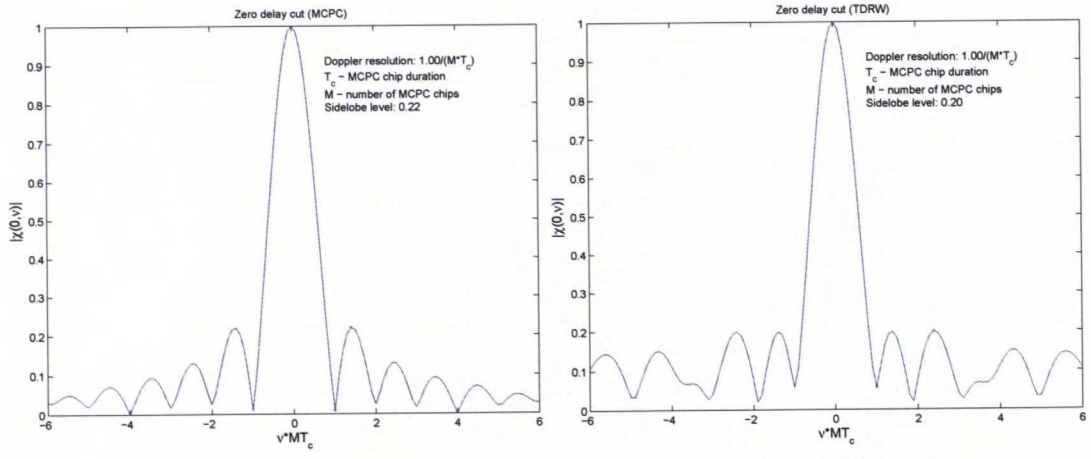

(a) MCPC (b) TDRW

Figure 32: Zero delay cut plots for MCPC ($N = 8$, $M = 8$, P3 code) and TDRW ($N = 8$, $M = 16$, P3 code) signals. The TDRW shows lower sidelobe level.

It is observed that the two signals have equal Doppler resolution. Nevertheless, the sidelobe level corresponding to the TDRW is lower than the ones corresponding to a MCPC signal. This is also the case for the zero Doppler cut plots Figure 33.

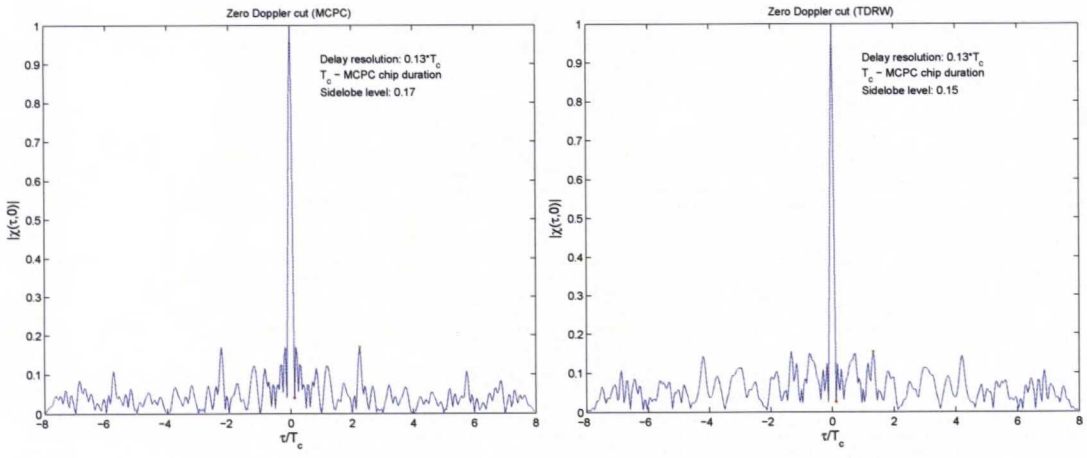

(a) MCPC (b) TDRW

Figure 33: Zero Doppler cut plots for MCPC ($N = 8$, $M = 8$, P3 code) and TDRW ($N = 8$, $M = 16$, P3 code) signals. The TDRW shows lower sidelobe level.

where it is shown that the two signals offer equal delay resolution as well. It can be concluded that by utilizing a longer modulation code the radar performance of the TDRW is the same as for the previous one ($M = 8$).

An even longer modulation code ($M = 24$) is chosen for the TDRW next. The spectrum, in comparison to the one of the reference MCPC signal, is presented in the following figure:

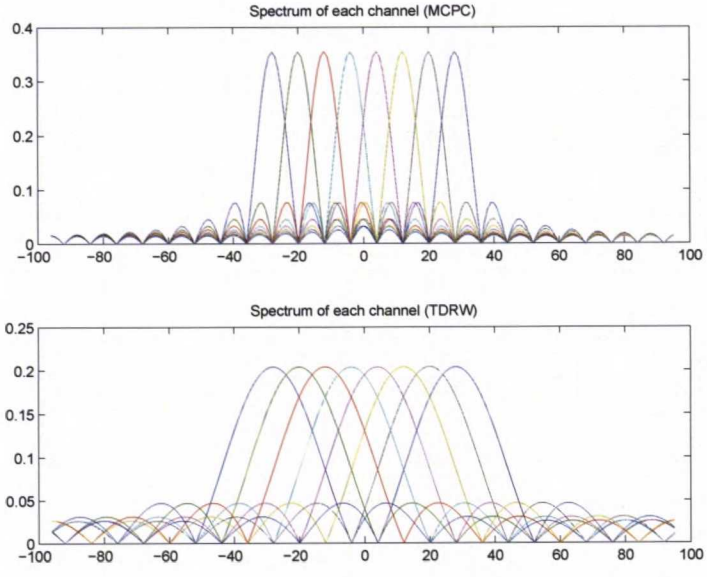

Figure 34: Spectrum of each subchannel for MCPC ($N = 8$, $M = 8$, P3 code) and TDRW ($N = 8$, $M = 24$, P3 code) signals.

The radar performance is investigated in the ambiguity plots from Figure 35.

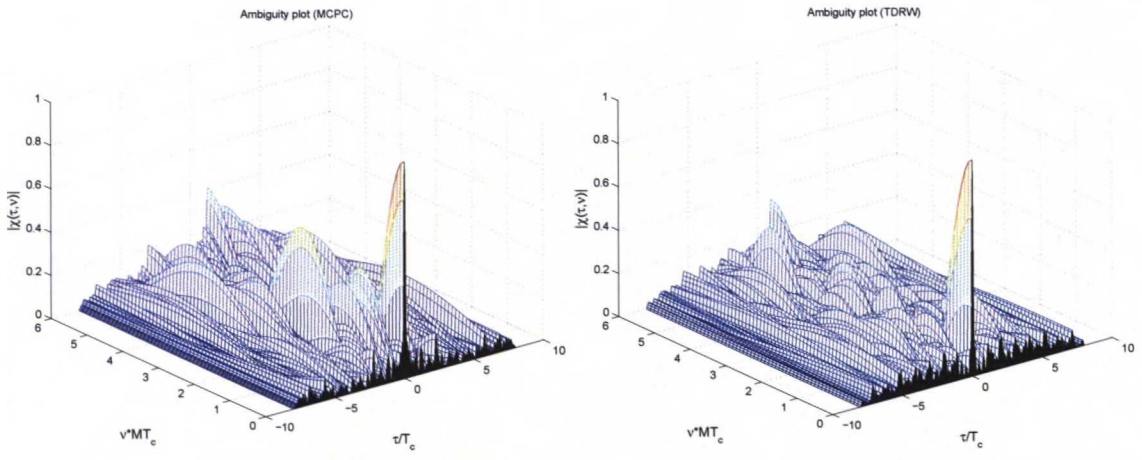

(a) MCPC (b) TDRW

Figure 35: Ambiguity plots for MCPC ($N = 8$, $M = 8$, P3 code) and TDRW ($N = 8$, $M = 24$, P3 code) signals. The sidelobes corresponding to the TDRW are lower.

The previously observed lower sidelobes for the ambiguity plot corresponding to the TDRW is present here as well. For the Doppler resolution the following zero delay cut plots are investigated in Figure 36.

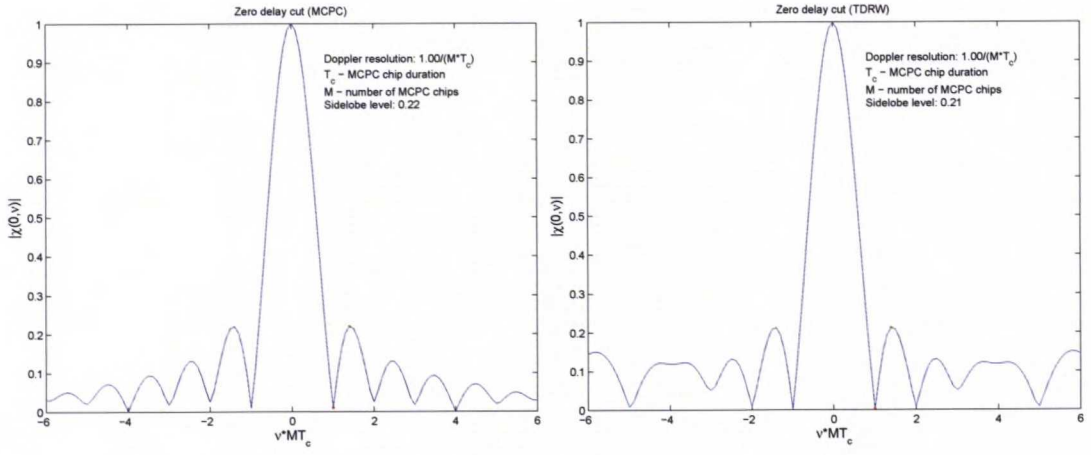

(a) MCPC (b) TDRW

Figure 36: Zero delay cut plots for MCPC ($N = 8$, $M = 8$, P3 code) and TDRW ($N = 8$, $M = 24$, P3 code) signals. The TDRW shows lower sidelobe level.

It is observed that the two signals offer equal resolution. Nevertheless, the sidelobe level corresponding to the TDRW is lower. This is the case as well for the zero Doppler cut plots in Figure 37.

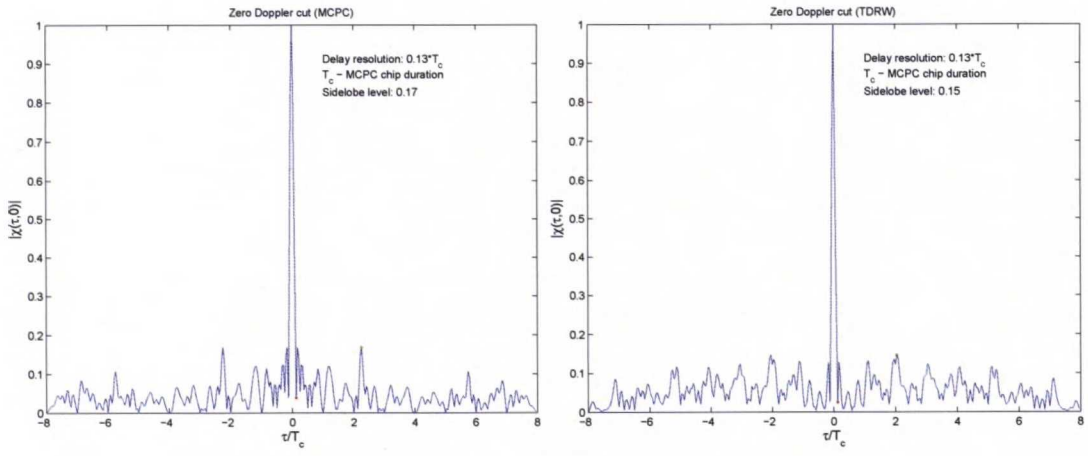

(a) MCPC (b) TDRW

Figure 37: Zero Doppler cut plots for MCPC ($N = 8$, $M = 8$, P3 code) and TDRW ($N = 8$, $M = 24$, P3 code) signals. The TDRW shows lower sidelobe level.

It can be observed that the signals offer equal delay resolution as well.

The second case, where the TDRW has larger number of subcarriers than the MCPC signal, is considered next. The spectrum associated with such signal is presented in Figure 38 where it is compared to the spectrum of the reference MCPC signal.

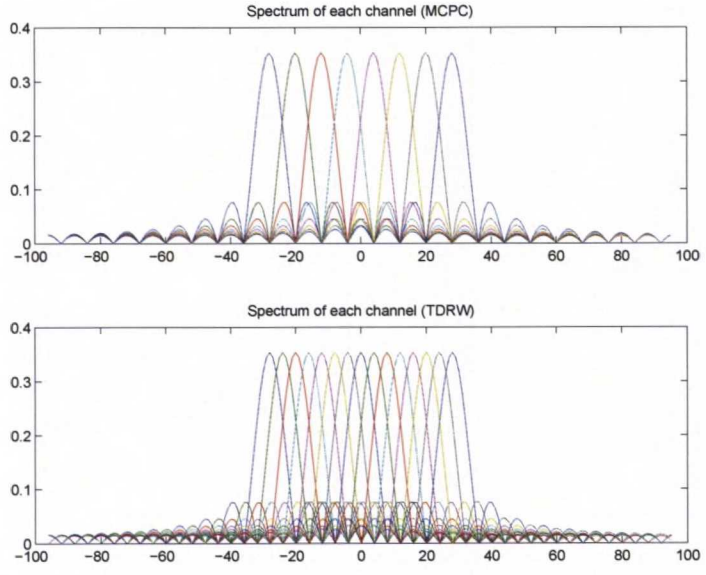

Figure 38: Spectrum of each subchannel for MCPC ($N = 8$, $M = 8$, P3 code) and TDRW ($N = 15$, $M = 8$, P3 code) signals.

The radar performance is investigated using the ambiguity plot of the signal, which is presented in Figure 39 along with the one corresponding to the MCPC reference.

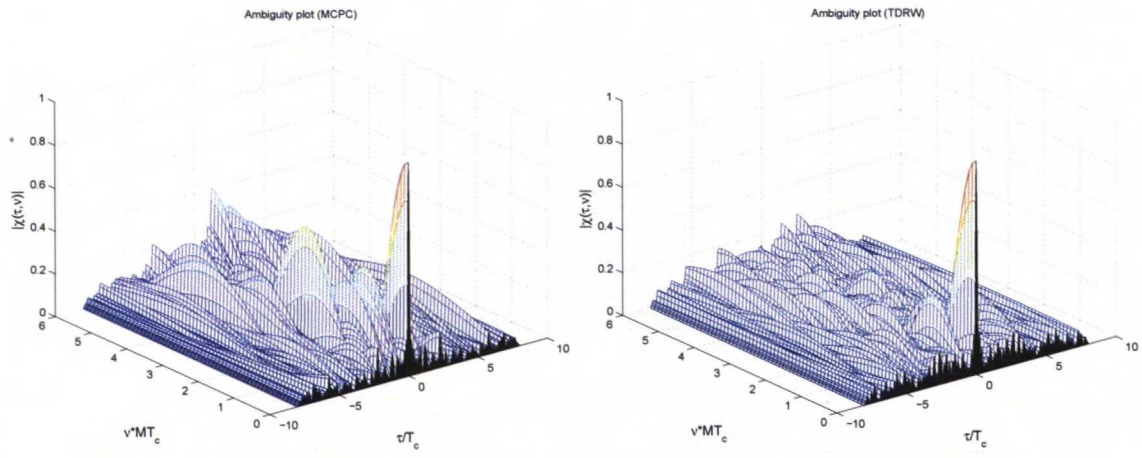

(a) MCPC (b) TDRW

Figure 39: Ambiguity plots for MCPC ($N = 8$, $M = 8$, P3 code) and TDRW ($N = 15$, $M = 8$, P3 code) signals. The sidelobes corresponding to the TDRW are lower.

It is again observed that the ambiguity plot corresponding to the TDRW has lower sidelobes than the one corresponding to the reference signal. The Doppler resolution can be seen from the zero delay cut plots in Figure 40.

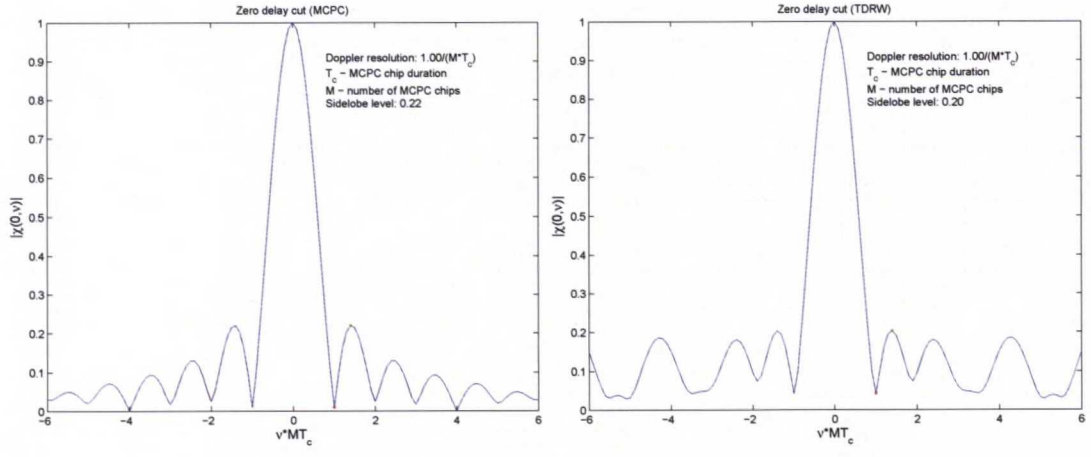

(a) MCPC (b) TDRW

Figure 40: Zero delay cut plots for MCPC ($N = 8$, $M = 8$, P3 code) and TDRW ($N = 15$, $M = 8$, P3 code) signals. The TDRW shows lower sidelobe level.

It shows an equal Doppler resolution for the two signals. Nevertheless, the sidelobe level corresponding to the TDRW is lower than the one corresponding to the reference signal. This is not the case for the zero Doppler cut plots in Figure 41.

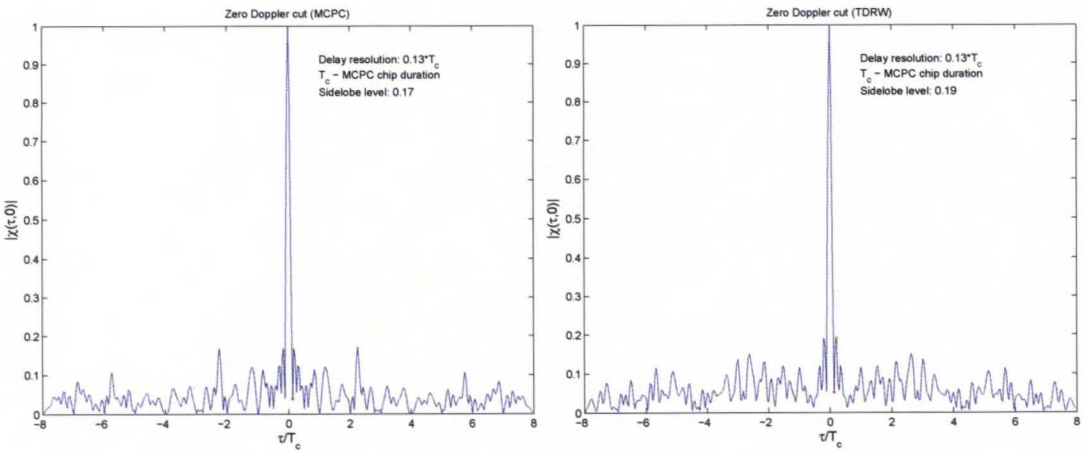

(a) MCPC (b) TDRW

Figure 41: Zero Doppler cut plots for MCPC ($N = 8$, $M = 8$, P3 code) and TDRW ($N = 15$, $M = 8$, P3 code) signals. The TDRW shows higher sidelobe level.

It shows that the two signals offer equal delay resolution and a higher sidelobe level corresponding to the TDRW. The reason for this

A longer modulation code ($M = 16$) is chosen next for the TDRW and the spectrum becomes:

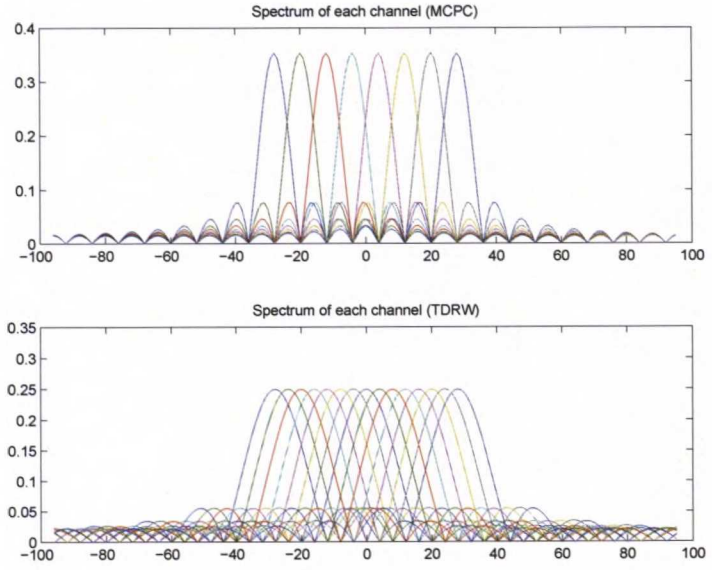

Figure 42: Spectrum of each subchannel for MCPC ($N = 8$, $M = 8$, P3 code) and TDRW ($N = 15$, $M = 16$, P3 code) signals.

The radar performance is investigated using the ambiguity plot of the signal, presented in Figure 43.

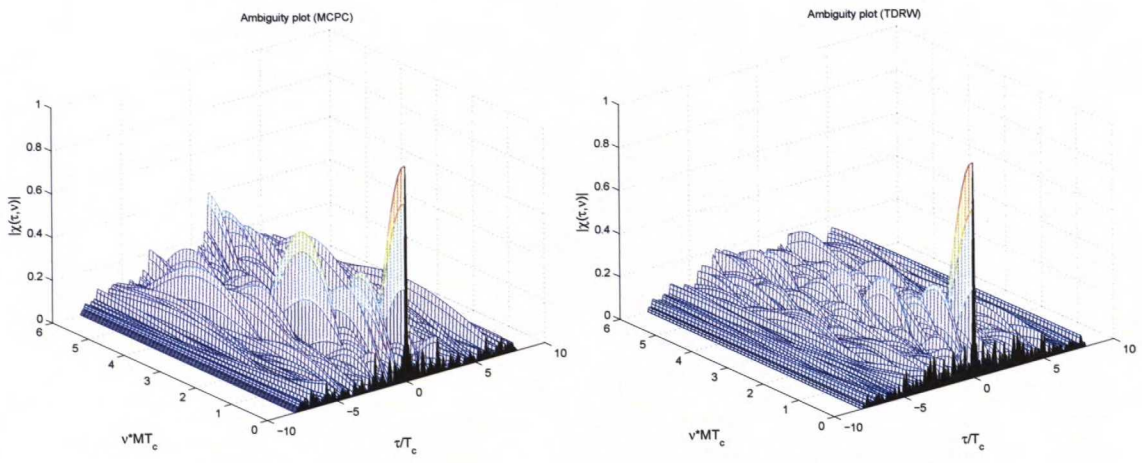

(a) MCPC (b) TDRW

Figure 43: Ambiguity plots for MCPC ($N = 8$, $M = 8$, P3 code) and TDRW ($N = 15$, $M = 16$, P3 code) signals. The sidelobes corresponding to the TDRW are lower.

It may be observed that the ambiguity plot corresponding to the TDRW has lower sidelobes than the one corresponding to the reference MCPC signal. The Doppler resolution is seen from the zero delay cut plots in Figure 44.

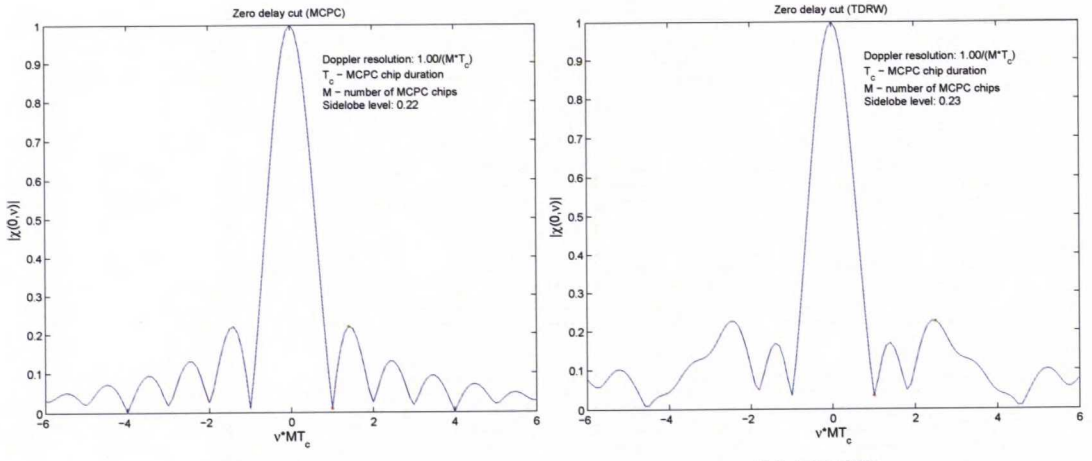

(a) MCPC (b) TDRW

Figure 44: Zero delay cut plots for MCPC ($N = 8$, $M = 8$, P3 code) and TDRW ($N = 15$, $M = 16$, P3 code) signals. The TDRW shows higher sidelobe level.

It shows that the two signals offer equal Doppler resolution. However, the sidelobe level corresponding to the TDRW is higher than the one corresponding to the reference signal. This is not the case for the zero Doppler cut plots as seen in Figure 45.

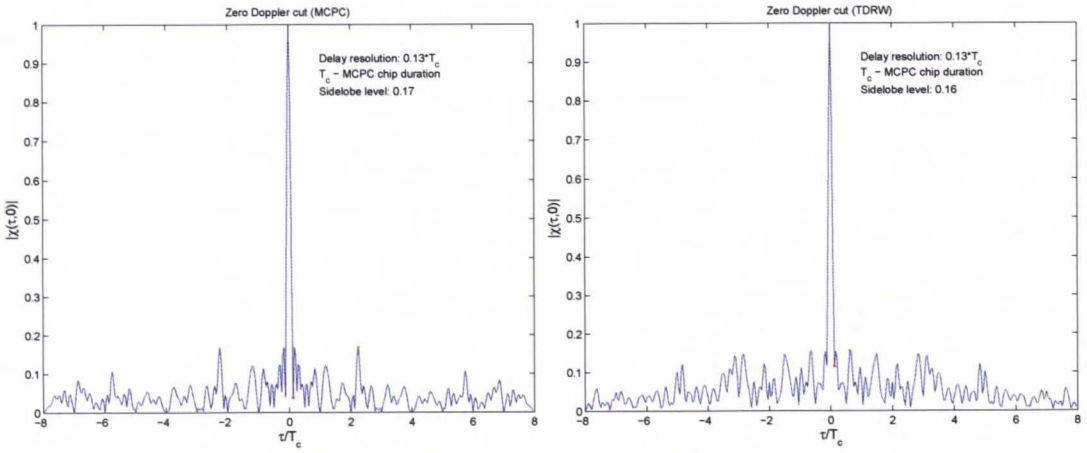

(a) MCPC (b) TDRW

Figure 45: Zero Doppler cut plots for MCPC ($N = 8$, $M = 8$, P3 code) and TDRW ($N = 15$, $M = 16$, P3 code) signals. The TDRW shows lower sidelobe level.

It can be observed that both signals offer equal delay resolution, while the sidelobe level corresponding to the TDRW is lower than the one corresponding to the reference signal.

An even longer modulation code ($M = 24$) is chosen next for the TDRW. The corresponding spectra are depicted in Figure 46.

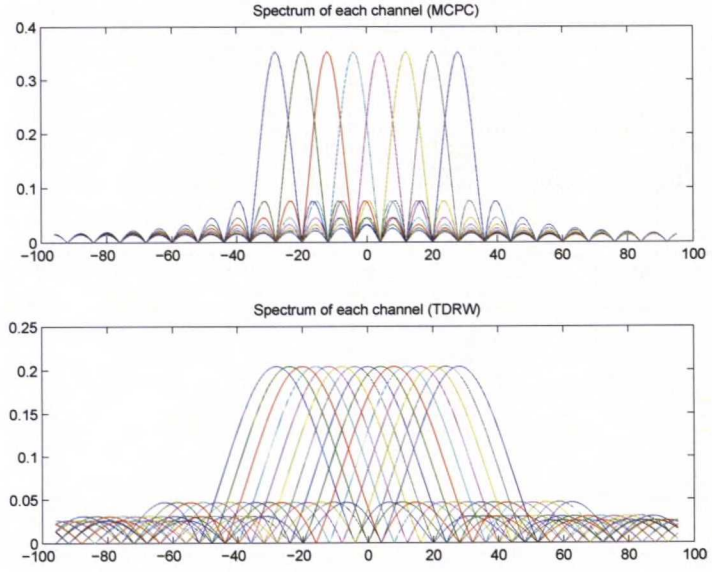

Figure 46: Spectrum of each subchannel for MCPC ($N = 8$, $M = 8$, P3 code) and TDRW ($N = 15$, $M = 24$, P3 code) signals.

The radar performance is investigated using the ambiguity plot of the signal, which is presented in Figure 47.

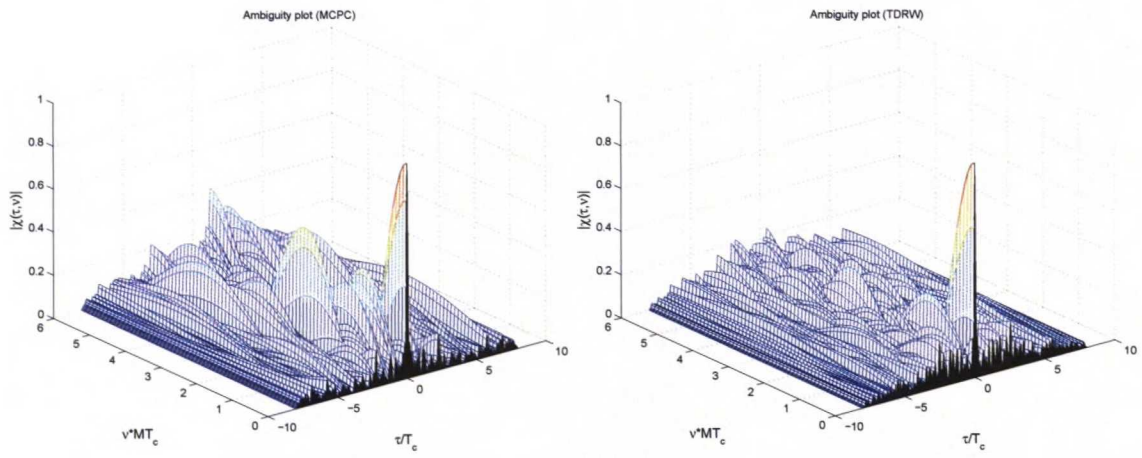

(a) MCPC (b) TDRW

Figure 47: Ambiguity plots for MCPC ($N = 8$, $M = 8$, P3 code) and TDRW ($N = 15$, $M = 24$, P3 code) signals. The sidelobes corresponding to the TDRW are lower.

It is again observed that the ambiguity plot corresponding to the TDRW has lower sidelobes than the one corresponding to the reference signal. The Doppler resolution is obtained from the zero delay cut plots depicted in Figure 48.

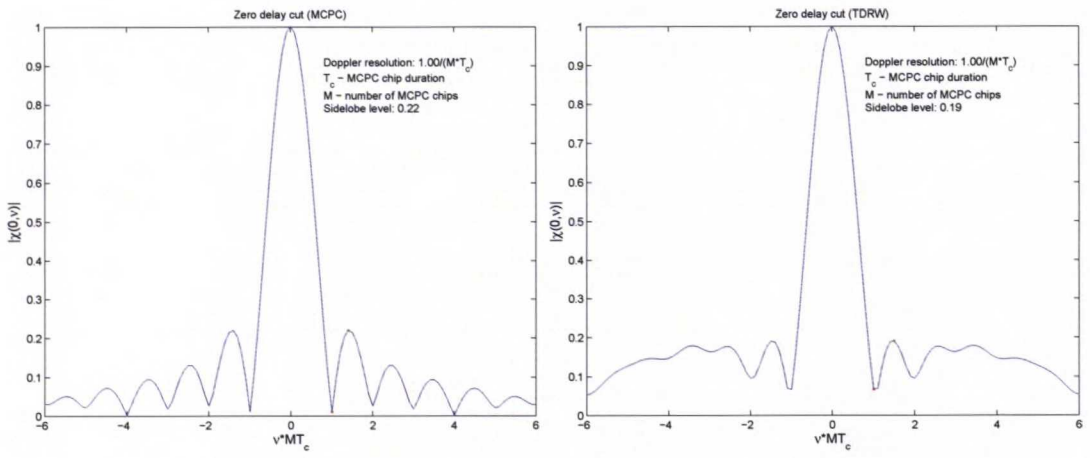

(a) MCPC (b) TDRW

Figure 48: Zero delay cut plots for MCPC ($N = 8$, $M = 8$, P3 code) and TDRW ($N = 15$, $M = 24$, P3 code) signals. The TDRW shows lower sidelobe level.

It shows that an equal Doppler resolution for both signals is achieved. Nevertheless, the sidelobe level corresponding to the TDRW is lower than the one corresponding to the reference. This is not the case for the zero Doppler cut plots as seen in Figure 49.

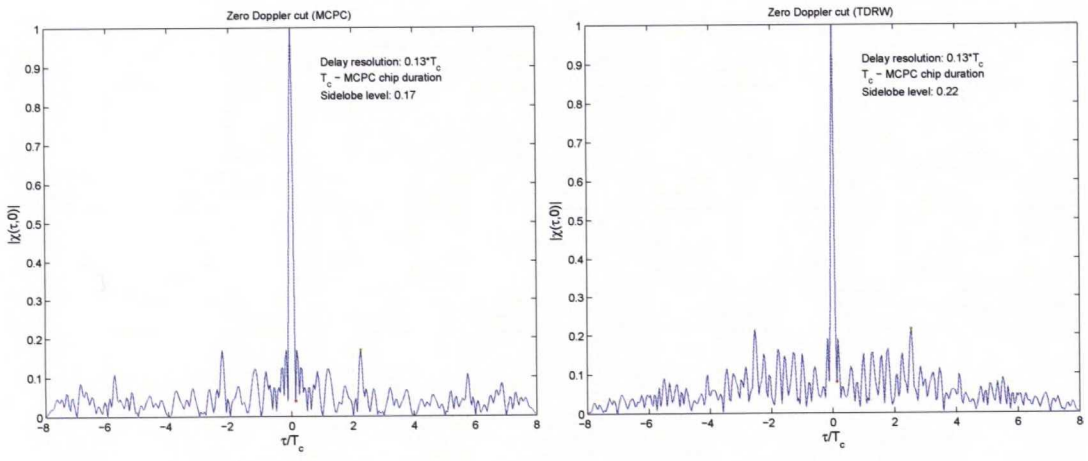

(a) MCPC (b) TDRW

Figure 49: Zero Doppler cut plots for MCPC ($N = 8$, $M = 8$, P3 code) and TDRW ($N = 15$, $M = 24$, P3 code) signals. The TDRW shows higher sidelobe level.

It shows an equal delay resolution for the two signals and higher sidelobe level corresponding to the TDRW.

For the third case, where the TDRW has smaller number of subcarriers than the MCPC signal, a new MCPC signal is used as a reference. The number of subcarriers is $N = 5$, the length of the modulating codes is $M = 5$ and the codes are obtained from an ideal sequence of $P4$ codes. The modulating codes on each subcarrier are obtained again through cyclic shifts. The shift sequence [3 5 2 1 4] is chosen as described in [15]. Also the TDRW is modified accordingly. It has $N = 3$ subcarriers and utilizes codes based on an ideal sequence of $P4$ codes. The spectrum of the two signals for codes of equal length ($M = 5$) is presented in Figure 50.

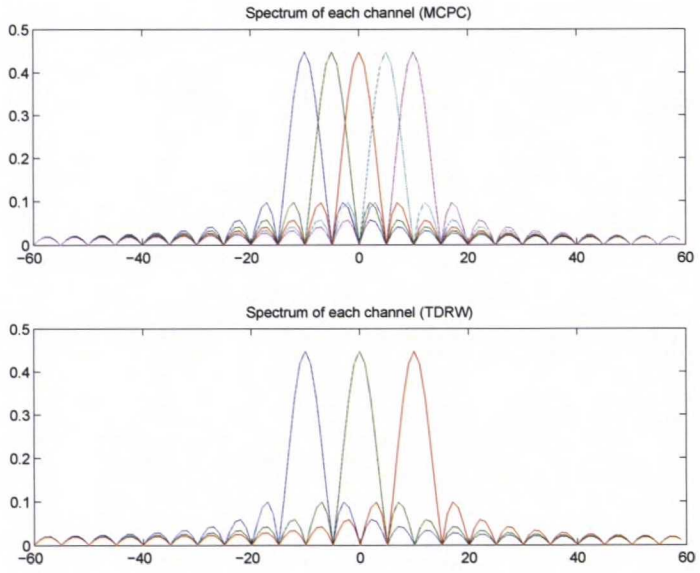

Figure 50: Spectrum of each subchannel for MCPC ($N = 5$, $M = 5$, P4 code) and TDRW ($N = 3$, $M = 5$, P4 code) signals.

It is clear from the previous figure that in this case the subchannels of the TDRW do not overlap and though these do not interfere these are not orthogonal either. This is because the spectrum is utilized in an inefficient manner. The radar performance is investigated using the ambiguity plots presented in Figure 51.

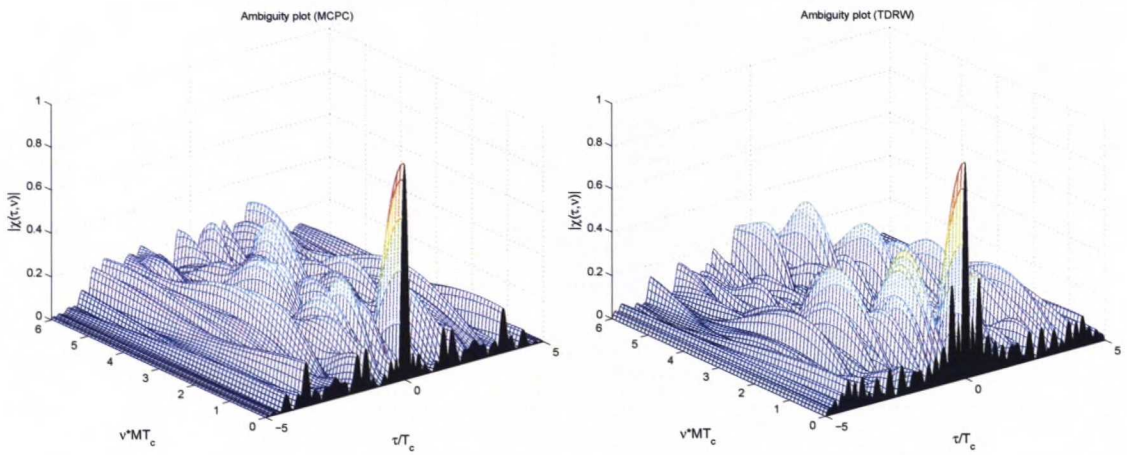

(a) MCPC (b) TDRW

Figure 51: Ambiguity plots for MCPC ($N = 5$, $M = 5$, P4 code) and TDRW ($N = 3$, $M = 5$, P4 code) signals.

The Doppler resolution can be seen from the zero delay cut plots presented in Figure 52.

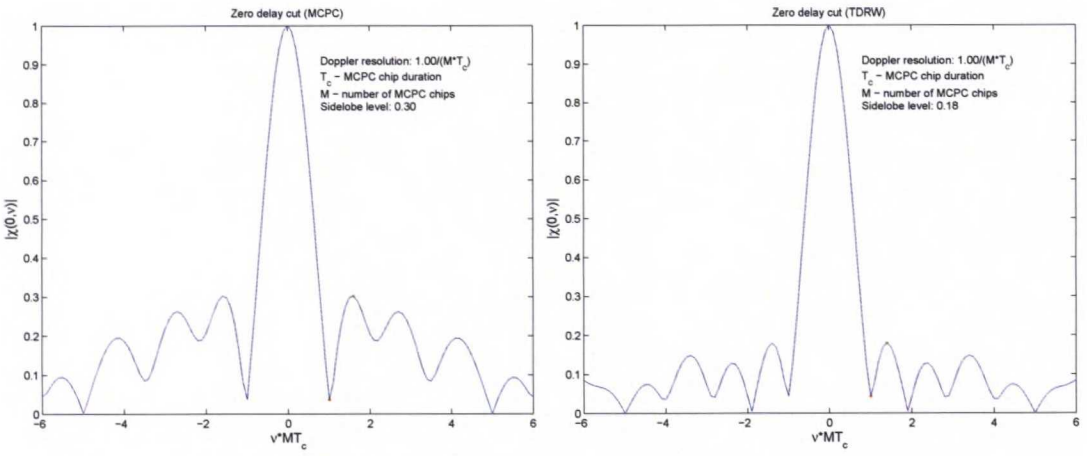

(a) MCPC (b) TDRW

Figure 52: Zero delay cut plots for MCPC ($N = 5$, $M = 5$, P4 code) and TDRW ($N = 3$, $M = 5$, P4 code) signals. The TDRW shows lower sidelobe level.

It reveals that the two signals offer equal Doppler resolution, while the TDRW gives a lower sidelobe level. For the delay resolution the zero Doppler cut plots in Figure 53 are investigated.

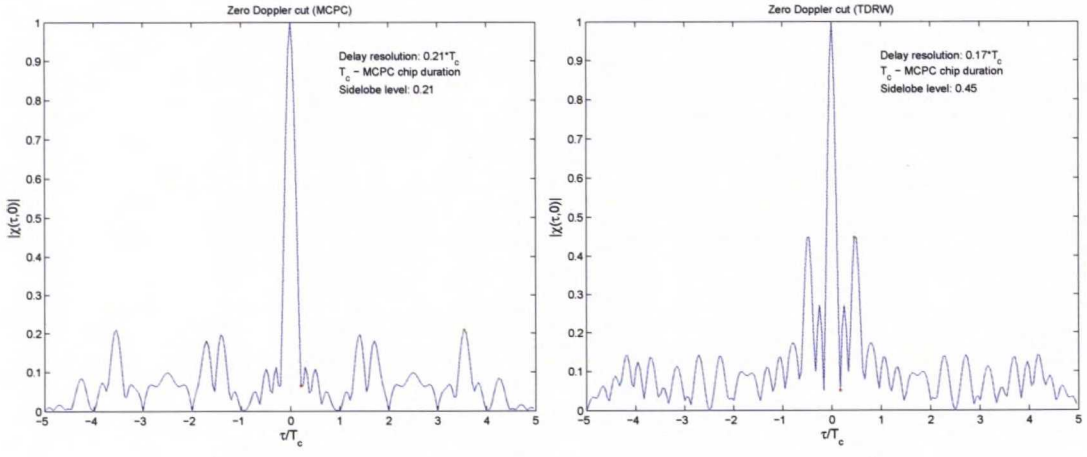

(a) MCPC (b) TDRW

Figure 53: Zero Doppler cut plots for MCPC ($N = 5$, $M = 5$, P4 code) and TDRW ($N = 3$, $M = 5$, P4 code) signals. The TDRW shows higher sidelobe level.

It can be observed that the TDRW offers a better delay resolution than the MCPC signal. However, the sidelobe level corresponding to the TDRW is far from desirable and way higher than the sidelobe level corresponding to the MCPC signal.

A longer modulation code ($M = 10$) is chosen for the TDRW and the resulting spectrum is depicted in Figure 54.

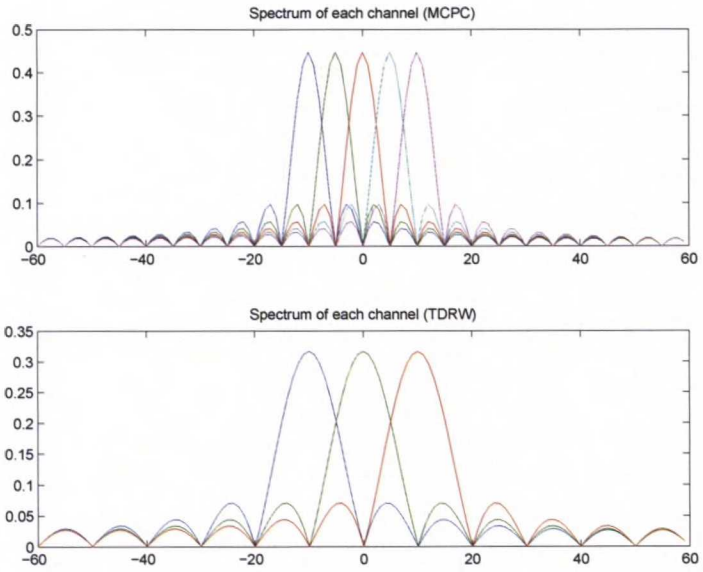

Figure 54: Spectrum of each subchannel for MCPC ($N = 5$, $M = 5$, P4 code) and TDRW ($N = 3$, $M = 10$, P4 code) signals. In this case the TDRW becomes a MCPC signal with less subcarriers.

In this case the TDRW becomes again a MCPC type of signal. However, the number of subcarriers is smaller than the one considered for the reference MCPC signal. The radar performance is investigated in the ambiguity plots presented in Figure 55.

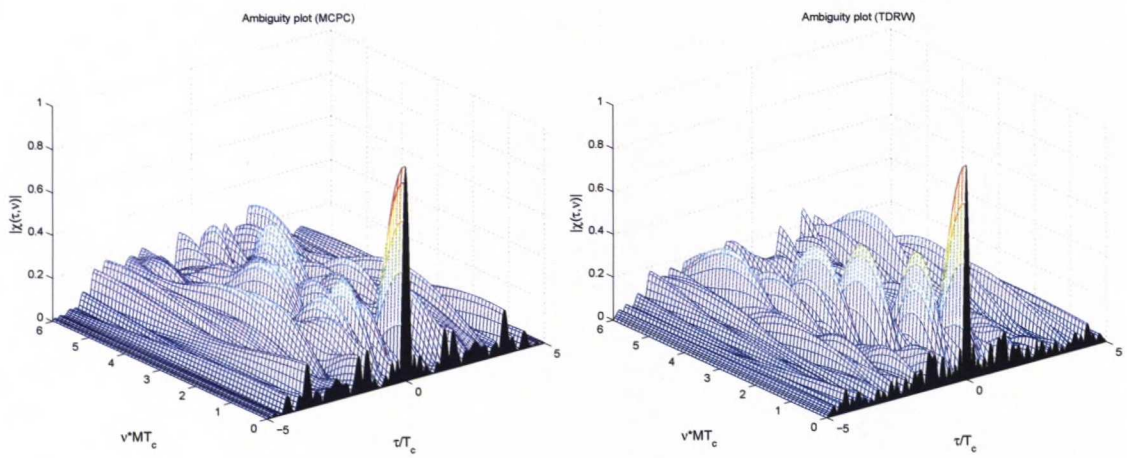

(a) MCPC (b) TDRW

Figure 55: Ambiguity plots for MCPC ($N = 5$, $M = 5$, P4 code) and TDRW ($N = 3$, $M = 10$, P4 code) signals.

The Doppler resolution is obtained from the zero delay cut plots in Figure 56.

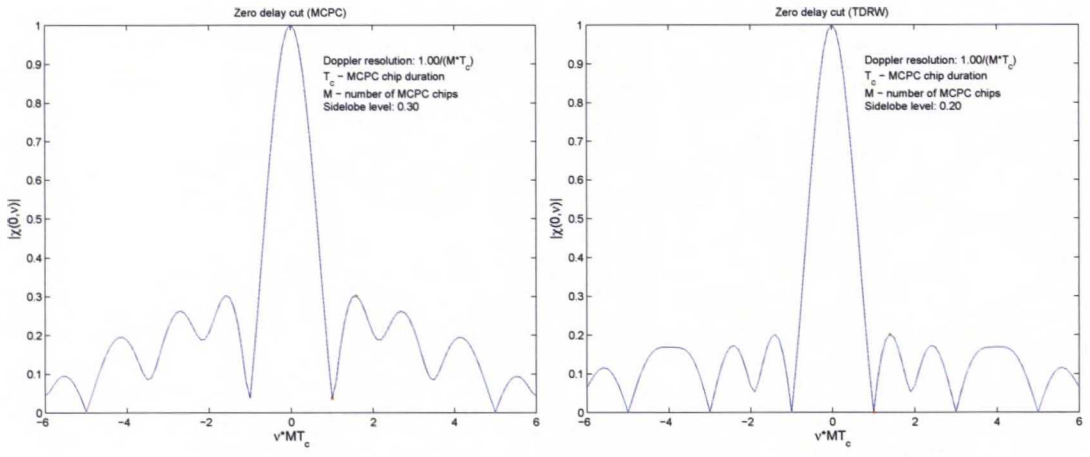

(a) MCPC (b) TDRW

Figure 56: Zero delay cut plots for MCPC ($N = 5$, $M = 5$, P4 code) and TDRW ($N = 3$, $M = 10$, P4 code) signals. The TDRW shows lower sidelobe level.

It shows that both signals have equal Doppler resolution. However, the sidelobe level corresponding to the TDRW is lower than the one corresponding to the reference signal. The zero Doppler cut plots are depicted in Figure 57.

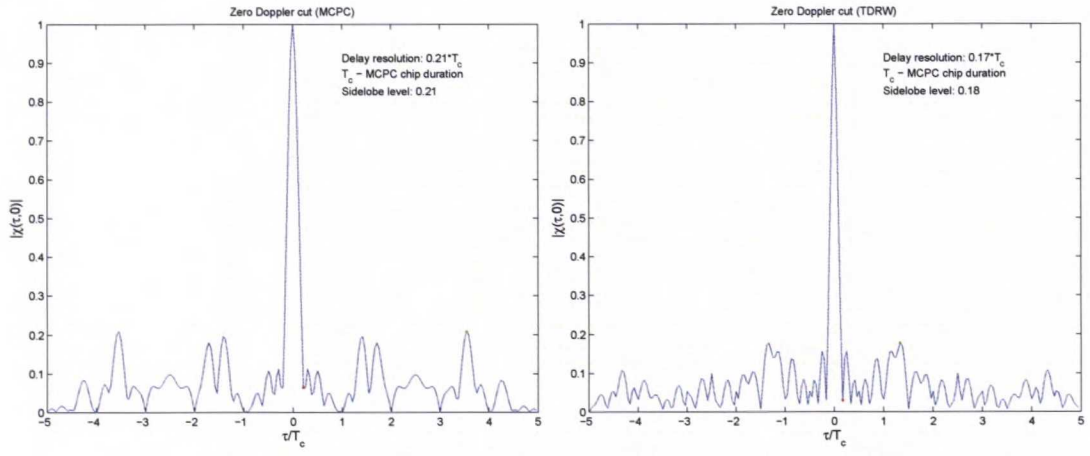

(a) MCPC (b) TDRW

Figure 57: Zero Doppler cut plots for MCPC ($N = 5$, $M = 5$, P4 code) and TDRW ($N = 3$, $M = 10$, P4 code) signals. The TDRW shows better delay resolution and lower sidelobe level.

It shows an improved delay resolution and lower sidelobe level when corresponding to the TDRW.

An even longer modulation code ($M = 15$) is chosen next for the TDRW and the resulting spectrum is shown in Figure 58.

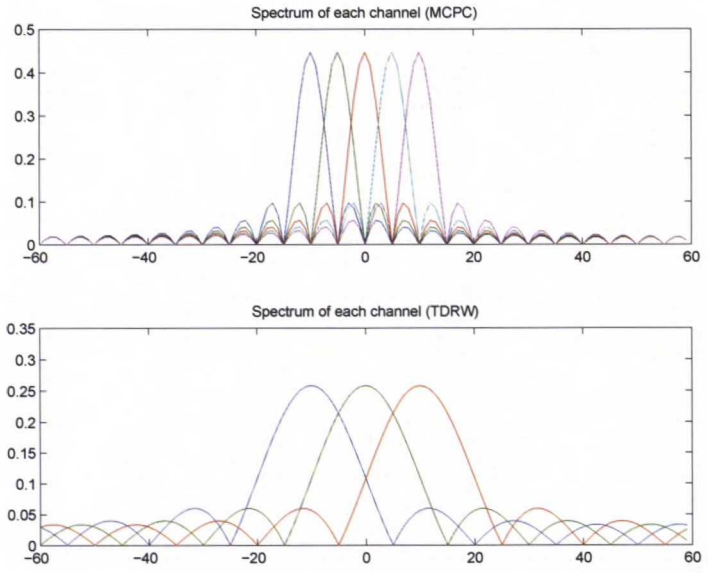

Figure 58: Spectrum of each subchannel for MCPC ($N = 5$, $M = 5$, P4 code) and TDRW ($N = 3$, $M = 15$, P4 code) signals.

The radar performance is investigated in the ambiguity plots presented in Figure 59.

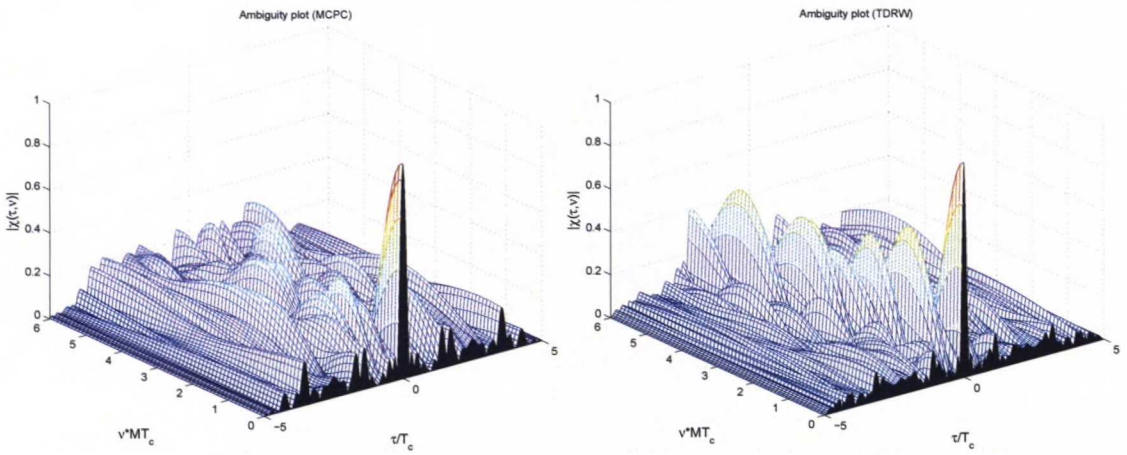

(a) MCPC (b) TDRW

Figure 59: Ambiguity plots for MCPC ($N = 5$, $M = 5$, P4 code) and TDRW ($N = 3$, $M = 15$, P4 code) signals.

The Doppler resolution is found from the zero delay cut plots in Figure 60.

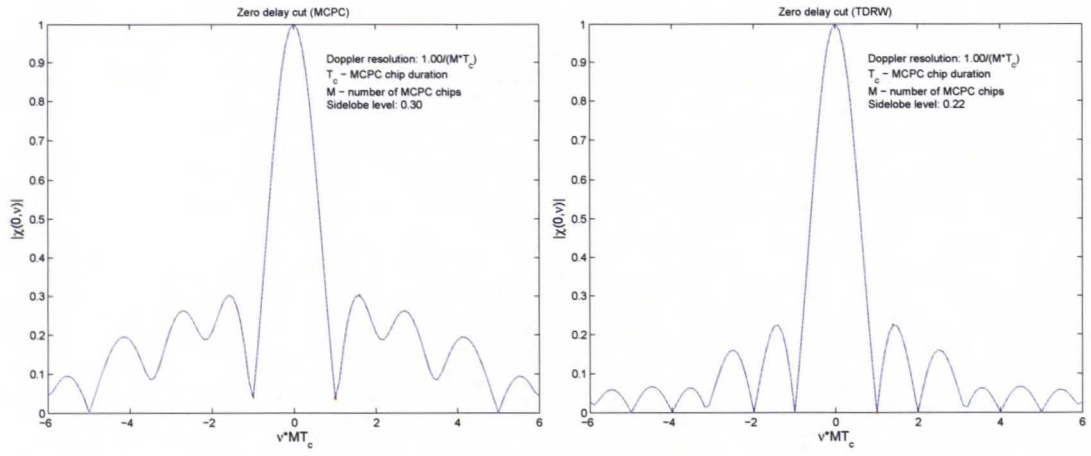

(a) MCPC (b) TDRW

Figure 60: Zero delay cut plots for MCPC ($N = 5$, $M = 5$, P4 code) and TDRW ($N = 3$, $M = 15$, P4 code) signals. The TDRW shows lower sidelobe level.

It can be seen that the two signals offer equal Doppler resolution. Nevertheless, the TDRW offers lower sidelobe level. The zero Doppler cut plots are shown in Figure 61.

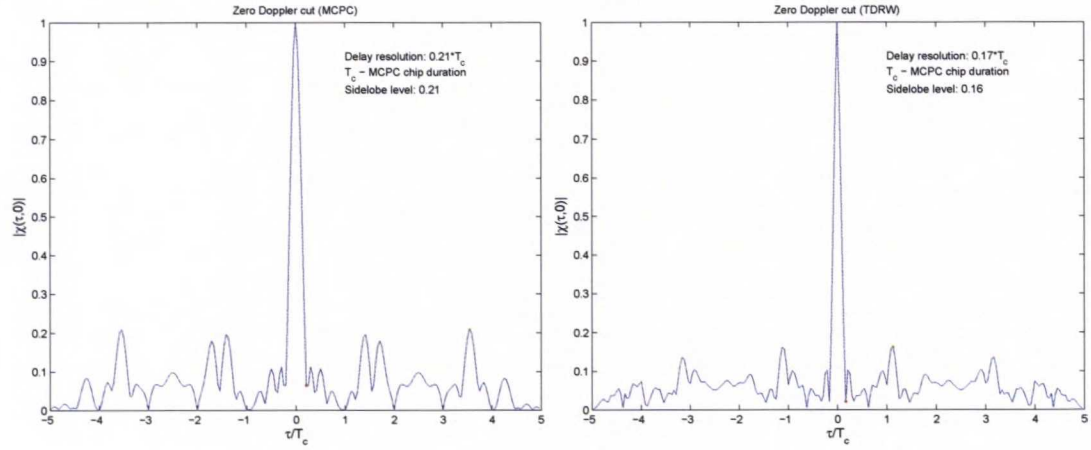

(a) MCPC (b) TDRW

Figure 61: Zero Doppler cut plots for MCPC ($N = 5$, $M = 5$, P4 code) and TDRW ($N = 3$, $M = 15$, P4 code) signals. The TDRW shows better delay resolution and lower sidelobe level.

It can be seen that the TDRW offers lower sidelobe level. More than that, the delay resolution offered by the TDRW is better than the one offered by the MCPC reference signal.

Table 7 summarizes the radar performance observed in all three cases for the generated signals with the developed model:

	Signal	Zero Doppler Cut		Zero Delay Cut	
		Delay Resolution	**Sidelobes level**	**Doppler Resolution**	**Sidelobes level**
	MCPC P3 code N = 8, M = 8	$0.13T_c$	0.17	$\frac{1}{MT_c}$	0.22
Case 1	TDRW P3 code N = 8, M = 8	$0.13T_c$	0.16	$\frac{1}{MT_c}$	0.21
Case 1	TDRW P3 code N = 8, M = 16	$0.13T_c$	0.15	$\frac{1}{MT_c}$	0.20
Case 1	TDRW P3 code N = 8, M = 24	$0.13T_c$	0.15	$\frac{1}{MT_c}$	0.21
Case 2	TDRW P3 code N = 15, M = 8	$0.13T_c$	0.19	$\frac{1}{MT_c}$	0.20
Case 2	TDRW P3 code N = 15, M = 16	$0.13T_c$	0.16	$\frac{1}{MT_c}$	0.23
Case 2	TDRW P3 code N = 15, M = 24	$0.13T_c$	0.22	$\frac{1}{MT_c}$	0.19
	MCPC P4 code N = 5, M = 5	$0.21T_c$	0.21	$\frac{1}{MT_c}$	0.30
Case 3	TDRW P4 code N = 3, M = 5	$0.17T_c$	0.45	$\frac{1}{MT_c}$	0.18
Case 3	TDRW P4 code N = 3, M = 10	$0.17T_c$	0.18	$\frac{1}{MT_c}$	0.20
Case 3	TDRW P4 code N = 3, M = 15	$0.17T_c$	0.16	$\frac{1}{MT_c}$	0.22

Table 7: Summary of the radar performance for the TDRWs generated using the general model

The performance of the TDRWs is summarized in the following and few recommendations are made for choosing the waveform parameters. A first glance at Table 7 illustrates the fact that a TDRW can offer a better radar performance than an equivalent MCPC signal already proposed in [16, 15, 22]. A closer look brings up several interesting findings that are discussed in the following.

Both the TDRW and MCPC signal are special cases of the generalized multicarrier radar model introduced in this report. These two signals are identical under certain parametrization. Nevertheless, the MCPC signal is a particular case of TDRW. This can be seen in the first case when the TDRW has $N = 8$ and $M = 8$ and in the third case when the TDRW has $N = 3$ and $M = 10$. However, in none of the cases where TDRW becoms a MCPC signal the two are identical. This is because different shifts are considered for the coding matrices of the two signals.

For the first case, when $N = 8$ and $M = 8$, the difference between the TDRW and the MCPC signal is in the utilized coding matrix. To be more precise, the considered shifts are different, as both coding matrices are based on the same ideal sequence. The obtained sidelobe level is lower for the TDRW than for the MCPC signal. Both signals offer the same Doppler and delay resolution. Thus, it can be concluded that the shifts utilized for the construction of the coding matrix influence the resulting sidelobe level.

For the third case, when $N = 3$ and $M = 10$, the differences between the TDRW and the MCPC signal are not only the utilized coding matrix but the number of subcarriers and code length also. A better delay resolution and lower sidelobe level are obtained for the TDRW signal. Comparing to the first case, it can be concluded that lowering the number of subcarriers and increasing the code length while keeping these orthogonal to each other can improve the delay resolution.

In the first case the TDRW has the same number of subcarriers as the MCPC signal, while in the second case it has a larger number of subcarriers than the MCPC signal. Analyzing the results for the first and second cases, for all the considered parameters, it can be concluded that a higher number of subcarriers does not improve either Doppler or delay resolution. This happens irrespective of the length of the code. However, this is not the case with the sidelobe level. First case offers lower sidelobe levels than the MCPC reference, regardless of the code length. A longer code induces a higher intercarrier interference because it spreads the signal more. However, this does not prevent obtaining lower sidelobe levels in the first case. Second case leads to higher sidelobe levels than both first case and MCPC reference. Taking the higher number of subcarriers of the second case into account, it can be concluded that the increased interference, caused by the smaller intercarrier spacing, accounts for the increased sidelobe level. Thus, a trade-off between the number of subcarriers and code length is needed in order to keep the intercarrier interference at tolerable level. Finding such trade-off is out of the scope of this work, nevertheless it is a future research topic.

For the third case the TDRW has a larger number of subcarriers than the MCPC signal. This is the only case where the TDRW offers better delay resolution than the reference MCPC signal. Taking into account that compared to the first two cases the number of subcarriers is smaller, it can be concluded that this is desirable in order to obtain better performance than the MCPC signal. It is also observed that increasing the code length the obtained sidelobe level becomes lower. Thus, employing a lower number of subcarriers and a longer spreading code provides overall improved performance than the MCPC waveform.

6 Conclusions

Multicarrier waveforms bring several major advantages over single carrier waveforms in radar systems. One major advantage, if not the most significant, is frequency diversity. As many carrier frequencies are available at the same time, it is easy to overcome problems like jamming, interference or attenuation by allocating power to subcarriers where the channel quality is high. Another great advantage that multicarrier waveforms bring to radar is that the time on target is greatly reduced. Only one pulse is required to obtain range and Doppler information. Waveform diversity is also an advantage. Designing the waveforms both in time and frequency brings in additional degrees of freedom. Last but not least, the possibility to optimize the transmitted waveform is important for radar systems. Traditionally, only the receiver has been adaptive and optimized in radars. The hardware requirements are very similar to those in commercial communication systems which facilitates cost efficient implementation of multicarrier radars.

In this work we developed a generalized model for multicarrier radar. This novel model includes most commonly used radar waveforms as special cases. For example, waveforms that employ OFDM [14, 13, 20, 26], MCPC waveforms [16, 15, 22], spread spectrum waveforms and frequency hopping waveforms. The model is provided using matrix representation. It facilitates implementing different multicarrier waveform designs. All it is needed is to fill in the elements to corresponding matrices accordingly. Depending on the waveform design some of the matrices remain unchanged. Moreover, the model is easy to implement and use in Matlab environment.

A few different multicarrier waveforms are generated using the derived model and their performance is investigated against already proposed waveforms in the literature. A spread spectrum waveform is proposed and generated using the derived model. Such waveform is called TDRW and is a generalization of the MCPC waveforms [16, 15, 22]. It is demonstrated that for some parameters the TDRWs offer a better radar performance than MCPC signals. Some concluding remarks and recommendations of the waveforms and their performance are made:

- sidelobe level depends on the chosen code matrix
- orthogonality in both frequency and code domain can improve delay resolution
- a trade-off between the number of subcarriers and length of the code is required to improve radar performance

Finding an optimal coding matrix that offers the best radar performance is a future research topic. Rules of thumb for choosing the shifts may also be established in future work.

References

[1] J.R. Bellegarda and E.L. Titlebaum. Time-frequency hop codes based upon extended quadratic congruences. *IEEE Transactions on Aerospace and Electronic Systems*, 24(6):726–742, November 1988.

[2] L. Bomer and M. Antweiler. Polyphase barker sequences. *Electronics Letters*, 25(23):1577–1579, November 1989.

[3] S. Boyd. Multitone signals with low crest factor. *IEEE Transactions on Circuits and Systems*, 33(10):1018–1022, October 1986.

[4] M. Braun, C. Sturm, and F.K. Jondral. Maximum likelihood speed and distance estimation for ofdm radar. In *Proceedings of IEEE Radar Conference*, pages 256–261, May 2010.

[5] Jr. Cimini, L. Analysis and simulation of a digital mobile channel using orthogonal frequency division multiplexing. *IEEE Transactions on Communications*, 33(7):665–675, July 1985.

[6] B.P. Crow, I. Widjaja, L.G. Kim, and P.T. Sakai. Ieee 802.11 wireless local area networks. *IEEE Communications Magazine*, 35(9):116–126, September 1997.

[7] K. Fazel and S. Kaiser. *Multi-Carrier and Spread Spectrum Systems: From OFDM and MC-CDMA to LTE and WiMAX*. Wiley, 2008.

[8] A. Ghosh, D.R. Wolter, J.G. Andrews, and R. Chen. Broadband wireless access with wimax/802.16: current performance benchmarks and future potential. *IEEE Communications Magazine*, 43(2):129–136, February 2005.

[9] R. Gold. Optimal binary sequences for spread spectrum multiplexing. *IEEE Transactions on Information Theory*, 13(4):619–621, October 1967.

[10] S.W. Golomb. Two-valued sequences with perfect periodic autocorrelation. *IEEE Transactions on Aerospace and Electronic Systems*, 28(2):383–386, April 1992.

[11] S.W. Golomb and H. Taylor. Constructions and properties of costas arrays. *Proceedings of the IEEE*, 72(9):1143–1163, September 1984.

[12] H. Holma and A. Toskala. *LTE for UMTS - OFDMA and SC-FDMA Based Radio Access*. Wiley, 2009.

[13] G. Lellouch, R. Pribic, and P. van Genderen. Wideband ofdm pulse burst and its capabilities for the doppler processing in radar. In *Proceedings of International Conference on Radar*, pages 531–535, September 2008.

[14] G. Lellouch, P. Tran, R. Pribic, and P. van Genderen. Ofdm waveforms for frequency agility and opportunities for doppler processing in radar. In *Proceedings of IEEE Radar Conference*, pages 1–6, May 2008.

[15] N. Levanon. Multifrequency complementary phase-coded radar signal. *IEE Proceedings - Radar, Sonar and Navigation*, 147(6):276–284, December 2000.

[16] N. Levanon. Multifrequency radar signals. In *Proceedings of IEEE International Radar Conference*, pages 683–688, 2000.

[17] N. Levanon and E. Mozeson. Multicarrier radar signal - pulse train and cw. *IEEE Transactions on Aerospace and Electronic Systems*, 38(2):707–720, April 2002.

[18] D.G. Luenberger. On barker codes of even length. *Proceedings of the IEEE*, 51(1):230–231, January 1963.

[19] Bassem R. Mahafza. *Radar Systems Analysis and Design Using MATLAB.* CHAPMAN & HALL/CRC, 2000.

[20] R. Mohseni, A. Sheikhi, and M.A. Masnadi Shirazi. Wavelet packet based ofdm radar signals. In *Proceedings of International Conference on Radar*, pages 552–557, September 2008.

[21] E. Mozeson and N. Levanon. Multicarrier radar signals with low peak-to-mean envelope power ratio. *IEE Proceedings - Radar, Sonar and Navigation*, 150(2):71–77, April 2003.

[22] Eli Mozeson Nadav Levanon, editor. *Radar Signals.* John Wiley & Sons, Inc., 2004.

[23] G. Porter. Error distribution and diversity performance of a frequency-differential psk hf modem. *IEEE Transactions on Communication Technology*, 16(4):567–575, August 1968.

[24] B.M. Povovic. Complementary sets based on sequences with ideal periodic autocorrelation. *Electronics Letters*, 26(18):1428–1430, August 1990.

[25] H. Sari and G. Karam. Orthogonal frequency-division multiple access and its application to catv networks. *IEEE Transactions on Consumer Electronics*, 9(6):507–516, November-December 1998.

[26] S. Sen and A. Nehorai. Adaptive design of ofdm radar signal with improved wideband ambiguity function. *IEEE Transactions on Signal Processing*, 58(2):928–933, February 2010.

[27] Merrill I. Skolnik, editor. *Radar Handbook.* McGraw-Hill, 3rd edition, 2008.

[28] C. Sturm, T. Zwick, and W. Wiesbeck. An ofdm system concept for joint radar and communications operations. In *Proceedings of 69th IEEE Vehicular Technology Conference*, pages 1–5, April 2009.

[29] C. Sturm, T. Zwick, W. Wiesbeck, and M. Braun. Performance verification of symbol-based ofdm radar processing. In *Proceedings of IEEE Radar Conference*, pages 60–63, May 2010.

[30] K. Taura, M. Tsujishita, M. Takeda, H. Kato, M. Ishida, and Y. Ishida. A digital audio broadcasting (dab) receiver. *IEEE Transactions on Consumer Electronics*, 42(3):322–327, August 1996.

[31] R.F. Tigrek, W.J.A. de Heij, and P. van Genderen. Solvind doppler ambiguity by doppler sensitive pulse compression using multi-carrier waveform. In *Proceedings of European Radar Conference*, pages 72–75, October 2008.

[32] E. Van der Ouderaa, J. Schoukens, and J. Renneboog. Peak factor minimization using a time-frequency domain swapping algorithm. *IEEE Transactions on Instrumentation and Measurement*, 37(1):145–147, March 1988.

[33] R. van Nee, G. Awater, M. Morikura, H. Takanashi, M. Webster, and K.W. Halford. New high-rate wireless lan standards. *IEEE Communications Magazine*, 37(12):82–88, December 1999.

[34] Zhendao Wang and G.B. Giannakis. Wireless multicarrier communications. *IEEE Signal Processing Magazine*, 17(3):29–48, May 2000.

[35] M. Zimmerman and A. Kirsch. The an/gsc-10 (kathryn) variable rate data modem for hf radio. *IEEE Transactions on Communication Technology*, 15(2):197–204, April 1967.